Structural and Functional Characterization of 2-Hydroxypropyl-β-Cyclodextrin and Sugammadex as Active Pharmaceutical Ingredients by NMR Spectroscopy

PhD thesis

Eszter Kalydi

Doctoral School of Pharmaceutical Sciences
Semmelweis University

Supervisor: Szabolcs Béni, Ph.D.

Official reviewers: Orsolya Tőke, Ph.D.
Arash Mirzahosseini, Ph.D.

Head of the Complex Examination Committee: István Antal, Ph.D.

Members of the Complex Examination Committee: Zoltán Szakács, Ph.D.
Gergő Tóth, Ph.D.

Budapest
2025

TABLE OF CONTENTS

LIST OF ABBREVIATIONS

1D	1-Dimensional
2D	2-Dimensional
2-Me-β-CD	Heptakis-2-*O*-Methyl-β-Cyclodextrin
3-Me-β-CD	Heptakis-3-*O*-Methyl-β-Cyclodextrin
6-Me-β-CD	Heptakis-6-*O*-Methyl-β-Cyclodextrin
a.r.	Analytical Reagent Grade
API	Active Pharmaceutical Ingredient
ASN	α-Solanine
BCD	β-Cyclodextrin
BCS	Biopharmaceutics Classification System
CD	Cyclodextrin
CE	Capillary Electrophoresis
CIS	Complexation-Induced Shift
COSY	Correlation Spectroscopy
DEPT	Distortionless Enhancement by Polarization Transfer
DMSO	Dimethyl Sulfoxide
DS	Average Degree of Substitution
EXSY	Exchange Spectroscopy
GC	Gas Chromatography
GCD	γ-Cyclodextrin
GP	α-1,4-Glucopyranose
GRAS	Generally Recognized as Safe
HMBC	Heteronuclear Multiple Bond Correlation
HP	2-Hydroxypropyl
HPBCD	2-Hydroxypropyl-β-Cyclodextrin
HPLC	High Performance Liquid Chromatography
HSQC	Heteronuclear Single Quantum Coherence
IR	Infrared
ITC	Isothermal Titration Calorimetry

MALDI-TOF	Matrix-Assisted Laser Desorption/Ionization Coupled to Time-Of-Flight
Me-BCD	Randomly Methylated-β-Cyclodextrin
MS	Molar Substitution
MSpec	Mass Spectrometry
MTT	3-(4,5-dimethylthiazol-2-yl)-2,5-diphenyltetrazolium bromide
NMR	Nuclear Magnetic Resonance
NOE	Nuclear Overhauser Effect
NOESY	Nuclear Overhauser Effect Spectroscopy
NPC	Niemann-Pick Type C
OH	Hydroxyl
PhEur	European Pharmacopoeia
PS	Pattern of Substitution
ROESY	Rotating Frame Overhauser Effect Spectroscopy
RS	Randomly Substituted
SB-GCD	Sulfobutylether-γ-Cyclodextrin
SGM	Sugammadex
SI	Single Isomer
SN	Solanidine
SS	Solasodine
TLC	Thin Layer Chromatography
TOCSY	Total Correlation Spectroscopy
USP	United States Pharmacopoeia
UV-VIS	Ultraviolet-visible

1. INTRODUCTION

1.1. Cyclodextrins

1.1.1. Structure and properties of cyclodextrins

Cyclodextrins (CDs) are natural cyclic oligosaccharides, produced via enzymatic treatment of starch. CDs are composed of various number of α-1,4-glucopyranose (GP) rings. The most common members are known as α-CD, β-CD, and γ-CD, comprised of six, seven and eight GP units, respectively (Figure 1A). CDs possess a unique three-dimensional structure, resembling a hollow truncated cone (Figure 1B). While the secondary hydroxyl (OH) groups (OH-2 and OH-3 based on the conventional atom numbering of monosaccharides) are situated on the wider rim of the toroid, the primary OH-6 are located on the narrower edge. Due to their free rotation, the primary side entrance is partially blocked by these sidechains. In contrast, the secondary OHs are unable to rotate, providing more rigidity to the secondary side. The structure is further stiffened by the H-bond belt formed between the non-bonding electron pair of the oxygen atom of OH-2 and the hydrogen atom of OH-3 of the adjacent subunit, in the clockwise direction. Due to the OH groups pointing towards the outside of the cone, CDs have hydrophilic surface, while H-3, H-5 and the glycosidic oxygens are facing the inside of the cavity, creating a hydrophobic character inside the hollow (1).

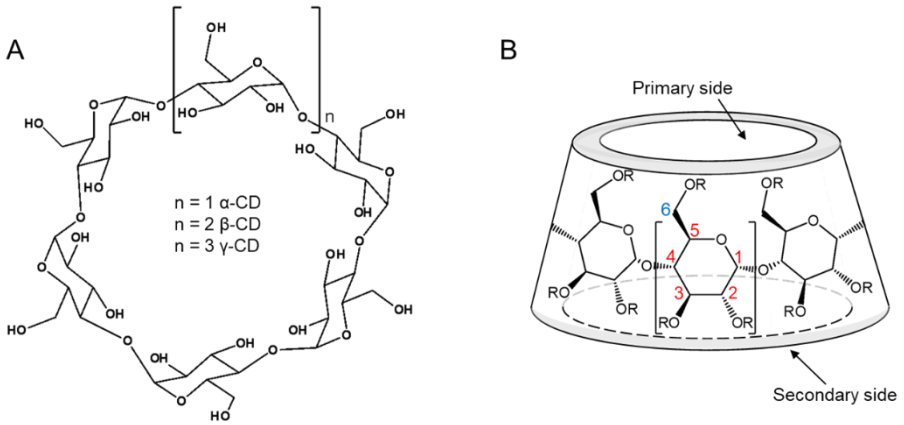

Figure 1. Schematic representation of cyclodextrins' (CDs) structures a) structure of native CDs B) schematic three-dimensional structure of CD derivatives with atom numbering of the glucopyranose (GP) unit.

Depending on the number of the joint GP units, the physico-chemical properties of CDs vary (Table 1). The increasing number of GP moieties results in wider cavity diameter,

as well as outer diameter, while the height of the torus remains constant, given by the height of the GP unit. The aqueous solubility of α-, β- and γ-CD shows a seemingly anomalous behavior: while α-CD and γ-CD have relatively high solubility of 145 mg/ml (149 mM) and 232 mg/ml (179 mM), respectively, β-CD with the middle-sized cavity possesses much more restricted solubility of 18.5 mg/ml (16.3 mM) at 25 °C. This unusual behavior can be explained by the high rigidity of the H-belt around the cavity, resulting in lower mobility of secondary OH hydrogens.

Table 1. Physico-chemical properties of native cyclodextrins (2).

Cyclodextrin	Number of glucose units	Cavity diameter (Ä)	Cavity height (Ä)	Solubility* (mg/ml)
α-CD	6	4.7 – 5.3	7.9	145
β-CD	7	6.0 – 6.5	7.9	18.5
γ-CD	8	7.5 – 8.3	7.9	232

** In water at 25 °C.*

1.1.2. The complexation phenomenon

Due to the hydrophobic cavity and hydrophilic surface, CDs are able to encapsulate hydrophobic compounds in aqueous environment by non-covalent host-guest type complex formation. The encapsulation is thermodynamically favored, driven by the replacement of the unfavored polar-apolar interactions between the water molecules and the cavity as well as between the apolar guest molecule(s) and bulk water with more favorable van der Waals and electrostatic interactions and hydrogen bonding (3). The relative contribution of the different forces depends on the type of the interacting host and guest. The inclusion process is reversible, and the strength of the complex can be quantitatively characterized by the association constant K_a (also referred as the stability constant or formation constant):

$$[CD] + [Guest] \rightleftharpoons [Complex] \qquad (1) \qquad \text{and} \qquad K_a = \frac{[Complex]}{[CD]\,[Guest]} \qquad (2).$$

The cavity size defines the nature of guest molecules suitable for complexation: α-CD is mostly capable of capturing aliphatic chains, while β-CD is well-suited for complexation of small aromatic molecules (4) or adamantane-derivatives (5). γ-CD with the widest cavity is able to incorporate condensed aromatic rings or steroids (6,7).

The complexation of the guest molecules can affect their physico-chemical properties, such as the aqueous solubility (8), stability (9), reactivity (10) or bioavailability (11). Given their advantageous toxicological profile, including GRAS (Generally Recognized as Safe) designation and biodegradability, CDs are extensively utilized for their complexation ability across a wide range of applications. Nearly half of the uses are related to the pharmaceutical field (12), where CDs are mainly employed as excipients to increase the solubility, stability, and bioactivity of active pharmaceutical ingredients (APIs), or for odor and taste masking to improve palatability of oral drugs (13). They are also widely utilized in the food (14) and cosmetic industry (15) as well as in packaging (16), e.g., by flavor, fragrance or preservative encapsulation, but have also met applications in agriculture (17) and environmental remediation (18). In the latter case, CDs are not used to encapsulate active compounds but to extract undesirable, toxic components from soil, or wastewater (19). Besides industrial applications, due to the intrinsic chirality of the glucose units, CDs are also used as chiral selectors in various analytical methods (20–22).

1.1.3. Chemically modified cyclodextrins

As native BCD, historically the first CD to become industrially available at a reasonable price, suffered from limited aqueous solubility, and in order to design hosts with increased specificity, a wide variety of semisynthetic derivatives have been developed. All GP subunits bear three OH groups, thus native α-, β-, and γ-CD have 18-, 21-, and 24 sites for chemical modification, enabling nearly limitless variability in compound design.

Modified CDs can be structurally classified based on various aspects, such as the site of modification, the number of modified groups, or the type of modification. From the pharmaceutical and analytical point of view, modified CDs can be divided into two main classes: single isomer (SI) CDs and randomly (or statistically) substituted (RS) CD derivatives.

SI derivatives can be described by one well-defined structure, independently from the site and number of modifications. SI CDs comprise mono-substituted derivatives (23,24) (mono-2, mono-3, and mono-6 substitution), persubstituted derivatives (25–27) (per-2, per-3, and per-6 substitution and their combination) and those multiply substituted in a selective manner (28,29).

In contrast, RS CDs cannot be described by an individual structure, as these derivatives are composed of a complex mixture of isomers, differing in the number and position of substitution.

Both classes of CDs have their own advantages: while the structural characterization of SI CDs is straightforward and identity is easy to verify, their synthesis is often laborious with yields compromised due to the necessity for consecutive reactions involving selective protection, modification and deprotection (30). The purification of the intermediates and the final product is also challenging and hardly scalable due to the often-inevitable use of chromatography, highly increasing the cost of production. These difficulties make their industrial-scale production non-favorable. Due to the structural uniformity, however, the interactions of SI CDs with other molecules and structure-activity relationship can be simply explored (31).

On the other hand, RS derivatives are usually synthesized in one-step, followed by a simple purification process (32). The average structure of such derivatives, however, is highly dependent on the applied synthetic conditions (33,34), and for proper characterization, a more sophisticated and complex analytical approach is required (32). Nevertheless, the preparation approach is usually well-scalable and more economical, therefore suitable for industrial-scale production. Furthermore, the complexation properties of RS derivatives are often superior to those of their SI-counterparts (35), but identifying the specific fraction responsible for the interaction can be challenging.

1.1.4. Pharmaceutical use of cyclodextrins

1.1.4.1. Cyclodextrins as excipients

Due to their favorable safety profile, native CDs and some of their derivatives are extensively exploited in pharmaceutical formulations as excipients. As a consequence of intrinsic hydrophilicity, orally administered CDs lack absorption from the gastrointestinal tract, leading to very low bioavailability with only few exceptions (RAMEB is adsorbed 11-12%) (36). The smaller ring sized CDs α- and β-CDs are stable against α-amylase present in the saliva, but γ-CD is promptly digested by the same enzyme as well as by pancreatic α-amylase. After parenteral administration, CDs are primarily eliminated in their intact form by renal excretion. Besides native CDs, various derivatives with improved solubility and complexation capabilities are also developed and accepted as pharmaceutical excipients, listed in Table 2.

Table 2. Cyclodextrin derivatives currently used as excipients, accepted by the European Medicines Agency (37).

Cyclodextrin	MS* / DS**	Molecular weight	Solubility (mg/ml)
α-CD	-	972	145
β-CD	-	1135	18.5
γ-CD	-	1297	232
HPBCD	0.65 / 4.55	1400	>600
Methylated-BCD	1.8 / 12.6	1312	>500
SBEBCD	0.9 / 6.3	2163	>500
HPGCD	0.6 / 4.8	1576	>500

* MS: molar substitution; average number of attached substituents per glucopyranose unit
**DS: degree of substitution: average number of substituents attached to one cyclodextrin molecule

The route of administration covers a wide variety, including oral, parenteral, nasal, ocular, rectal, and transdermal delivery. The toxicity profile of the single derivatives depends on the route of administration. For example, β-CD exhibited renal toxicity when administered parenterally at certain concentrations and dosage regimens, while some methylated derivatives showed hemolytic activity. However, they were found to be safe in oral, nasal, or ocular applications (38).

According to the Biopharmaceutics Classification System (BCS) for oral delivery, CDs show beneficial enhancement of bioavailability of drugs with low aqueous solubility, classified in BCS Class II (high permeability) and BCS Class IV (low permeability) (36).

1.1.4.2. Cyclodextrins as active pharmaceutical ingredients

Although the application of CDs is still dominated by their use as excipients (pharmacologically inert additives), in the past decades there has been a paradigm shift towards their utilization as APIs.

1.1.4.2.1. Sugammadex

The first example of a CD used as an API is the octatiopropionic acid derivative of γ-CD, known as sugammadex (SGM) (sold under the brand name Bridion®) (Figure 2). SGM is the first selective relaxant binding agent, specifically designed for the reversal of the neuromuscular blockade induced by rocuronium (Figure 2), an aminosteroid-type muscle relaxant used in anesthesia (39). The application was patented in 2001 and has been used in clinical practice ever since. After intravenous administration, SGM captures the muscle relaxant by forming a host-guest complex with exceptional stability, causing quasi-immediate cessation of the anesthetized state (40,41). The high selectivity eliminates

prolonged side effects following the surgical intervention. SGM has an elimination half-life of approximately two hours via renal clearance, generally without adverse side effects and has been found to be biologically inactive and well tolerated (42). Its medical use is approved in the European Union, in the United States and in Japan.

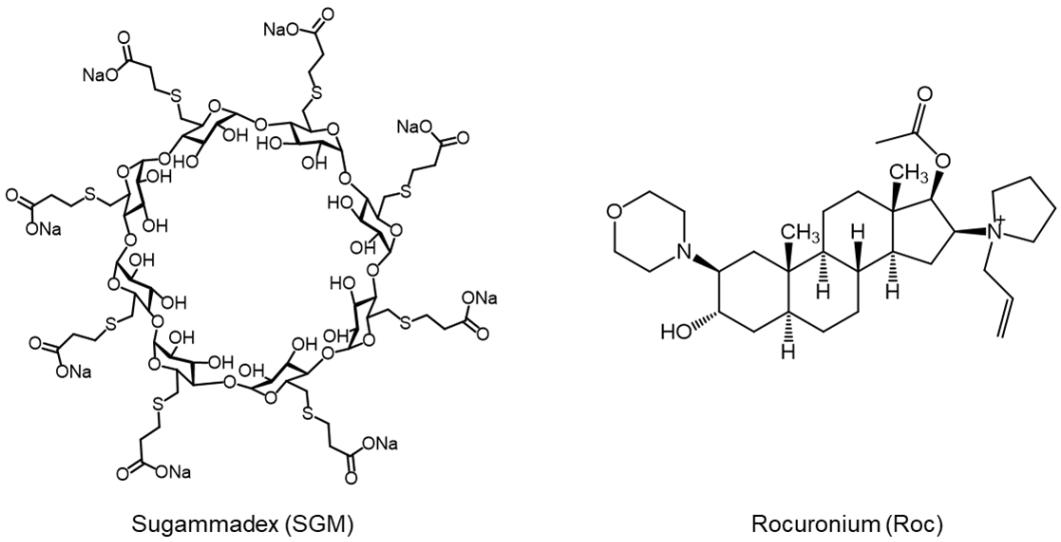

Figure 2. Structure of sugammadex (SGM) and rocuronium.

The high selectivity of SGM towards the aminosteroid is attributed to the formation of a particularly stable inclusion-type complex (43). The reported binding affinity for the SGM/Rocuronium complex of $K_a = 1.8 \times 10^7$ M^{-1} is among the highest ever reported for CD inclusion complexes. SGM is similarly used to reverse the effect of two other muscle relaxants with analogous structures, vecuronium and pancuronium bromide. Similar selectivity and efficacy were shown, the reported stability constants for SGM/vecuronium and SGM/pancuronium complexes are 5.7×10^6 M^{-1}, and 2.6×10^6 M^{-1}, respectively (40). The high binding affinity is due to the tight fit of the steroid backbone into the extended CD cavity, stabilized by the emerging intermolecular ionic interactions between the carboxylic sidechains of SGM and the amino head of the steroids (44).

1.1.4.2.2. 2-Hydroxypropyl-β-CD

2-Hydroxypropyl-β-CD (HPBCD) is a RS derivative of *β*-CD (Figure 3), one of the most significant CD derivatives. Beyond its substantial role as an excipient, HPBCD also received orphan drug status in 2015 for the treatment of Niemann-Pick type C disease (NPC) (45), a fatal inherited metabolic disorder. NPC is associated with erroneous cholesterol metabolism causing the accumulation of cholesterol in the late endosomes and

lysosomes in cells, leading to dysfunctions in various organs and resulting in progressive neurodegeneration, and ultimately in premature death (46).

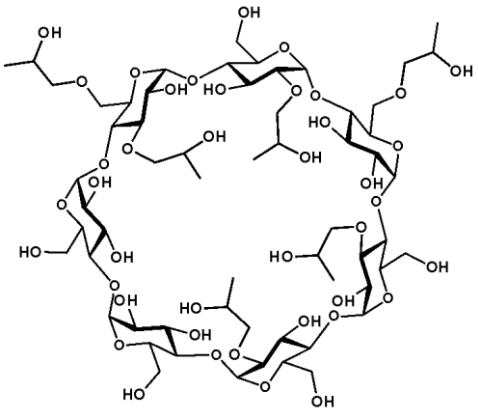

Figure 3. Representative structure of 2-hydroxypropyl-β-CD (HPBCD).

Although the exact mechanism of action of HPBCD is not yet fully understood and remains largely unexplored, it is known to modify cholesterol trafficking by encapsulating and removing excess cholesterol (45). The success of HPBCD in clinical application prompted research to explore its further therapeutic potential for various related disorders associated with elevated levels of cholesterol, such as atherosclerosis and various neurodegenerative diseases like Alzheimer's- and Parkinson's disease (47).
Despite being granted orphan drug status, the broader application of HPBCD as an API is hampered by its complex composition. HPBCD is synthesized by reacting native β-CD with propylene oxide under aqueous basic conditions (48). The basicity of the reaction medium typically impacts all OH groups, albeit to varying degrees depending on the reaction conditions (33), generating a randomly substituted compound.
The earlier works of Pitha and his research group presented detailed studies to assess the effect of the synthetic conditions on the extent of derivatization and the distribution of substituents on the various positions (pattern of substitution, PS). They have shown that besides the evident influence of the molar excess of propylene oxide on the obtained DS, the regioselectivity changes by varying the alkaline concentration (34). Low alkali concentration favors OH-2 substitution, while increasing the basicity, OH-6 substitution becomes pronounced. The variation in both DS and PS remarkably influences the average structure, cavity dimensions, and ultimately pharmaceutically crucial parameters, such as solubility, complex forming ability, and toxicity (32,49–55).

To define the structural needs of HPBCDs, both the European Pharmacopoeia (PhEur) and United States Pharmacopoeia (USP) only prescribe a range of molar substitution (MS) expressing the number of HP sidechains per GP unit. However, a more common way to describe the extent of substitution is to calculate the average degree of substitution (DS), which defines the average number of HP per CD molecule (MS·7 in case of HPBCD). The accepted range for the average substitution of HPBCD is between MS 0.4-1.5 equivalent to DS 2.8-10.5, representing a rather wide acceptance interval and no specific data requirements exist for establishing the PS.

1.1.5. Analytical methods for the characterization of cyclodextrins and cyclodextrin complexes

1.1.5.1. Analysis of cyclodextrins

Although modern analytical techniques provide a wide variety of methods for structural and physico-chemical analysis, several challenges remain during CD characterization. Native CDs and most of their derivatives do not have intrinsic absorption in the ultraviolet-visible (UV-VIS) wavelength range, making their detection with separation techniques difficult. They also tend to form aggregates, which can cause issues ranging from sample preparation to detection. Additionally, their complexation ability may lead to unwanted interactions with solvents, additives, or even the stationary phase during separation (56).

The most frequently applied techniques to characterize CDs include thin layer chromatography (TLC), high performance liquid chromatography (HPLC), gas chromatography (GC), mass spectrometry (MSpec), and nuclear magnetic resonance (NMR) spectroscopy, or the coupled version of such techniques.

While TLC, HPLC and GC are used to monitor reactions, identify byproducts and other impurities such as reagent or solvent residues, from MSpec data indirect structural information can be drawn. The most comprehensive information can be obtained from liquid state NMR spectroscopy, that provides direct atomic level structural information on the CD structure while simultaneously allowing qualitative and quantitative determination of byproducts and impurities.

The proper characterization of RS CDs is particularly challenging, given that they are made up of a myriad of different structural analogues, with diverse molecular weight and constitution. The most important characteristics of a statistically substituted CD are DS,

DS distribution and PS. While the total DS can be calculated using NMR spectroscopy, techniques such as TLC, HPLC, or MALDI-TOF-MSpec can be used to generate a fingerprint chromatogram or mass spectrum, revealing the distribution of components with varying DS in the sample. However, these methods do not provide information about the positions of the side chains.

At present, the generally applied method to determine the distribution of the substituents in a RS CD derivative is the Hakomori method (57). The method is developed for oligo- and polysaccharide characterization and comprises four consecutive steps of modifications before GC-MSpec analysis (Figure 4). The carbohydrate derivative is first permethylated to protect free OH-groups, and consecutively hydrolyzed to its monomers. After reduction of the furanose or pyranose monosaccharide units to open chain derivatives, peracetylation is carried out to facilitate GC-MSpec analysis.

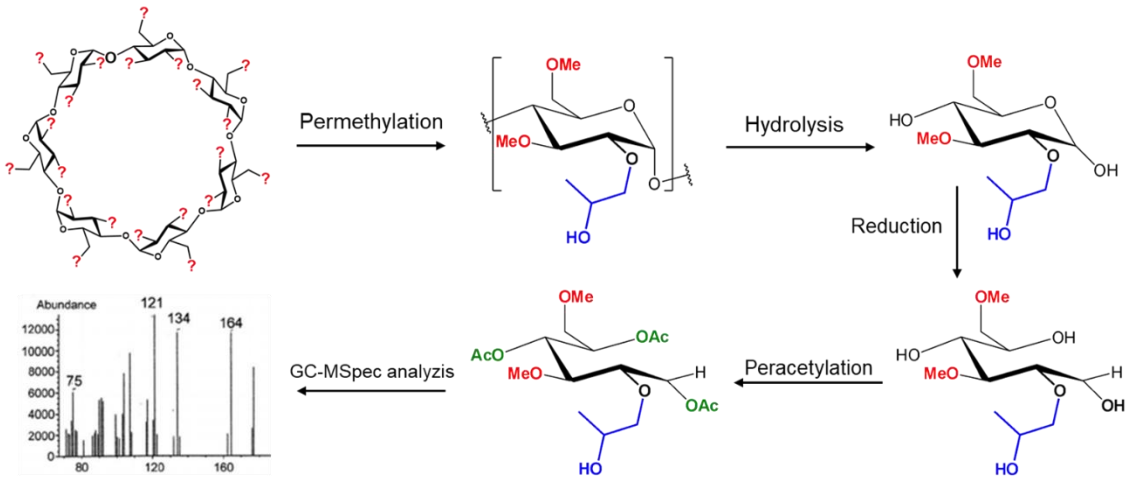

Figure 4. The schematic flowchart of the Hakomori-method used to determine the substituent distribution of CD derivatives.

The Hakomori procedure, as a destructive method, consumes and alters the sample during the analysis. The multiple manipulation steps that are necessary for conducting an appropriate analysis can lead to sample loss, which can affect the accuracy of the analysis. Derivatization of the analyte involves chemical reactions, and the efficiency of these reactions can vary; incomplete or inefficient derivatization can lead to inaccurate results.

1.1.5.2. Analysis of cyclodextrin complexes

The characterization of CDs' complex formation includes various aspects and often requires complementary techniques for comprehensive assessment. The choice of

analytical method highly depends on the nature of the guest and the complex. For example, UV-VIS and fluorescent spectroscopy are sensitive techniques, but only applicable in the presence of a chromophore. As the vast majority of CDs do not have such moieties, only UV-active guests are suitable for this method, or a special set-up, competitive titration with a UV-active guest (or host) can be applied as an indirect method.

To determine the nature of the complex, phase solubility diagrams are recorded by determining the solubility of the guest in the presence of increasing concentrations of CD (Figure 5), usually carried out by HPLC analysis (58). The recorded isotherm reveals if the formed host-guest complex is soluble (A-type), has limited solubility (B_S) or insoluble (B_I).

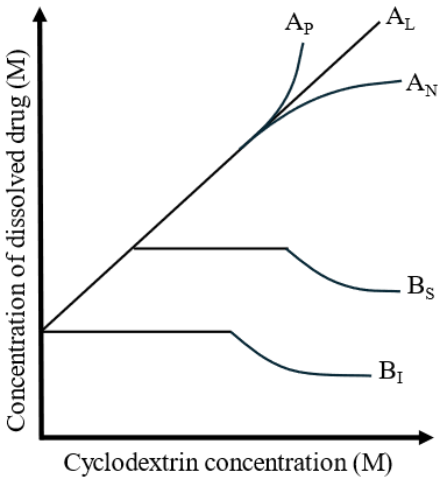

Figure 5. Theoretical phase solubility diagram for various types of CD complexes (59).

Regarding the soluble complexes, the isotherm also provides information on the complex stoichiometry. In case of equimolar (1:1) complexes, the solubility of the guest molecule increases linearly with increasing CD concentrations (A_L-type), while higher order complexes are indicated by positive (A_P) or negative (A_N) deviation from linearity. Aggregation or self-association of the complexes or the limited solubility guest may also occur, influencing the shape of the curve. Consequently, the stoichiometry of the inclusion complex cannot be strictly derived from the phase solubility diagram.

To determine complex stoichiometry, and complex stability (i.e., the complex stability constant K_a) there are plenty of methods available. The most common and straightforward technique is isothermal titration calorimetry (ITC). It provides detailed thermodynamic

parameters of the complex formation process, including the stability constant (K_a), stoichiometry of the supramolecular association and changes in molar enthalpy (ΔH), and entropy (ΔS), by measuring the released or absorbed heat upon binding (60). ITC requires small amounts of sample, and due to its sensitivity, it is suitable for higher affinity systems up to K_a of 10^8 M^{-1} (61).

In addition to ITC, a variety of spectroscopic or chromatographic techniques are available to evaluate complex affinity. These methods typically rely on detecting changes in a suitable physical or chemical property of the guest molecule upon inclusion complex formation. The most common techniques include UV-VIS and fluorescent spectroscopy, NMR, HPLC and capillary electrophoresis (CE) (62). In spectroscopic techniques, the detected parameter is the absorbed wavelength, whereas in chromatographic methods, the retention time of the guest is altered due to guest-CD interaction (63). The stoichiometry of the complex can be determined using spectroscopic approaches such as Job's continuous variation method (64). The stability constant can be calculated using the spectral shift method, where the observed physical property is plotted against CD concentration.

NMR is one of the techniques providing the most comprehensive information on CD complexes. It is not only suitable to gain information on the structure of the complex at the atomic level through mapping intermolecular interactions, but the stoichiometry, complex stability and various thermodynamic parameters can also be obtained.

1.1.5.3. NMR spectroscopic characterization of cyclodextrins and their complexes

1.1.5.3.1. Structural elucidation

While the structural elucidation of a wide range of molecules is mainly carried out by NMR spectroscopy, the determination of carbohydrate structures –including CDs– is often challenging, as most of their ^{1}H NMR chemical shifts fall into a relatively narrow range leading to severe spectral overlap. With the increase in signals dispersion at higher magnetic field, modern NMR instruments are well-suited for the investigation of more complex carbohydrate derivatives as well.

Due to the high symmetry of the native CDs, their spectra are simplified to one set of frequencies corresponding to the GP unit. The field strengths of commonly available

instruments (e.g. 400 MHz) are sufficient to differentiate the various frequencies of GP in 1-dimensional (1D) ^{1}H and ^{13}C spectra (65).

Regarding the ^{1}H NMR spectrum, the signals of unmodified CDs can be separated into two well-separated regions: the anomeric region between 5.0 – 5.2 ppm, and the core region typically between ~3.4 – 4.3 ppm comprising the rest of the proton frequencies (H2-H6). In case of modified derivatives, the signals of the attached sidechains can appear in the aliphatic region mostly separated from the core region at lower chemical shifts, or in the aromatic region between 6.0-9.0 ppm, depending on the nature of the substituent.

In the ^{13}C spectra, a higher signal dispersion is observed due to the broader frequency range. The anomeric carbon is usually found around 100 ppm, the core protons between 60 – 80 ppm, while the carbon frequencies of aliphatic substituents typically have lower frequencies (10-60 ppm) and the aromatic carbons are typically found between 120-160 ppm.

For complete structural elucidation, 1D ^{1}H and ^{13}C spectra are typically complemented with common 2D experiments (Figure 6) (66). The anomeric signals serve as a useful entry point for the resonance assignment, as they are distinctly separated from the other signals in both frequency ranges (65,67). To map the adjacent connectivities, COSY is used, while with help of TOCSY non-equivalent GP units of the CD can be separated. ROESY correlations are used to connect the GP rings by finding the correlation between an anomeric proton and the H4 proton, corresponding to the neighboring GP unit in the clockwise direction. Using HMBC the same information can be obtained, by finding correlation between the proton of an anomer and the carbon of the adjacent GP unit, or vice versa. Similarly, the position of substitution can be revealed by HMBC correlation between the α-carbon (or hydrogen) of the substituent and the hydrogen (or carbon) of the substituted position (66,68).

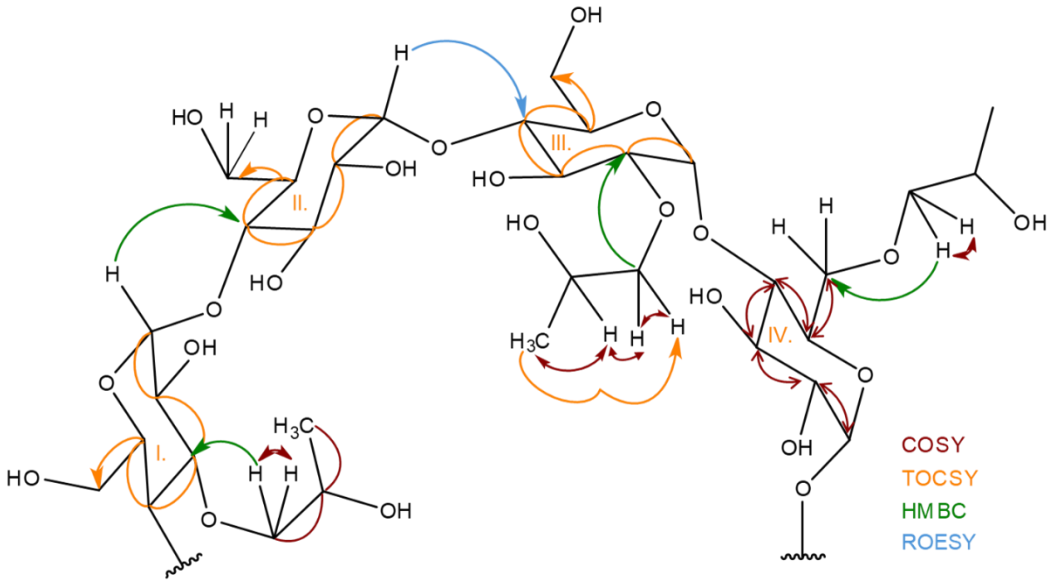

Figure 6. Homo- and heteronuclear correlations used for CD structural elucidation shown on the partial structure of HPBCD.

The structural assignment of symmetrically substituted CDs is straightforward, however the elucidation of unsymmetrically modified CDs is more complex and –depending on the number and nature of the substituent– often requires extensive analysis of various more sophisticated spectra. As the number of substituents increases, the spectral complexity also grows due to the greater number of individual frequencies overlapping within the same spectral region. For SI derivatives, however, it is possible to identify the individual units, as demonstrated by the complete signal assignment of selectively disubstituted-β-CD (28) derivatives and a hepta-differentiated-β-CD (29), comprising seven different GP units.

On the other hand, in the case of RS derivatives, the complete assignment often fails due to several reasons: as RS CD derivatives are composed of a great number of substitutional isomers rather than a single component, the signals in the NMR spectra are apparently broadened, which is a consequence of similar but not identical chemical environment of the nuclei due to microheterogeneity (69). It leads to reduced dispersion and more pronounced overlaps of the frequencies in the already crowded spectral regions. Additionally, in 2D correlation spectra, it causes more diffuse, less definite cross-peaks, leading to ambiguous assignments (70). Due to signal overlap, only partial differentiation of the structural isomers is possible.

From the practical point of view, these spectral features restrict the NMR structural characterization of RS CDs to the calculation of the DS. However, as not only the DS is the decisive feature influencing the complexing ability, but also distribution of substituents has a crucial role, there is a demand for a more comprehensive characterization of such derivatives with a simple and reliable method to pave the way to the application of RS CDs as APIs.

1.1.5.3.2. Investigation of complexes

The appearance of the NMR spectrum of CD complexes highly depends on the strength of the complex, or more precisely the rate of association/dissociation, which is in the vast majority of cases correlating with binding affinity. That is, by increasing binding affinity, the exchange between the two states (free and that in complex) is slower and vice versa (71). The expression "NMR timescale" refers to the ability of NMR to distinguish between frequencies. If the chemical shift difference between the two exchanging sites is smaller than the exchange rate, then the process is described as fast exchange on the NMR timescale (72). In the fast exchange regime, the time averaged spectrum of the free and complex form of the host and guest are observed (73) (Eq. 3 and 4),

$$\delta_{\mathrm{obs}}(\mathrm{H}) = x_{\mathrm{H}}\delta_{\mathrm{H}} + x_{\mathrm{HG}}\delta_{\mathrm{HG}}(H) \qquad (3)$$

$$\text{and} \quad \delta_{\mathrm{obs}}(\mathrm{G}) = x_{\mathrm{G}}\delta_{\mathrm{G}} + x_{\mathrm{HG}}\delta_{\mathrm{GH}}(G) \qquad (4),$$

where δ_{obs}(H) and δ_{obs}(G) are the observed chemical shifts for nuclei of the host and the guest, respectively, $x_{\mathrm{H}}\delta_{\mathrm{H}}$ and $x_{\mathrm{G}}\delta_{\mathrm{G}}$ are the molar fraction-weighted chemical shift of the host and guest, and $x_{\mathrm{HG}}\delta_{\mathrm{HG}}$(H) and $x_{\mathrm{HG}}\delta_{\mathrm{HG}}$(H) are those of the complexed form.

In contrast, distinct frequencies appear in the NMR spectrum when the exchange rate is lower than the chemical shift difference between the two forms. The slow exchange rate indicates formation of a high affinity complex, and it is not commonly observed in the case of CD complexes, as the majority of these assemblies fall in the stability range of K_{a} = 10 – 10^5 M^{-1}.

When the equilibrium is in the slow exchange regime, exchange spectroscopy (EXSY) can be used to determine the quantitative exchange rate (k) of the process. While EXSY shares similarities with NOESY and ROESY experiments, it specifically differs in its application to study equilibrium exchange processes (74).

Due to chemical exchange, both in NOESY and ROESY spectra, off-diagonal cross-peaks can be observed between the frequencies of the exchanging forms. In NOESY

spectra, the exchange peaks have the same sign as the diagonal and the cross-peaks, thus it is not always straightforward to identify the exchanging sites. In contrast, in ROESY spectra the exchange cross-peaks appear with opposite signs to the diagonal or peaks making it straightforward to recognize (Figure 7).

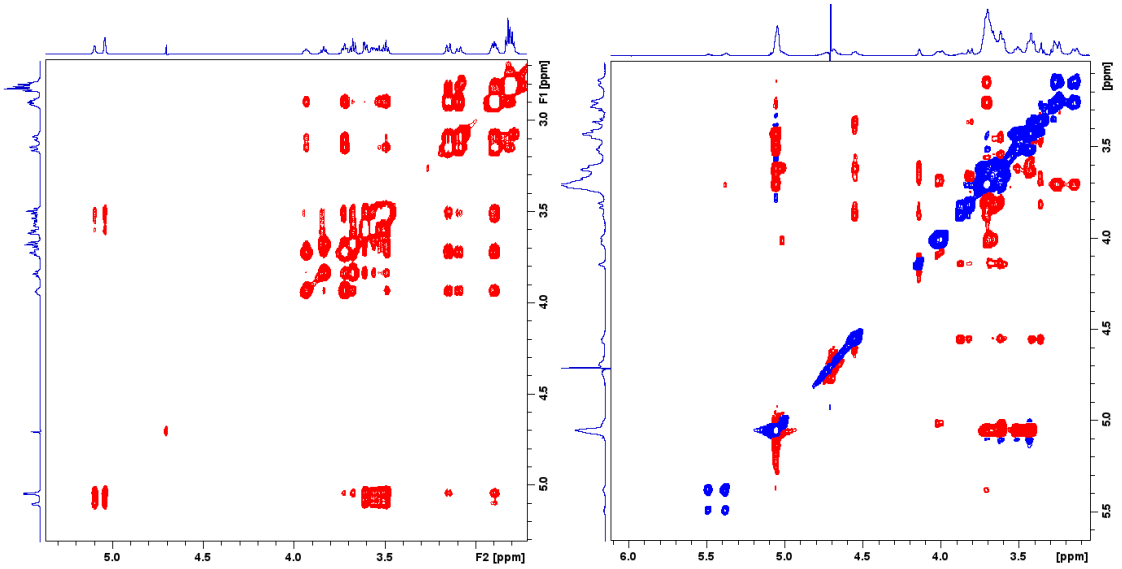

Figure 7. NOESY (left) and ROESY (right) spectra of sugammadex/solasodine complex (75).

The exchange rate can be calculated from the volume integrals of the diagonal and off-diagonal cross-peaks, according to the following formulas (76):

$$ln\left(\frac{r+1}{r-1}\right) = k_{ex}t_{mix} \quad (5) \qquad \text{and} \qquad r = \frac{I_{Ha,Ha}+I_{Hb,Hb}}{I_{Ha,Hb}+I_{Hb,Ha}} \quad (6),$$

where $I_{Ha,Ha}$ and $I_{Hb,Hb}$ are the volume integral of the diagonal cross-peaks, and $I_{Ha,Hb}$ and $I_{Hb,Ha}$ are those of the off-diagonal cross-peaks and t_{mix} is the mixing time in the experiment. According to equations 5 and 6, recording one spectrum is sufficient to determine the exchange rate, however, by recording a series of spectra with various t_{mix} values, the accuracy can be improved (74). Plotting the obtained k_{ex} values against t_{mix} provides a linear relationship with the slope corresponding to the exchange rate of equilibrium.

Using the linear form of the Eyring-equation (Eq. 7), the temperature dependence of the reaction rates can be described.

$$ln\frac{k}{T} = \frac{-\Delta H^{\ddagger}}{RT} + ln\frac{k_B}{h} + \frac{\Delta S^{\ddagger}}{R} \quad (7),$$

where k is the reaction rate constant, $\Delta H^{\ddagger}$ and $\Delta S^{\ddagger}$ are the enthalpy and entropy of activation, respectively, k_B is the Boltzmann constant, and R is the gas constant. In the Eyring plot, the slope corresponds to $-\Delta H^{\ddagger}/R$, and the y-intercept equals to $ln\frac{k_B}{h} + \frac{\Delta S\ddagger}{R}$. The Gibbs energy of activation is given by Eq. 8

$$\Delta G^{\ddagger} = \Delta H^{\ddagger} - \mathrm{T}\Delta S^{\ddagger} \qquad (8).$$

1.1.5.3.3. Determination of complex stoichiometry

Job's method of continuous variation (or Job's plot) is generally used to determine the stoichiometry of a binding event of two species. In this method, the total molar concentration of the two binding partners is kept constant, while their mole fractions are systematically varied. An observable parameter, which correlates with complex formation, is then plotted as a function of the mole fractions of the two components. The mole fraction at the maximum or minimum on the plot indicates the stoichiometry of the two species, provided that the response is directly proportional to the concentration of the species (Figure 8). In NMR spectroscopy, the registered variable is the observed chemical shift of the guest nuclei (most commonly ^{1}H), as it is proportional to the extent of binding in the fast exchange regime (Eq. 3 and 4). The Job plot is obtained by plotting the chemical shift change ($\Delta\delta$) weighted with the mole fraction of the guest as a function of the molar fraction. In slow exchange equilibria, the integrals of the discrete free and bound forms can be used in a similar manner to calculate the complex stoichiometry (73).

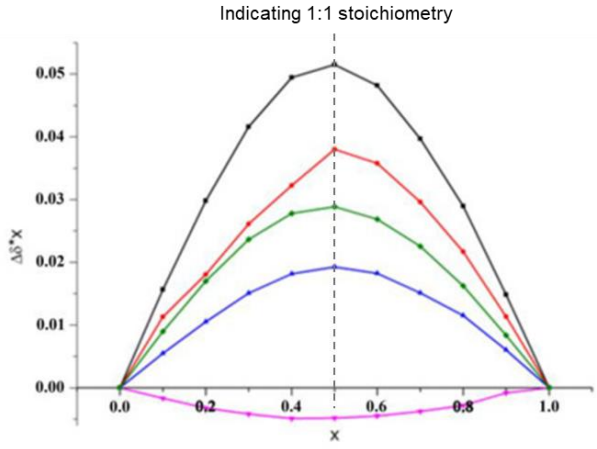

Figure 8. Job's plot of 3,4-methylenedioxypyrovalerone SBE-β-CD complex (63).

1.1.5.3.4. Determination of the association constant

To determine the stability constant for supramolecular systems, there are a wide variety of NMR-based techniques available (73). Among these, the simplest and most widely applied method is NMR chemical shift titration (generally referred as spectral shift method), where the chemical shift is recorded as a function of the binding partner's concentration. Generally, the concentration of the guest is kept constant while that of the host is varied.

Considering equimolar complex formation (Eq. 1), the stability constant K_a is expressed by the concentrations of the free and bound species (Eq. 2). As Eq. 3 shows, δ_{obs} is dependent on the extent of complexation, which is determined by the stability constant. K_a is determined either with graphical methods (such as the Benesi-Hildebrand method) or curve fitting methods (73). In both cases, known complex stoichiometry is necessary to choose the right fitting model. For equimolar complexes the binding affinity can be determined by fitting the data to the following function:

$$\Delta\delta/\Delta\delta\text{max} = [\text{H}]/(K_d + [\text{H}]) \qquad (9).$$

Evidently, for slow exchange systems this approach does not apply, as the chemical shift is not dependent on the extent of complexation, but distinct resonances of the free and bound form are observed, usually when $K_a > 10^5$ M^{-1}. The range suitable for NMR titration can be extended by applying competition methods, where two hosts are competing for the same guest (or vice versa). The method requires the known stability constants for one complex from an independent measurement, as the experiment provides the ratio of the two binding affinities as a result by the following correlations (73):

$$\delta_{\text{obs}} = x_{\text{H1G}}\delta_{\text{H1G}} + x_{\text{H2G}}\delta_{\text{H2G}} \qquad (10),$$

$$\text{x}_{\text{H2G}} = (\delta_{\text{obs}} - \delta_{\text{H1G}}) \,/\, (\delta_{\text{H2G}} - \delta_{\text{H1G}}) \qquad (11),$$

$$\text{and } K_{rel} = \frac{K_2}{K_1} = [\text{H2G}][\text{H1}] \,/\, [\text{H2}][\text{H1G}] \qquad (12),$$

where δ_{H1G} and δ_{H2G} are the limiting chemical shifts of the distinct complexes, from which the weaker is known from the independent titration.

1.1.5.3.5. Exploring the structure of the complex

As NMR spectroscopy provides the advantage of atomic level insights, comprehensive structural information for host-guest complexes can be obtained through 1- and 2D experiments.

Comparing the ^{1}H NMR spectra of the host, guest, and their mixture typically reveals complexation-induced shifts (CIS) in proton frequencies upon host-guest encapsulation (77). Particularly, the cavity protons of the CD (H3 and H5) usually become less shielded and shift to higher chemical shift, while opposite CIS is observed for the anomeric protons. The CIS of H2 and H4 protons indicate spatial rearrangement of the CD ring.

On the other hand, the CIS of the guest protons provides information about the included moieties: the protons entering the cavity tend to suffer the highest CIS. In this manner, the orientation of the guest inside the cavity can be assessed.

However, the 1D ^{1}H spectrum provides information about the complex in a fast and simple way, 2D ^{1}H-^{1}H through space correlation spectra (NOESY and ROESY) offer more detailed and more accurate structural information of the complex.

In case of CD complexes, if the guest enters the cavity, NOE cross-peaks are observed between the protons of the guest and H3 and H5 of the CD, facing the hollow of the cone (Figure 9) (21,78). In comparison, if the interaction occurs on the surface of the CD, proximity of the guest to H2 and H4 of the CD are observed. To decipher the orientation, analyses of the relative intensities of the correlations between the guest protons and H3, H5 and H6 of the CD usually provide sufficient evidence (79).

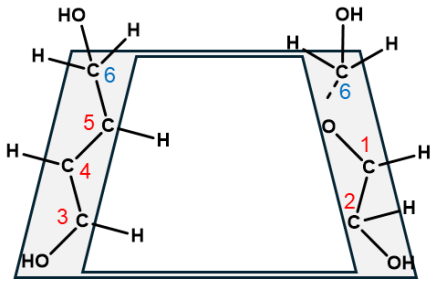

Figure 9. Schematic representation of the CD cone, emphasizing the orientation of the GP protons in respect to the cavity.

1.1.5.4. Isothermal Titration Calorimetry

Besides NMR spectroscopy, ITC provides the most comprehensive data of molecular interactions in solution, including micelle formation, self-assembling systems, binding of small molecules to macromolecules (such as substrate-ligand interactions of proteins), or formation of host-guest type complexes (80–82). Although ITC is not suitable to explore the structure of the assembly, it offers complete thermodynamic characterization of the binding event.

The technique is based on the measurement of the generated or absorbed heat upon interaction between molecules. The instrument is composed of two cells, the reference cell, containing solvent and the sample cell (Figure 10A) The temperature of both cells is regulated, while the instrument is recording the heat power necessary to maintain equal temperature of the sample cell relative to the reference cell.

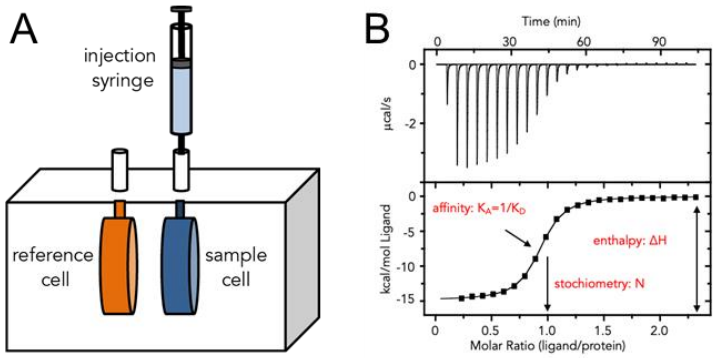

Figure 10. Schematic figure of the isothermal titration calorimeter (A) and the obtained thermogram and derived parameters from data fitting (B) (83).

The sample cell contains the solution of one of the binding partners and is titrated by small volumes of the solution of the interacting molecule from a syringe. Through the heat power changes, the generated or absorbed heat upon the molecular interaction is recorded.

The data obtained from the titration experiment includes enthalpy (ΔH), entropy (ΔS), stoichiometry (n) and binding affinity (K_a) (Figure 10B). Energetically favorable binding processes have negative Gibbs free energy (ΔG) values, expressed as

$$\Delta G = RT\ln K_a \qquad (13),$$

where R is the gas constant, and is determined by the contribution of enthalpy and entropy components as follows:

$$\Delta G = \Delta H - T\Delta S \qquad (14).$$

From the thermogram, ΔH is measured directly.

1.2. Aminosteroid phytotoxins

Toxic steroid-type alkaloids occur in large quantities in nature (84). The nightshade family (*Solanaceae*), which includes many species important for human consumption, also contains plants that accumulate large amounts of toxic glycoalkaloids with diverse structures during ripening (85). This includes *Solanum tuberosum*, the plant responsible for producing potatoes. Improper storage of potatoes can cause them to turn green and begin germinating, leading to the production of toxic substances in the buds and skin, primarily α-solanine and α-chaconine, glycoalkaloids with related structures (86). Thus, the consumption of immature or sprouted potatoes leads to poisoning, which manifests mainly in gastrointestinal and nervous system symptoms, such as vomiting, diarrhea, cardiac arrhythmia, or convulsions, in extreme cases even with fatal outcomes.

Poisoning may occur by confusion of toxic species with edible plants. *Solanum dulcamara*, *Solanum nigrum* and *Veratrum viride* are species also containing toxic glycoalkaloids (α-solanine, solasonine, solamargine, veratridine) whose berries can easily be mistaken for forest fruits, especially by children, posing potential poisoning risk (86–88).

Despite the diverse range of *Solanaceae* phytotoxins, most share chemical structures with aminosteroid backbones. Currently, there is no available antidote to eliminate these toxins from the body in case of intoxication, with treatment limited to supportive therapy aimed at symptom relief, spasm alleviation, and hydration management.

2. OBJECTIVES

The objective of my work was to advance our understanding of the structure and interactions of two pharmaceutically approved cyclodextrin derivatives, HPβCD and sugammadex, with the goal of extending their broader applicability as active pharmaceutical ingredients (APIs).

In one hand, we aimed to develop a fast, reliable and robust analytical method for the structural characterization of HPBCD, that provides more comprehensive information about its substitution pattern. Our goal was to develop an NMR spectroscopy-based method to characterize the PS of HPBCD using commonly available instrumentation and pulse sequences. Our first goal was to carry out a comprehensive signal assignment of the ^{1}H and ^{13}C spectra of HPBCD using standard 2D experiments, including COSY, HSQC and HMBC, and consecutively identify the unique signals corresponding to the substituents at the various substitution sites. Thereafter, we sought to develop a method to quantitatively determine the extent of substitution on each position to define an average structure for a given batch of this complex mixture of isomers. Ultimately, we aimed to compare the PS of various HPBCD batches synthetized under various conditions, to confirm the feasibility of the method. The approach we aimed to develop could serve as a tool for regulatory purposes to control the uniformity and the quality of HPBCD from various resources.

On the other hand, our goal was to explore the potential of SGM in capturing natural aminosteroid phytotoxins, which have analogous structures to the clinically used muscle relaxants, with the aim of evaluating its potential as an antidote in intoxication cases. We focused on investigating the complexation of SGM with various natural toxins, including solasodine (SS), a steroid containing a secondary amine moiety, solanidine (SN) an aminosteroid with tertiary amine group, and α-solanine (ASN), the glycoside of SN containing a trisaccharide chain (Figure 11).

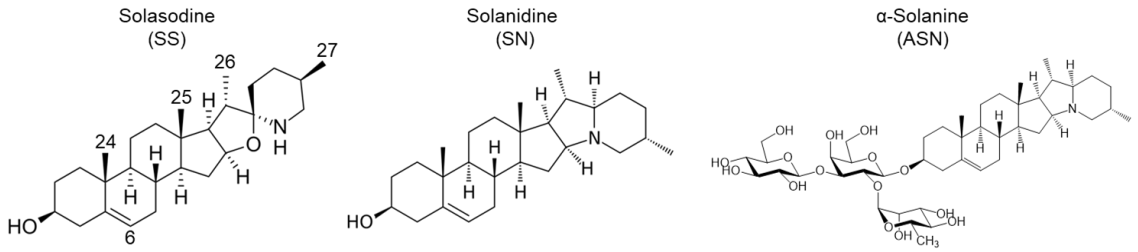

Figure 11. Chemical structures of solasodine (SS), solanidine (SN), and α-solanine (ASN), natural aminosteroids used as model compounds for *Solanaceae* phytotoxins in our study with partial numbering of protons

Our objective was to investigate the complexation behavior of these compounds with SGM using NMR spectroscopy, ITC, and other complementary techniques. We aimed to determine the stability of the resulting complexes by evaluating the stability constants, as well as their temperature and pH dependence. Additionally, we sought to explore how different amino groups and glycosylation affect complex stability. Finally, we planned to assess SGM's ability to mitigate the toxicity of the selected compounds through cytotoxicity assays.

3. METHODS

3.1. Materials

3.1.1. Materials used for syntheses of HPBCDs and their characterization

(±)-Propylene oxide ReagentPlus®, ≥99%, sodium hydroxide reagent grade, 97% (powder), Activated Charcoal Norit®, Norit® GAC 1240W were purchased from Sigma-Aldrich. (R)-propylene oxide, ≥98%, and (S)-propylene oxide, ≥98%, were purchased from TCI. Hydrochloric acid (3 N), 1-propanol (analytical reagent grade, a.r.), ammonia aqueous solution 25% (a.r.), ethyl acetate (a.r.), methanol (a.r.), 2-butanone (a.r.) were products of Molar Chemical Kft. β-Cyclodextrin (CAVAMAX® W7), commercial HPBCD DS 4.5 (CAVASOL® W7 HP), and methyl-β-cyclodextrin (CAVASOL® W7 M) were products of Wacker (Wacker Chemie, Munich, Germany), while HPBCD DS 6.3 (KLEPTOSE®) was purchased from Roquette (Roquette Frères, Lestrem, France). Strong acid cation exchange resin (Purolite® Resin C 100 E) was from Purolite®. Heptakis-2-*O*-methyl-β-CD (2-Me-β-CD), heptakis-3-*O*-methyl-β-CD (3-Me-β-CD) and heptakis-6-*O*-methyl-β-CD (6-Me-β-CD) were the fine chemicals of Carbohyde Zrt (Budapest, Hungary). Membrane filter for vacuum filtration set, hydrophilic, mixed cellulose esters, 0.45 μm was a product of Sartorius.

3.1.2. Materials used to study complexation of the aminosteroids with SGM.

Dimethyl sulfoxide (DMSO), and methanol (a.r.) were products of Molar Chemical Kft. (Halásztelek, Hungary), 3-mercaptopropionic acid and sodium methoxide were purchased from Merck (Merck KGaA, Darmstadt, Germany) while Per-6-iodo-GCD, was the product of CarboHyde Zrt. (Budapest, Hungary).

SS, SN, and ASN were purchased from PhytoLab (PhytoLab GmbH & Co. KG, Vestenbergsgreuth, Germany), while deuterium oxide (D_2O), dimethyl sulfoxide-d_6 (DMSO-d_6), and methanol-d_4 (CD_3OD) were obtained from Merck (Merck KGaA, Darmstadt, Germany). γ-cyclodextrin (GCD) and sulfobutylether-γ-cyclodextrin (SB-GCD) were products of CarboHyde Zrt. (Budapest, Hungary).

3.2. Synthesis of cyclodextrin derivatives

3.2.1. Synthesis of HPBCD

The 2-hydroxypropylated β-CDs with various DS were synthesized under aqueous alkaline conditions by employing varying amounts of sodium hydroxide and increasing quantities of propylene oxide (32). Specifically, two distinct setups were executed, utilizing different base ratios (4 and 6 equivalents), and six different concentrations were investigated for the alkylating agent (1, 2, 3, 8, 10, 12 equivalents; the 8, 10 and 12 equivalents added in two equal portion). In total, 12 reactions were conducted. The progress of the reactions was monitored by TLC (1-propanol:ethyl acetate:H_2O:25% NH_3=6:1:3:1. The synthetic procedure was as follows:

β-CD (1.13 g, 1 mmol) was suspended in deionized water (3 ml) and vigorously stirred for 5 minutes. Sodium hydroxide (4 eq, 0.16 g; 6 eq, 0.24 g) was added to the mixture, resulting in complete solubilization with heat evolution. The solution was then cooled to 10 °C using an ice bath, and propylene oxide was added in one portion (Reaction 1: 1 eq, 70 µl; Reaction 2: 2 eq, 0.14 ml; Reaction 3: 3 eq, 0.21 ml; Reaction 4: 4 eq, 0.28 ml; Reaction 5: 5 eq, 0.35 ml; Reaction 6: 6 eq, 0.42 ml). The flask was flushed with an inert atmosphere, sealed, and stirred overnight. Reactions 1, 2 and 3 were worked-up after 1 day of stirring. For Reactions 4, 5 and 6, the mixtures were cooled to 10 °C using an ice bath, a second portion of propylene oxide was added (Reaction 4: 4 eq, 0.28 ml; Reaction 5: 5 eq, 0.35 ml; Reaction 6: 6 eq, 0.42 ml, respectively), and the flasks were then flushed with inert atmosphere, sealed, and stirred overnight.

During the work-up, the reaction mixture was extensively treated with cation exchange resin, adjusting the pH to neutral. The resin was removed by filtration using a sintered glass filter (porosity 2), extensively washed with water (3 x 15 ml), and the mother liquor was evaporated at 40 °C to dryness under reduced pressure using a rotavapor. The viscous residue, with viscosity proportionally increasing with the amount of propylene oxide, was suspended in 2-butanone (30 ml). The precipitate material was filtered using a sintered glass filter (porosity 3), extensively washed with 2-butanone (3 x 20 ml) and acetone (3 x 10 ml). The solid was dried overnight in a drying box under vacuum, with KOH and P_2O_5 as drying agents.

The material was solubilized in water (50 ml) and concentrated at 40 °C to half volume under reduced pressure using a rotavapor to remove residual volatiles. Activated charcoal

was added to the aqueous solution, and the black suspension was vigorously stirred for 10 minutes. It was then filtered using a sintered glass filter (porosity 4), membrane filtered, and the mother liquor was finally concentrated to dryness under reduced pressure using a rotavapor. The recovered amounts of materials, a white amorphous powder, varied between 0.62 and 1.35 g.

Table 3. Reaction conditions and yields of the reactions, as well as the DS of the obtained materials.

Reaction	BCD	H_2O	NaOH	Propylene Oxide	Yield (g)	DS
1	1.13 g (1 mmol)	3 ml	0.16 g (4 eq)	70 µl (1 eq)	1.12 g	0.5
2	1.13 g (1 mmol)	3 ml	0.16 g (4 eq)	0.14 ml (2 eq)	1.23 g	1.21
3	1.13 g (1 mmol)	3 ml	0.16 g (4 eq)	0.21 ml (3 eq)	1.06 g	2.53
4	1.13 g (1 mmol)	3 ml	0.16 g (4 eq)	(0.28+0.28) ml (8 eq)	0.83 g	3.39
5	1.13 g (1 mmol)	3 ml	0.16 g (4 eq)	(0.35+0.35) ml (10 eq)	0.67 g	7.05
6	1.13 g (1 mmol)	3 ml	0.16 g (4 eq)	(0.42+0.42) ml (12 eq)	0.76 g	9.18
7	1.13 g (1 mmol)	3 ml	0.24 g (6 eq)	70 µL (1 eq)	1.27 g	0.71
8	1.13 g (1 mmol)	3 ml	0.24 g (6 eq)	0.14 ml (2 eq)	1.16 g	1.43
9	1.13 g (1 mmol)	3 ml	0.24 g (6 eq)	0.21 ml (3 eq)	1.35 g	1.53
10	1.13 g (1 mmol)	3 ml	0.24 g (6 eq)	(0.28+0.28) ml (8 eq)	0.83 g	7.1
11	1.13 g (1 mmol)	3 ml	0.24 g (6 eq)	(0.35+0.35) ml (10 eq)	0.75 g	9.8
12	1.13 g (1 mmol)	3 ml	0.24 g (6 eq)	(0.42+0.42) ml (12 eq)	0.62 g	10.7

3.2.2. Synthesis of SGM

Per-6-iodo-GCD (21.76 g (0.01 mol) was pre-solubilized in dimethyl sulfoxide (DMSO, 50 ml) in a Schott Duran bottle of adequate volume. DMSO (100 ml) was added to the reaction vessel under an inert atmosphere and 3-mercaptopropionic acid (16 ml, 19.1 g, 0.18 mol) was then poured sequentially. The reaction mixture was cooled down in a water bath (T < 15 °C) and sodium methoxide-methanol solution (25% w/w, 32 ml , 0.36 mol) was slowly added (79). The reaction mixture turned from a colorless solution to an intense pinkish solution with heat evolution. The DMSO-CD solution was added in one portion to the reaction mixture causing almost immediate formation of a massive white precipitate. The suspension was stirred at room temperature for 1 h. The reaction mixture was filtered and the solid was extensively washed with methanol (3 x 100 ml) until a white solid was obtained. The solid was placed into a drying box and dried until constant weight (17.64g, 81% yield).

3.3. Sample preparation

3.3.1. Preparation of HPBCD NMR samples

The samples were prepared by dissolving 20 mg of the material in 600 µl D_2O resulting in clear solutions of 21-25 mM. The solutions were then transferred to standard 5 mm NMR tubes. For quantitative ^{13}C NMR, 75 mg HPBCD was dissolved in 600 µl D_2O.

3.3.2. Sample preparation for the SGM-phytotoxin interaction studies

Samples of individual compounds were prepared by dissolving the solid in the given solvent (D_2O for SGM and CD_3OD for SS, SN and ASN), sonicated for 1 minute and transferred to a standard 5 mm NMR tube. If the compound's solubility in the selected solvent was limited, the mixture was sonicated and then centrifuged at 13.4k rpm for 5 minutes. The supernatant was subsequently transferred to a standard 5 mm NMR tube.

For the SS-SGM interaction study SS was dissolved by adding small amount of HCl to become fully protonated, and a 10.6 mM SS stock solution was prepared in a solvent mixture of 10% DMSO-d_6 and 90% D_2O. The pD of the stock solution was 8.21. The initial concentration of the SGM samples was 3.2 mM. The titration was performed by stepwise addition of SS stock solution, until the ratio of SGM:SS was 2:1. To study the effect of DMSO on complex formation, samples with the same total concentrations of SGM and SS were prepared using 100% D_2O or a mixture of 25% DMSO-d_6 and 75% D_2O as solvent.

SGM/SN and SGM/ASN complexes were prepared by grinding an excess amount of the phytotoxin (~1.2 mM) with SGM (~2 mg, 0.9 mmol) for 5 min using mortar and pestle. The mixture was then transferred to an Eppendorf tube and dissolved in 700 µL D_2O by sonication for 1 minute. The solution was centrifuged at 13.4k rpm for 5 min and the supernatant was transferred to a standard 5 mm NMR tube. For the pH-dependent experiments, DCl or NaOD solutions were used to adjust the pH, which was checked with the Hydrion MicroFine pH test paper set (Sigma-Aldrich).

3.4. NMR experiments

3.4.1. Characterization of HPBCD

The NMR experiments were carried out either on a Varian Mercury Plus (^1H: 400 MHz, ^{13}C: 100 MHz), a Bruker Avance III (^1H: 500 MHz, ^{13}C: 125 MHz) or a BRUKER Avance

III (^{1}H: 600 MHz, ^{13}C: 151 MHz) instrument. Each pulse program was taken from the available software library (VnmrJ or TopSpin, respectively). ^{1}H experiments were recorded using 90° pulse angle and 10s relaxation delay. Quantitative ^{13}C-NMR was recorded using inverse gated ^{1}H-decoupling (BRUKER pulse program zgig). The mixing time used for TOCSY was set to 100 ms. In heteronuclear correlation experiments $^{1}J_{CH}$ = 145 Hz (for HSQC) and $^{2,3}J_{CH}$ = 8 Hz (for HMBC) were used. For quantitative ^{13}C spectrum 2048 scans were accumulated with 4.8 s acquisition time and 4 s relaxation delay. The spectra were recorded in standard 5 mm NMR tubes at 25 °C. The residual solvent signal was used as a chemical shift scale reference. The spectra were processed using MestReNova v9.0.1-13254 (Mestralab Research, S.L., Santiago de Compostela, Spain) or TopSpin 3.6.5 (Bruker Biospin GmbH, Rheinstetten, Germany) software. For each homo- and heteronuclear 2D spectra 2048 x 256 datapoints were collected using 16 or 32 scans per increment.

3.4.2. SGM-phytotoxin interaction studies

NMR experiments were recorded on a 600 MHz Varian DDR NMR spectrometer equipped with a 5 mm inverse-detection gradient probe for structural assignment of SS and on a Bruker Avance III 700 MHz instrument operating at 700.05 MHz using a Prodigy TCI H&F-C/N-D, z-gradient probe-head to study the SGM/SS complex. All samples were prepared in 5 mm standard NMR tubes. The measurements for resonance assignment were carried out at 298 K, and the temperature dependence of the SGM/SS complex formation was studied in the range 278–323 K. Temperature was calibrated against the methanol standard sample [3].

Resonance assignment was achieved using conventional 2D COSY, TOCSY (mixing time: 120 ms), ROESY (mixing time: 300 ms), ^{1}H-^{13}C HSQC, ^{1}H-^{13}C HMBC experiments. Chemical exchange was studied using 2D EXSY experiments with the Bruker standard *noesygpph19* pulse program, using the experimental setup of NS=8; 2048 × 512 complex points, and mixing time values were varied between 10μs and 500 ms. EXSY experiments with 100 ms mixing time were acquired in the 278 - 313K temperature range.

The ^{1}H NMR-titration was performed in reverse arrangement: Stock solution of SS was added to the solution of SGM, and changes in chemical shift of SGM protons were monitored.

To study SGM/SN and SGM/ASN complexes, experiments were carried out on a Bruker Avance 500 MHz instrument at 298 K and 313 K using an inverse BBI probe. 2D spectra were registered on a Bruker Avance III 500 MHz spectrometer equipped with a cryo probe-head. All the experiments were implemented using the pulse sequences from the Bruker library. Presaturation of the residual water peak in D_2O was applied using the *zgpr* pulse sequence. The mixing times used were 80 ms for 2D TOCSY and 300 ms for 2D ROESY spectra. In heteronuclear correlation experiments ^{1}J(CH) = 145 Hz or 130 Hz and $^{2,3}J$(CH) = 6 Hz were used.

3.5. X-Ray crystallography

Crystallization trials were set up using the vapor diffusion technique in 1.5 µl hanging drops. In brief, droplets containing a solution of SGM/SN complex prepared by grinding an equimolecular mixture of the solid components in an agate mortar and a low concentration of a precipitating agent were equilibrated against reservoirs containing solutions at higher concentrations of the same precipitating agent, leading to slow evaporation of water from the droplet until the precipitating agent concentrations of droplet and reservoir become approximately equal.

Crystals were obtained when drops containing 20-30 mM complex and 0.75-4.7 % (w/v) polyethylene glycol of mean MW 1500 (PEG 1500), were equilibrated against reservoirs with double the concentration of PEG 1500. The best crystals, from which useful data were collected, were obtained from a 20 mM complex and 0.75% PEG 1500 in the droplet (1.5% PEG 1500 in the reservoir). Crystallization conditions of such low concentration of PEG are very unusual. All the crystals were thin plates, which in the vast majority of cases grew in stacks that were impossible to separate into single crystals. The very few crystals that appeared single and somewhat thicker under the stereoscope were selected for harvesting.

The crystals were manually harvested from the drops and were immersed very quickly into a heavy vacuum oil for cryoprotection. The dataset used for structure determination was collected at cryogenic temperature (100 K) at beamline P13 of the PETRA III storage ring at the DESY/EMBL-Hamburg synchrotron source, set at wavelength 0.976 Å, from a crystal of approximate dimensions 80x60x15 µm. The space group was determined to be P4212, with cell dimensions a = b = 24.255 Å and c = 23.020 Å. The dataset extended to 0.98 Å resolution, with a total of 38256 observed reflections, however data up to 1.04

Å were used in the refinement. Two additional and very similar complete datasets from similar-looking crystals were collected, but these were of somewhat inferior quality and resolution.

3.6. ITC studies

ITC experiments were performed on a MicroCal PEAQ-ITC instrument (Malvern Panalytical, Worcestershire, UK). Stock solutions were prepared as follows: SGM was solubilized in 20 mM phosphate buffer at pH 7.4 to obtain 0.5 or 1.0 mM solution. ASN was solubilized in 20 mM phosphate buffer at pH 7.4 or pH 4.0 to obtain 50 µM solution. SS and SN were solubilized by the addition of various concentration of GCD or SB-GCD (of 0.5 – 5.0 mM) to the 20 mM phosphate buffer at pH 7.4 containing the weighted materials. The mixtures were stirred overnight at 37 °C. All the stock solutions were filtered through a 0.22 µm polyvinylidene difluoride filter membrane prior to filling into the instrument cell. Titration with 0.5 mM SGM consisted of 18–36 injections of 2–1 µl SGM solution, respectively, to reach saturation and a final 2.5–3.5-fold molar excess. The spacing between injections was 300–500 seconds, and a reference heat of 2.5 µcal/sec was used. The results were evaluated using MicroCal PEAQ-ITC Analysis Software using a competitive binding model (89). The binding parameters for the competitor weak binder GCD were fixed at various values to find the value that provided the same binding parameters for SGM to SS at all GCD concentrations. This allowed us to determine the binding constants for both SGM and GCD to SS.

3.7. Cytotoxicity studies

The cytotoxicity of CDs (SGM, SB-GCD, GCD) and SS, SN and ASN was assessed using the mHippoE-14 mouse hippocampal embryonic cell line, obtained from American Type Culture Collection. Cells were cultured in Dulbecco's modified Eagle's medium with 4.5 g/l glucose and L-glutamine, with phenol red (DMEM, Lonza), containing 1% fetal bovine serum (FBS, Euroclone S.p.A.), and 1% penicillin/streptomycin/amphotericin B (PSA, Lonza). The cells were incubated in a 5% CO_2/95% air humidified atmosphere at 37 °C.

Cells were seeded into 96-well plates at a density of 10^4 cells/well in 100 µl medium per well. After 24 hours of incubation, 10 µl of treating solution was added to each well. The treating solutions consisted of PBS with added DMSO and either CD (SGM, SB-GCD,

or GCD), or aminosteroid toxin (SS, SN, or ASN), or a combination of the two. Concentrations were set so that after adding 10 µl treating solution to 100 µl medium, the final concentrations in the wells were 1% DMSO; 0, 0.2, or 0.5 mM CD; and 0, 10 or 20 µM SS, and 0, 5 or 10 µM SN and ASN. After 72 hours of incubation, the medium was removed, the wells were washed with PBS, and 50 µl of fresh medium containing 0.5 mg/ml 3-(4,5-dimethylthiazol-2-yl)-2,5-diphenyltetrazolium bromide (MTT) was added to each well. After 3 hours of incubation, the medium was removed, wells were washed with PBS, and 50 µl DMSO was added. Absorbance at 570 nm was measured using a Synergy H4 plate reader (BioTek Instruments, Inc.). The absorbance values of wells containing cells were corrected by that of cell-free wells. The corrected values were then normalized against the absorbance of control samples treated with 1% DMSO. The cell viability was calculated by normalizing the survival rate, using the control cells treated with 1 % DMSO as 100% viability, thereby the relative survival rate of the cells after different treatments of SGM, AS, SN and their mixtures can be determined.

4. RESULTS

4.1. Characterization of the pattern of substitution of HPBCD

During the synthesis of HPBCD, all types of OH groups are alkylated to varying degrees depending on the reaction conditions. Assuming that only monosubstitution occurs at each GP unit, the resulting derivatized CD molecule contains four possible types of GP monomers: unsubstituted GP (GP_{unsub}), and those derivatized at the OH-2, OH-3, or OH-6 (GP_{2sub}, GP_{3sub}, or GP_{6sub}, respectively, as shown in Figure 12).

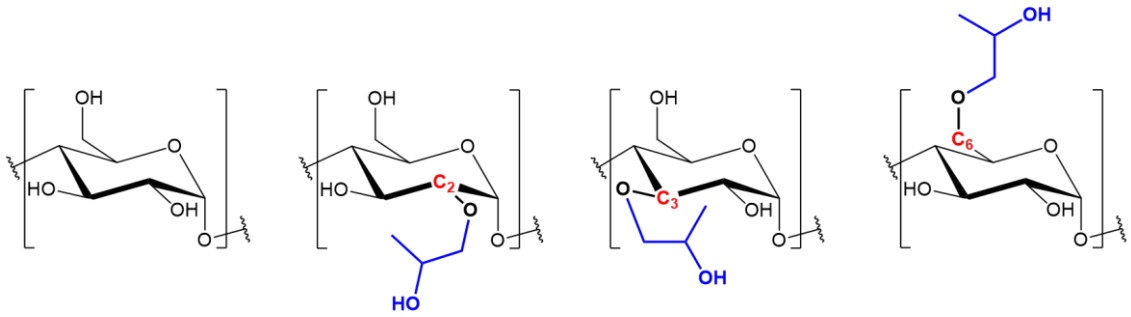

Figure 12. Possible structures of glucopyranose (GP) units present in HPBCD, assuming maximum one substituent per GP.

To resolve the substitution pattern, first the HP substituents at various positions must be differentiated in the spectrum.

To assign them, we used the following nomenclature, shown in Figure 13; numbers indicate the atoms of the GP unit, those without subscript indicate the unsubstituted type, while the subscripts indicate the position of substitution on the given GP.

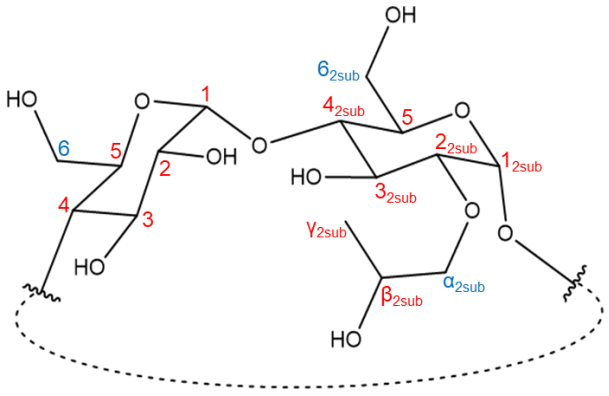

Figure 13. Nomenclature used for the NMR assignment of HPBCD. The single numbers refer to unsubstituted-type GP, while those bearing a subscript refer to substituted-type GP units, where the subscript indicates the position of the substitution of the same GP unit. The color coding resembles the appearance of the resonances in the multiplicity-edited HSQC spectrum (90).

4.1.1. Assignment of the ^{1}H NMR signals

Figure 14 shows the ^{1}H NMR spectra of HPBCD samples with various DS. The apparently broad signals are the consequence of the RS nature of HPBCD. Similarly to most carbohydrates, the signals can be assigned to three well-separated regions. The characteristic anomeric region is found above 5.0 ppm, the doublet of the terminal methyl of the HP sidechain (γ) is easily recognizable on the upfield end of the spectrum, while the methine and the methylene signals of the GP (H2-H6) as well as the Hα and Hβ of the HP sidechains are situated in a quite narrow range (~3.4-4.3 ppm).

From the ^{1}H NMR spectrum, the MS and DS can be calculated. The Pharmacopoeias recommend calculating the MS from the ^{1}H NMR spectrum by dividing the peak area of the methyl by three times the anomeric peak area. By multiplying the calculated MS by the number of GP units (7 in case of BCD-derivatives), the DS is obtained, describing the average extent of substitution for one CD molecule.

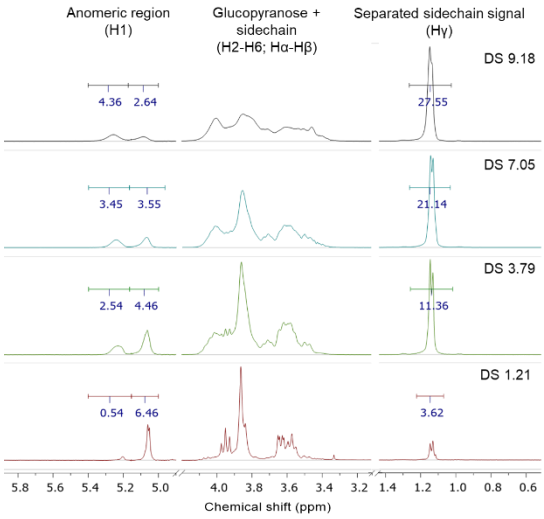

Figure 14. Series of ^{1}H NMR spectra of HPBCD samples with increasing average degree of substitution (DS) (90).

By comparing the spectra of HPBCD samples with different DS, two phenomena can be observed: with increasing DS, signal broadening increases rapidly (due to the microheterogeneous nature of the CD), leading to loss of resolution of distinct signals. Furthermore, as the DS increases, an additional anomeric signal arises. The resonances at higher chemical shift also exhibit increased integral values with greater degrees of substitution. However, the integral does not correlate linearly with the calculated DS. This suggests that although the emerging signal is associated with a substituted-type GP, it

does not represent the entire population of substituted GPs (GP_{sub}). Nevertheless, it provides a reasonable approximation for differentiating of the signals into GP_{sub} and GP_{unsub}.

To commence the assignment of the methine units of the GP_{sub} and GP_{unsub}, the anomeric protons serve as a good entry point due to the remarkable spectral separation. To execute the initial assignment, a sample with low DS was chosen, since, as Figure 14 shows, by increasing DS, the complexity of the spectrum increases. Starting from the anomers, by mapping the ^{1}H-^{1}H correlations using TOCSY- and COSY spectra, the various GP units can be differentiated, and the sequence of the CH(OH) backbone of the GP units can be determined, respectively.

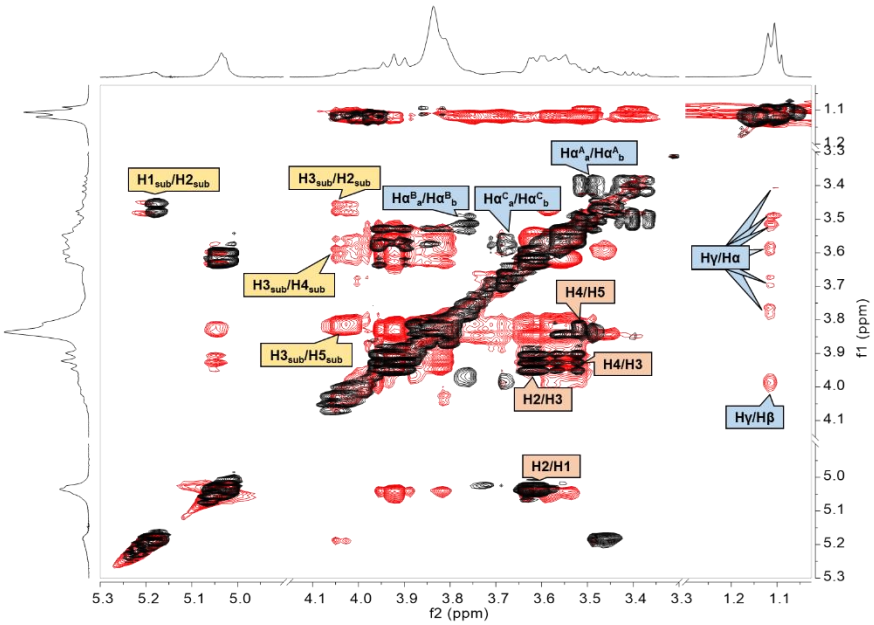

Figure 15. Superimposed COSY (black) and TOCSY (red) spectra of HPBCD DS 3.4 with partial assignment of the connectivities (400 MHz, D_2O, 298 K). Color coding is used to differentiate substituted-type GP (yellow), unsubstituted-type GP (orange) and the HP sidechains (blue) (90).

Similarly, the signals of the HP sidechains were identified by mapping the connectivities starting from the well separated Hγ signal at 1.1 ppm. First, in the TOCSY spectrum (Figure 15, red contours), the chemical shift of the sidechain α and β protons can be deduced. The single COSY correlation (Figure 15, black contours) of Hγ identifies one signal of Hβ, which further correlates with various types of α protons (Figure 15, blue rectangles). Three different Hα/Hβ correlations were identified, denoted by $H\alpha^{A}$, $H\alpha^{B}$, and $H\alpha^{C}$. All these protons exhibit an intensive COSY correlation, pointing to the geminal

proton of each, completing the assignment of the previously identified sidechain chemical shifts.

By defining the ^{1}H chemical shift of the units, the corresponding signals in the HSQC spectrum were identified (Figure 16). Based on the significant downfield shifting of the ^{13}C chemical shift of $C2_{sub}$ compared to C2, the substitution of GP_{sub} on OH-2 can be unambiguously determined(67) and denoted by GP_{2sub}.

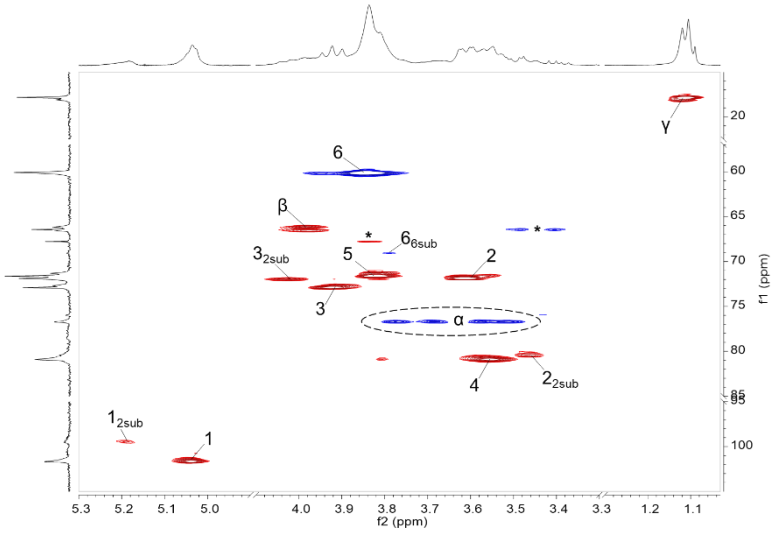

Figure 16. Multiplicity edited HSQC spectrum of HPBCD DS 3.4 presenting the assignment of the main resonances (400 MHz, D_2O, 298 K). The asterisk indicates the impurity detected in the sample, identified as propylene glycol (90).

Based on this assignment, the relative integrals of the two anomeric ^{1}H signals can be used to calculate the DS at C2. The signals corresponding to C6 and $C6_{6sub}$ of the GP backbone were definitively assigned by their sign (with the help of multiplicity editing in the ^{13}C dimension) and spectroscopic evidence. Specifically, $C6_{sub}$ experiences a downfield shift of 6-10 ppm compared to the unmodified C6 due to alkylation. This assignment was further confirmed through HMBC correlations (Figure 17).

For CD derivatives, the anomeric protons exhibit HMBC cross-peaks with C3 and C5 of the same GP unit as well as with C4 carbon of the neighboring GP unit in the clockwise direction. In this manner, also the partial separation of C5 and $C5_{sub}$ was recognized, as the latter one exhibits around 0.3 ppm upfield shift compared to the corresponding signal of the unsubstituted GP unit.

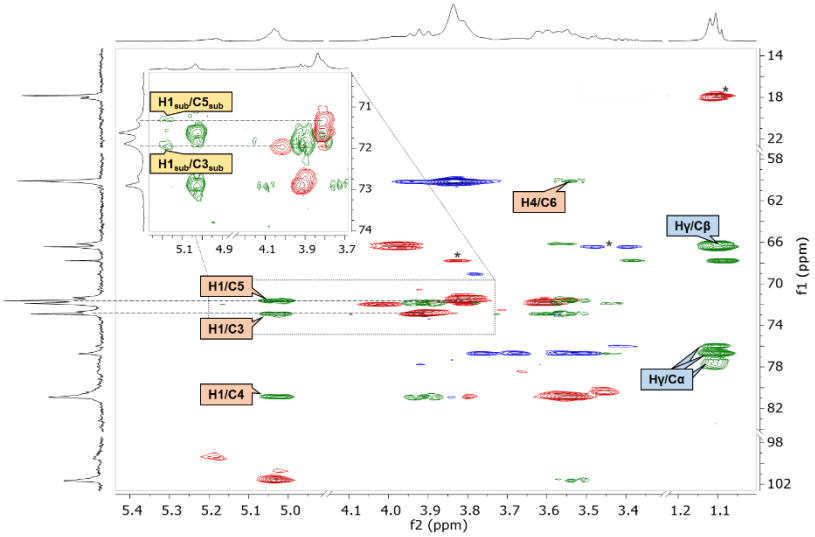

Figure 17. DEPT-HSQC (red and blue) and HMBC (green) spectra of HPBCD DS 3.4 with assignment of crucial HMBC correlations (400 MHz, D_2O, 298 K) (90).

4.1.2. Assignment of the substituent positions

After assigning the signals of GP_{unsub}, $GP_{2sub,}$ and three types of HP sidechains, the next step was to establish the connection points between the GP and HP spin systems to determine the location of the side chains. Using HMBC, the correlation between the carbon atom of the GP bearing the HP sidechain and the α-proton of the HP sidechain (or vice versa) were observed.

For this purpose, a sample with a higher average DS of 7.9 was selected and analyzed, as it displayed more intense HP signals in the HSQC spectrum (Figure 18). In the previously analyzed sample with a DS of 3.4, only three distinct α frequencies were identified (α^A, α^B, and α^C). In the case of higher DS, two less intense but clearly separated methylene signals were additionally detected at higher ^{13}C shifts (denoted by α^D and α^E, Figure 18). These latter resonances also exhibited characteristic HMBC correlations with Hγ, confirming their assignment as methylene signals of HP sidechains. The presence of five distinct pairs of α signals can be attributed to the chirality of the HP sidechain. Since the substituent contains a chiral center, there are six possible isomers: 2sub, 3sub and 6sub, each in (*R*) and (*S*) configurations. Due to the intrinsic chirality of the CD core, the pairs of (*R*) and (*S*) enantiomers become diastereomers, leading to distinct resonance frequencies. This interpretation is further supported by the consistent observation that the

signals of α^B and α^C appear with equal intensity at any given DS, indicating that they represent diastereomers.

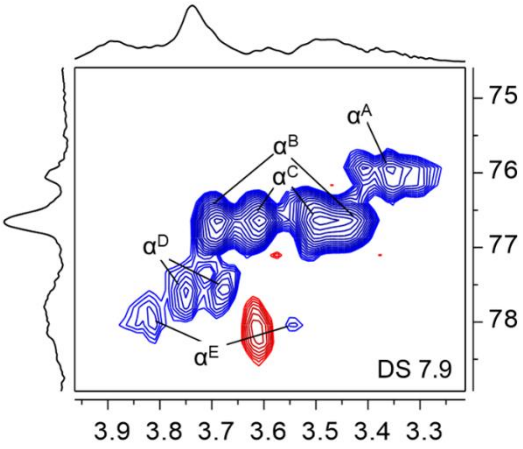

Figure 18. Hα region of the multiplicity-edited HSQC spectrum of HPBCD DS 7.9 exhibiting five separated pairs of methylene signals (400 MHz, D_2O, 298 K) (90).

Figure 19 shows the relevant region of the superimposed HMBC and HSQC spectra of HPBCD DS 7.9, comprising the signals corresponding to all potential direct connection points of the HP sidechain to the CD scaffold. Solid lines identify the signal (red and blue contours) of the correlating moieties in the HSQC spectrum, while dashed arrows confirm the correlations based on the probative HMBC cross-peak (in green contour). To facilitate the assignment, color-coding was used to distinguish the signals of the three types of HP sidechain.

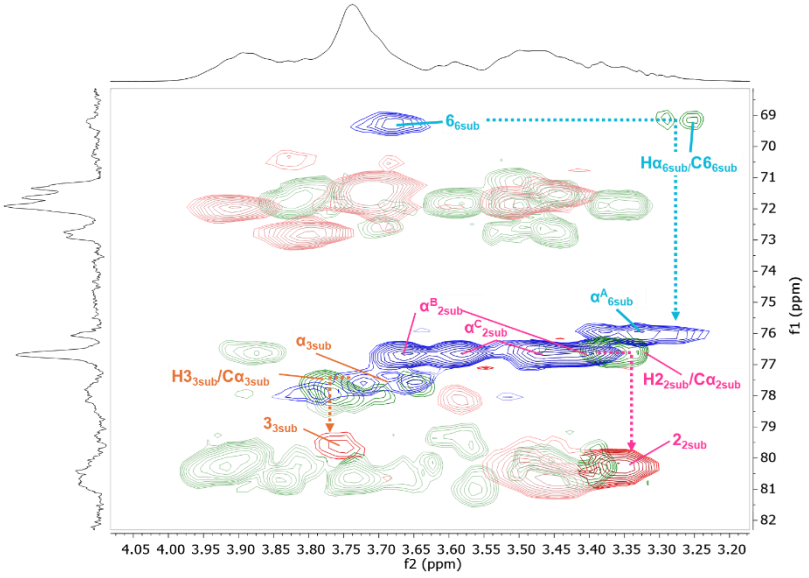

Figure 19. Superimposed HSQC (red and blue contours) and HMBC (green contours) spectra of HPBCD (DS 7.9), showing the three-bond correlations between Cα of HP and C2/C3/C6 of GP unequivocally confirming the position of substitution (400 MHz, D_2O, 298 K) (90).

Lacking any signal overlap in both axes, among all the α signals, the assignment of the HMBC correlation of α^A is the most straightforward and unambiguous. A clear correlation with $C6_{6sub}$ is readily identified (cyan in Figure 19), consequently, α^A is assigned as α_{6sub}. The apparent misalignment of the HMBC correlation with α^A is due to the splitting of the signal, similar to α^B and α^C. As it is shown in Figure 20, all pairs of α signals exhibit selective correlation. Only one proton of the split methylene signals of every diastereomer shows the three-bond HMBC correlations, specifically the one with a lower ^1H frequency. This phenomenon originates from the distinct coupling constants of the magnetically inequivalent protons on the same carbon.

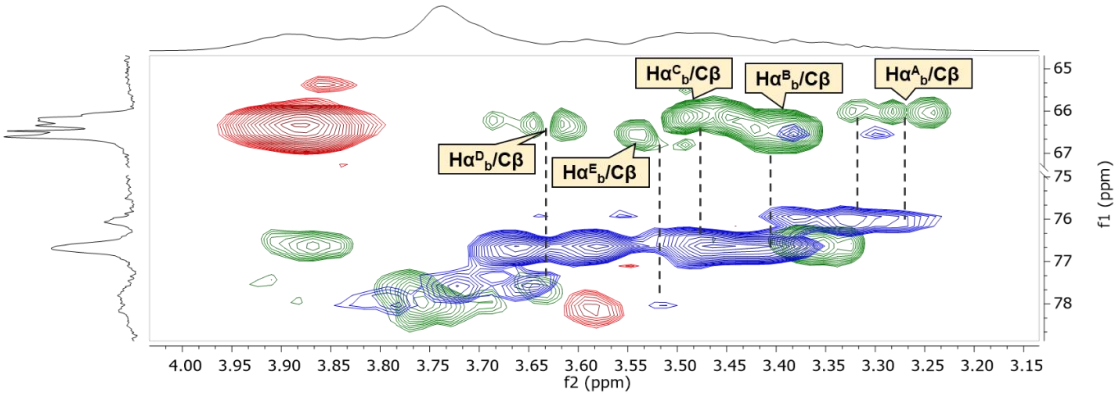

Figure 20. DEPT-HSQC (red and blue) and HMBC (green) spectra of HPBCD DS 7.9 demonstrating the selective three-bond correlations between Hα and Cβ frequencies (400 MHz, D_2O, 298 K) (90).

In the case of α^A, the signals of (*R*) and (*S*) sidechains overlap leading to the apparent partial alignment. The observation was independently proven by the synthesis of enantiopure HPBCD derivatives from (*R*)- and (*S*)-propylene oxide (90). Moving on to α^B and α^C, there is an obvious challenge in their individual discrimination. To assign the $H2_{2sub}$/Cα correlation (magenta in Figure 19) to the corresponding Cα resonance, a higher field instrument was used to register the spectrum with better resolution, as the chemical shifts of $C\alpha^B$ and $C\alpha^C$ overlap at 400 MHz (Figure 19).

As shown in Figure 21A, the signals of interest are slightly separated along the f1 axis, exhibiting ~0.05 ppm difference in ^{13}C chemical shift (Figure 19, blue contours) and both methylenes are clearly correlating with $H2_{2sub}$ (Figure 19, green contours). The separation of the resonances is also evident for the β and γ signals of the HP sidechain. However,

instead of splitting of the ^{1}H frequencies, a clear separation of the ^{13}C resonances is observed (Figure 21b, c).

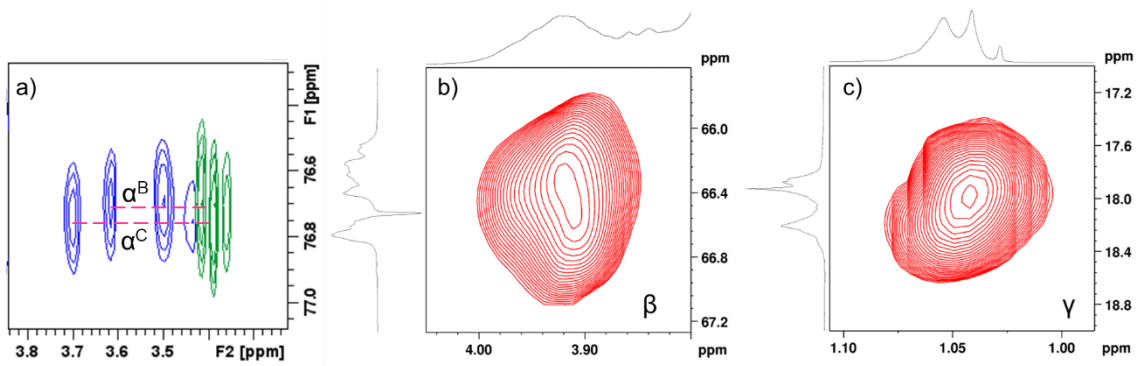

Figure 21. a) Superimposed multiplicity edited HSQC spectrum (red and blue) and HMBC spectra (green) of HPBCD (DS 4.6) emphasizing the correlations of $C\alpha^{B}$ and $C\alpha^{C}$ signals with $H2_{2sub}$ (500 MHz, D_2O, 298 K). b-c) Partial HSQC spectra of HPBCD (DS 6.3) showing the signals β (b) and γ (c) signals of the HP sidechains, showing the separation of ^{13}C frequencies (90).

As α^{B} and α^{C} were both identified as α_{2sub}, the remaining two methylene signals α^{D} and α^{E} were assumed to correspond to the α_{3sub} signals, accounting for both enantiomers of HP. Due to the multiple overlap of signals in both dimensions, only the $H3_{3sub}/C\alpha^{D}$ connection (orange color in Figure 19) could be distinguished from the rest of the correlations. However, since 3_{3sub} has not been assigned earlier, its assignment as C3 can be supported by two definite HMBC correlations, as shown in Figure 22. In Figure 22A, a clear correlation is observed with another methine-type cross-peak assigned as C4, as demonstrated by its HMBC correlations in Figure 22B. This cross-peak exhibits a well-separated correlation with one of the anomeric signals.

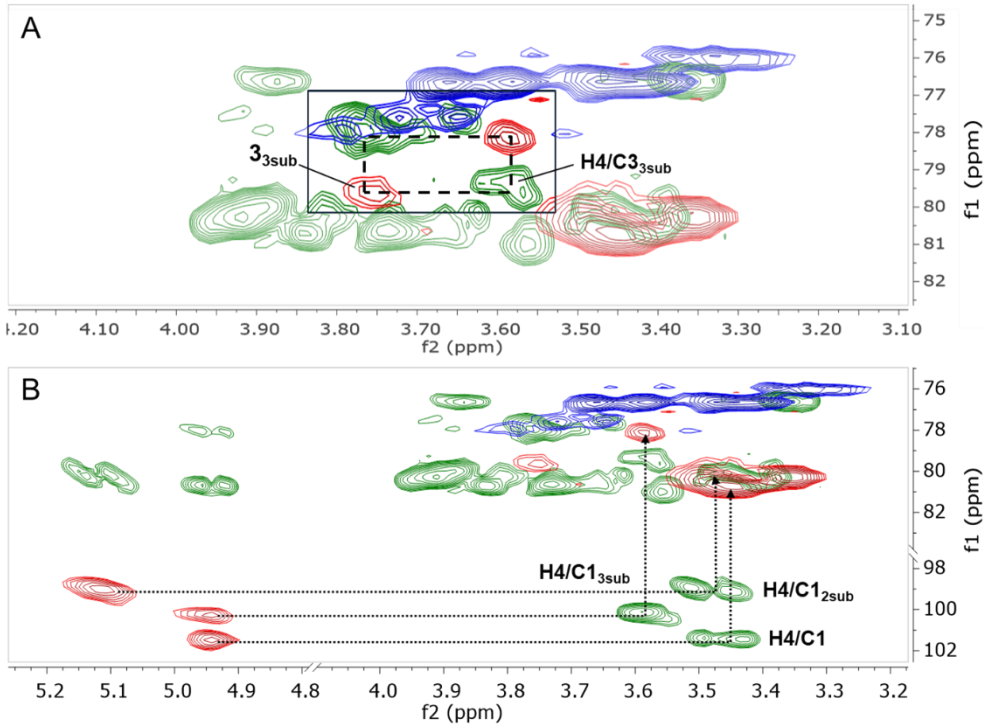

Figure 22. Superimposed HSQC and HMBC spectra of HPBCD (DS 7.9) showing the A) Indicative HMBC correlation of the assumed 3_{3sub} B) HMBC correlations of the anomeric signals confirming the identity of the 3_{3sub}-connected cross-peak (400 MHz, D_2O, 298 K) (90).

Although H1 has three-bond couplings with C3, C5 and the C4 of the neighboring GP unit clockwise, as illustrated in Figure 9B, in the C1 axis only H4/C1 can be detected, thus confirming the putative assignment of the observed methine as C4. Combining these three separate observations, C4 assignment, H4/C3 correlations and H3/Cα^D correlation, the assignment of 3_{3sub} and consequently α^D as α_{3sub} is verified.

4.1.3. Comparison with analogous methylated-β-CD

The NMR assignment of various HP sidechains was confirmed by the analysis of the analogous randomly substituted methylated-β-CD (Me-BCD). Me-BCD, similarly to HPBCD is a randomly alkylated RS CD derivative bearing methyl substituents. Due to the simplified spectra, the signals of Me-BCD are more straightforward to assign.

The relative location of the methyl-substituents (which resemble the α-moiety of the HP sidechains) shows identical patterns to those previously revealed for HPBCD, thus reinforcing the assignment disclosed. The chemical shifts of analogous sidechain types at different positions shift downfield in both ^1H and ^{13}C frequencies in the order of $\delta_3 > \delta_2 > \delta_6$ (Figure 23).

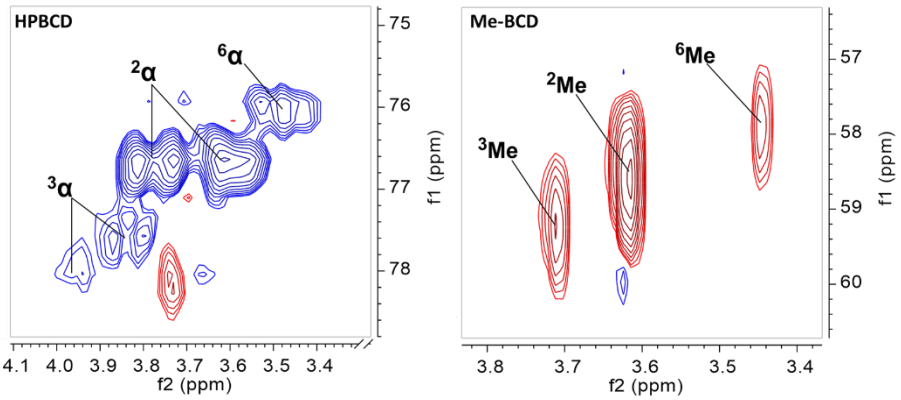

Figure 23. Partial multiplicity-edited HSQC spectrum of HPBCD (DS 7.9) and random methylated β-CD (Me-BCD, DS 12.5), illustrating the identity of chemical shift pattern of the substituents on various positions (400 MHz, D_2O, 298 K) (90).

4.1.4. NMR assignment of the glucopyranose signals

To achieve a *quasi*-full assignment of the HPBCD signals, an in-depth investigation of the anomeric frequencies was performed. As previously shown in the anomeric region of the HSQC spectrum of the HPBCD with DS 7.9, three well-separated signals were identified (Figure 22B). The resonance with the highest ^{1}H frequency was earlier assigned as 1_{2sub}. Consequently, the other two anomeric cross peaks situated at lower ^{1}H resonances should originate from GP_{unsub} and GP_{3sub} and GP_{6sub}. The chemical shift changes of the anomeric signals upon 2-hydroxypropylation indicate that lower ^{13}C frequency of the anomer was influenced by the OH-3 substitution, as it is in close vicinity to C1 compared to OH-6. The substitution of the OH-6 position is thought not to perturb the chemical shift of the anomer (Figure 24A).

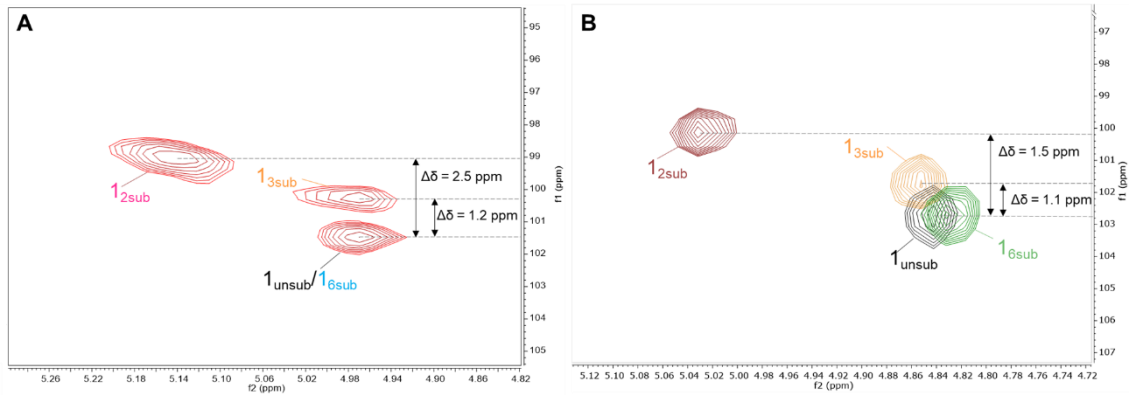

Figure 24. Partial HSQC spectrum of A) HPBCD (DS 7.9) and B) single isomer (SI) permethylated β-CD derivatives: heptakis-2-O-methyl-β-CD (maroon), heptakis-3-O-methyl-β-CD (orange) and heptakis-6-O-methyl-β-CD (green), and native β-CD (black), revealing the

identity of the pattern of chemical shift changes of the anomers upon alkylation on various positions (400 MHz, D_2O, 298 K) (90).

To support the putative assignment of the anomeric signals, SI permethylated β-CD derivatives were examined. Specifically, the spectra of heptakis-2-*O*-methyl-β-CD (2-Me-β-CD), heptakis-3-*O*-methyl-β-CD (3-Me-β-CD) and heptakis-6-*O*-methyl-β-CD (6-Me-β-CD) were compared to native β-CD. In this manner, we were able to elucidate the effect of alkylation at different positions on the chemical shift perturbation of the anomers.

The superimposition of the three SI-Me-β-CDs on the β-CD spectrum revealed that the methylation at the OH-2 position results in ~1.5 ppm shift of the C1 resonance towards lower frequencies (accompanied by concomitant deshielding of H1), while methylation at OH-3 evokes a ~1.1 ppm decrease in ^{13}C chemical shift along with a minor change in ^{1}H chemical shift. Finally, methylation at the OH-6 position has no chemical shift perturbation effect on the anomeric ^{13}C resonances. Aided by this comparative evaluation, the anomeric assignment of HPBCD was justified.

4.1.5. Assignment of the oligomerized sidechains

It is well-documented that the HP sidechains can also react with the alkylating agent, resulting in sidechain oligomerization, especially when large excess of propylene oxide is used. This phenomenon significantly influences the molecule's structural features and also poses a greater challenge in its characterization. When employing the standard procedure to calculate the DS, side-chain oligomerization causes a distorted or "apparent" value that does not accurately represent the true level of substitution. Consequently, it becomes vital to assess the extent of oligomerization.

By comparing the spectra of a series of HPBCD samples synthetized under high alkali conditions with increasing amount of propylene oxide and concomitantly progressive incrementing DS (from 7.1 up to 14.7), it becomes straightforward to distinguish a new set of methylene signals corresponding to the oligomerized sidechains (Figure 25c, orange rectangle). The increasing extent of OH-6 substitution can also be easily

recognized (Figure 25a-c, grey rectangles), and accordingly, the signal corresponding to $C5_{6sub}$ also becomes more intensive (Figure 25a-c, green rectangles).

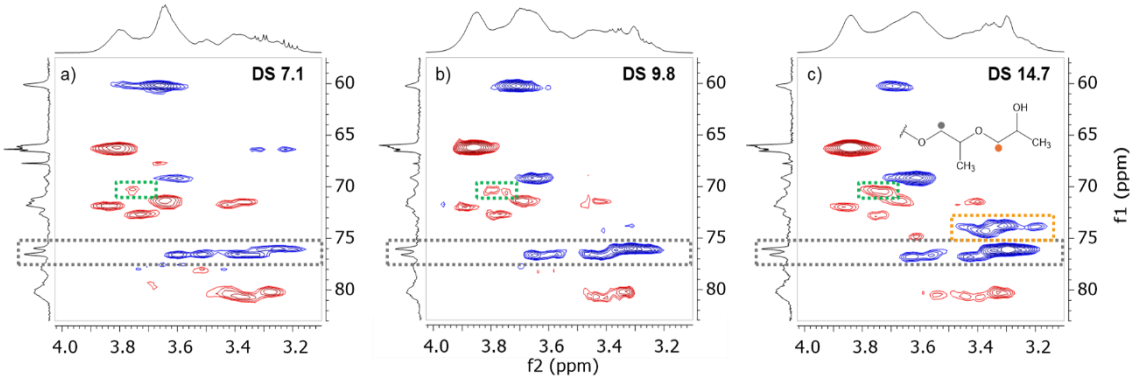

Figure 25. Multiplicity-edited HSQC spectra of HPBCD samples with increasing DS indicating the enhanced OH-6 substitution (grey rectangles), identification of $C5_{6sub}$ (green rectangles) and the oligomerized-type sidechain (orange rectangle) (400 MHz, D_2O, 298 K) (90).

4.1.6. Comparison of substituent distribution

With the signals representing the HP substituents at various positions identified, it becomes possible to compare the PS of various batches. To illustrate the influence of synthetic conditions on the PS, we have compared HPBCD samples possessing practically the same DS. Figure 26 shows the comparison of the ^{13}C spectra of two samples with calculated DS of 7.1 and 7.2. In the Cα region (~79-75 ppm) a remarkable difference in the $C\alpha_{2sub}/C\alpha_{6sub}$ ratio is evident. Variations in the extent of derivatization on the primary and secondary side can significantly impact complexation ability, as demonstrated in earlier studies.

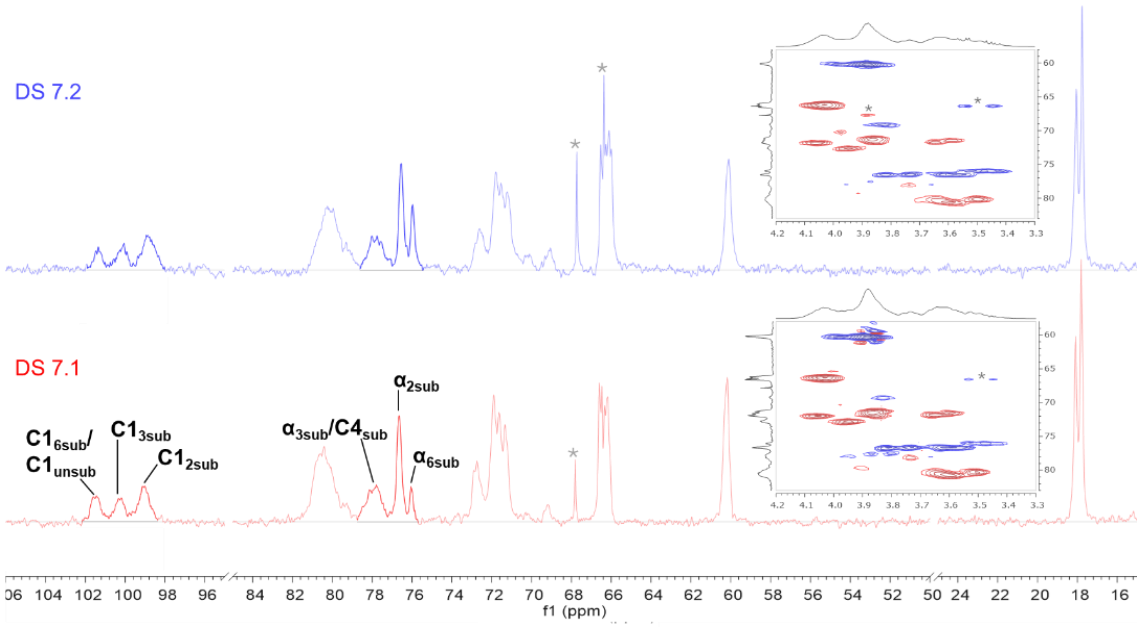

Figure 26. Comparison of the ^{13}C NMR spectra of two HPBCD samples with nearly identical DS values highlights clear differences in the substitution distribution confirming the disparity in their PS profiles (400 MHz, D_2O, 298 K). The asterisk denotes the signals of the propylene glycol impurity (90).

Using the presented assignment, it is possible to determine the extent of substitution at distinct positions directly from the ^{13}C spectrum. For quantitative analysis, inverse-gated decoupling is required.

First, the DS can be calculated based on the intensity ratios of the anomeric signals and the Cγ resonances. By normalizing the sum of integrals for all the anomeric signals to seven ($C1_{unsub}/C1_{6sub}$ + $C1_{3sub}$ + $C1_{2sub}$), the integral of Cγ provides the DS directly. To calculate the substituent distribution there are two possibilities, either through Cα signals or through the anomeric signals. Using the Cα signals, the substitution extent at C2 and C6 (DS_2 and DS_6, respectively) can be directly derived from the integrals of the corresponding signals. However, $C\alpha_{3sub}$ overlaps with a $C4_{sub}$-type frequency. Since the total DS, DS_2, and DS_6 are known, the extent of substitution at C3 (DS_3) can be calculated as $DS_3 = DS - DS_2 - DS_6$. Similarly, using the anomeric signals, DS_2 and DS_3 can be directly calculated, and DS_6 is derived as $DS_6 = DS - DS_2 - DS_3$.

An analysis of the PS of CAVASOL® W7 HP from Wacker was carried out using both approaches. The results showed very good agreement between the two methods (Table 4) as well as with the previously determined PS obtained by the Hakomori method.

Table 4. Calculated substitution distribution of CAVASOL® W7 HP (90).

DS = 4.49	**OH-2**	**OH-3**	**OH-6**
Cα	2.68 (60%)	4.49 – 2.68 – 0.44 = 1.37 (30%)	0.44 (10%)
C1	2.62 (58%)	1.43 (32%)	4.49 – 2.62 – 1.42 = 0.45 (10%)

4.2. Assessing the potential of sugammadex to capture aminosteroid phytotoxins

To evaluate the ability of SGM to capture natural aminosteroids phytotoxins, first SS was chosen as a model compound for a comprehensive binding study.

4.2.1. NMR spectroscopic study

4.2.1.1. ^{1}H NMR titration

NMR titration is commonly employed to study CD complexes through the stepwise addition of the CD to the guest molecule. In our case this approach was not feasible due to the extremely poor aqueous solubility of SS. To prepare a solution of SS, DMSO was chosen as co-solvent. First, SS was solubilized in a calculated amount of DMSO then it was diluted with D_2O to obtain a homogenous suspension in a solvent mixture of 10% DMSO in D_2O. To ensure consistent solvent conditions throughout the titration, an equivalent amount of DMSO was added to the SGM solution.

Upon the stepwise addition of SS to the SGM solution, alongside the emerging SS resonances a second set of SGM signals at lower frequencies appeared, with gradually increasing intensity without significant chemical shift changes (Figure 27A, signals labeled with c). Simultaneously, the intensities of the initial SGM signals gradually decreased.

The observation of two separate series of CD signals clearly indicates that SGM is complexing SS, and the formed complex is in slow exchange, suggesting a high binding constant (K_a>10^5 M^{-1}). When the SGM:SS molar ratio reached 2:1, the signals corresponding to the free form of SGM and that in complex (denoted by f, and c, respectively) displayed nearly equal intensities. This suggests that half of the SGM molecules are in the complexed form while the other half remain free. The further addition of SS up to an equimolar concentration led to the complete disappearance of the free SGM

resonances.

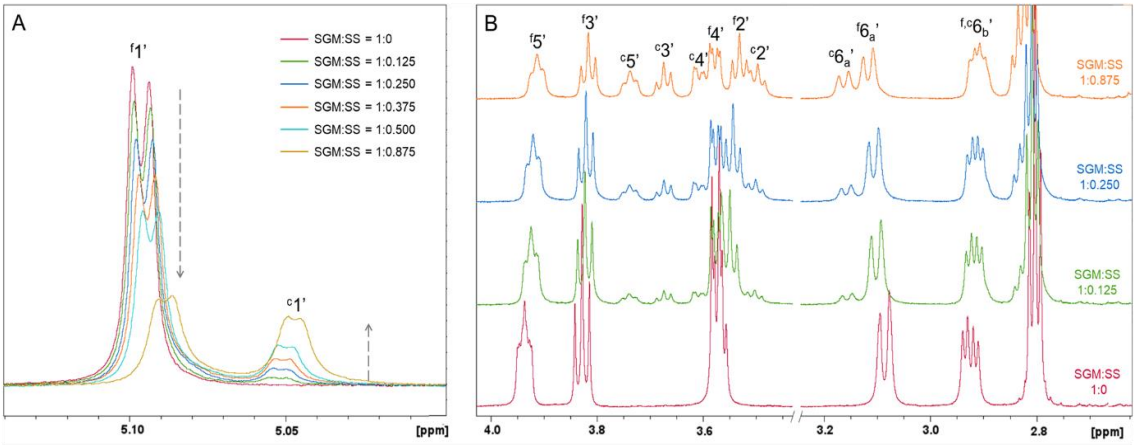

Figure 27. ^{1}H NMR spectra monitoring chemical shift changes upon titration of SGM with SS (700 MHz, 298K). (A) Spectral region for the 1' environment of SGM, and (B) for the 2',3', 4',5', 6' environments of SGM. Peaks corresponding to the free form are labeled with f, while the appearing new resonances belonging to the complex are denoted with c. Apostrophized numbers denote protons of SGM (75).

Continuing the addition of SS, an increasing amount of precipitate was observed, and no further changes occurred in the NMR spectra. Conversely, the addition of excess SGM completely solubilized the precipitate and the signals of free SGM appeared. The lack of free SS signals is attributed to the poor solubility of the steroid, in which keeps its free concentration in the solution below detectable levels. However, in presence of SGM, SS is solubilized (in equimolar ratio) by forming a well-soluble inclusion-type complex.

To justify the assignment of the distinguished set of SGM signals, a 2D ROESY experiment was carried out. Intermolecular NOE cross-peaks were only observed between the signals of SS and the more shielded set of SGM signals, but not with the initial SGM frequencies (Figure 28), confirming the nature of the two forms as complex and free form of SGM, respectively. As SS exhibited spatial proximity to the cavity protons of SGM (H3' and H5'), the inclusion of the steroid was also confirmed.

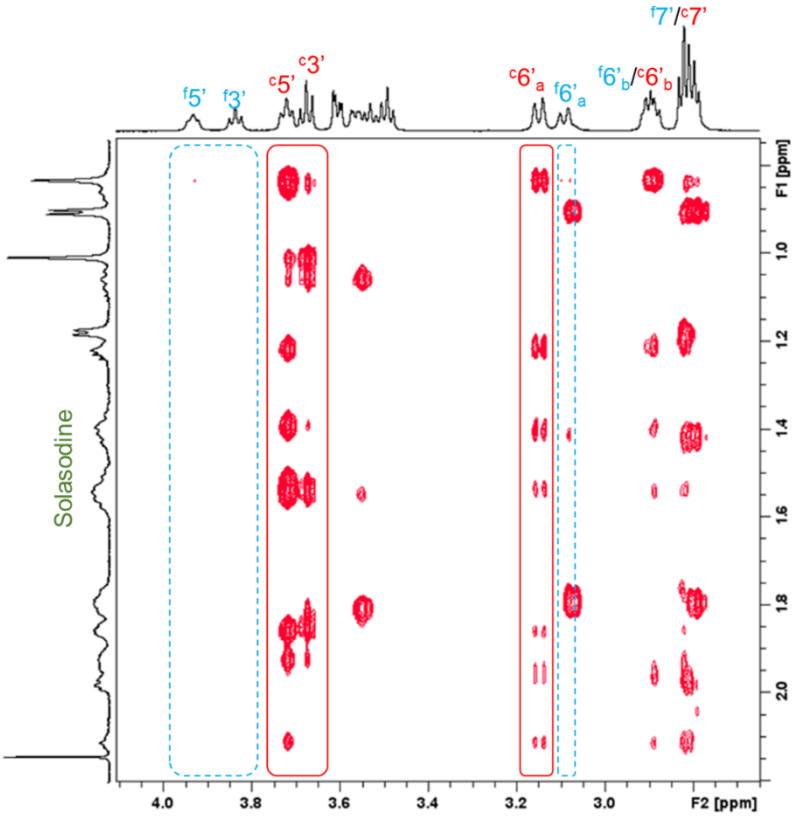

Figure 28. ^{1}H-^{1}H ROESY NMR spectrum of the SGM:SS 2:1 system (700 MHz, 298 K, 10% DMSO-d_6 in D_2O). The superscripts in the assignment and the color-coding stand for free and complexed form of SGM (blue with the superscript f and red, with the superscript c, respectively). The signals of free SGM do not have intermolecular correlations with SS frequencies, while between the complex form of SGM and SS multiple NOE correlations are present (75).

4.2.1.2. Structure of the complex

The unambiguous structure determination of the SGM/SS complex through NOE correlations is hindered by severe signal overlaps in the aliphatic region. However, the orientation of SS in the SGM cavity can be determined by analyzing the NOE cross-peaks of the four methyl groups of SS (H24, H25, H26, H27), situated at different parts of the steroid core (Figure 29). Strong intermolecular correlations were detected between H24 - H3'; H25 - H5'; H26 – H7'; H27 - H7' signals, indicating that the piperidine ring of SS is oriented towards the primary side of the SGM cavity (Figure 29B). This arrangement is further supported by the strong intermolecular NOE cross-peaks between H5' - H12 and H5' - H15 as well as between H3' – H1. These findings are in accordance with the expectations that SS penetrates the cavity in a manner that facilitates ionic interactions with the oppositely charged sidechains of SGM.

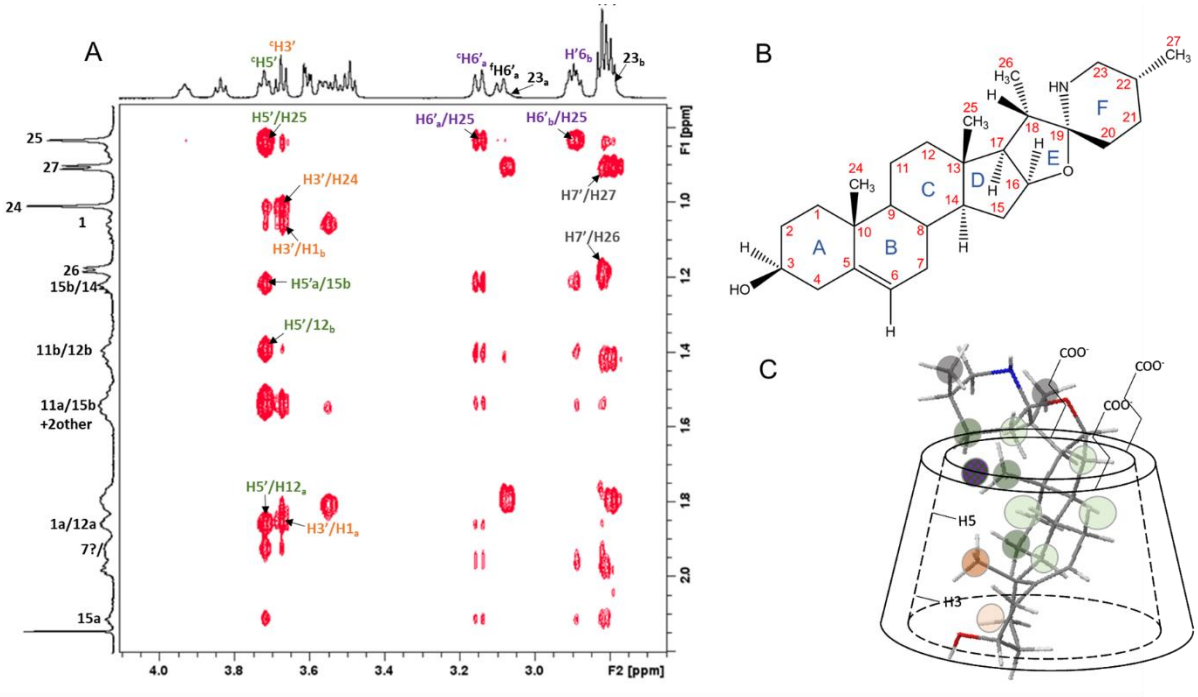

Figure 29. (A) ROESY NMR spectrum of the SGM:SS 2:1 system with the assignment of the crucial intermolecular NOE correlations to determine the guest's orientation (700 MHz, 298 K, 10% DMSO-d_6 in D_2O). Numbers without apostrophe denote the protons of SS while those apostrophized correspond to SGM. (B) Tentative structure of the SGM/SS complex based on the identified NOE correlations. Color coding is used to differentiate intermolecular correlations with the various protons of SGM: orange – interaction with H3'; green – interactions with H5'; purple – interaction with H6'; grey – interaction with H7'. The dark circles indicate strong correlation, while light circles stand for medium strength or weak NOE signals (75).

4.2.1.3. Effect of DMSO on the equilibrium

During the titration experiments, a minor fast exchange process was observed alongside the slow exchange process between SGM and SS, indicated by the slight shifts of resonances (Figure 30B). The effect was attributed to the influence of the DMSO content, suggesting a competitive binding between SS and DMSO to SGM. To confirm this hypothesis, additional series of titration experiments were performed, using solvents with 0% and 25% DMSO. By comparing the three conditions, it was found that increasing DMSO content decreased the fraction of bound SGM in the equilibrium and increased the shifting of the resonances (Figure 30). These findings confirm the competitive fast-exchange process, where DMSO competes with SS for inclusion in the SGM cavity.

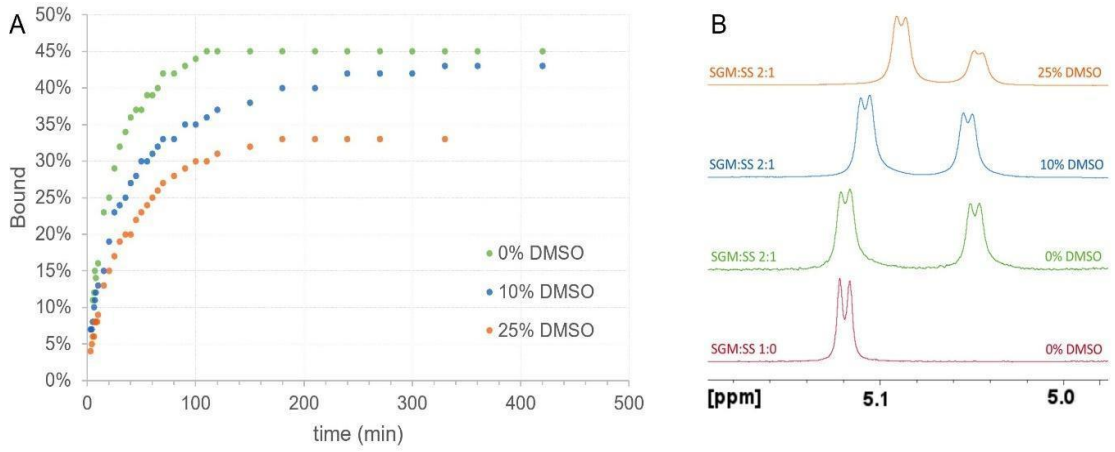

Figure 30. Effect of DMSO on the equilibrium between SGM and SS. (A) time dependence of the complex formation showing the fraction of SGM in complex for the SGM:SS 2:1 sample and (B) anomeric region of the ^{1}H spectrum with different DMSO contents. (700 MHz, 298 K, various solvent mixtures) (75).

4.2.1.4. Effect of temperature

The SGM/SS complex (2:1) was studied in the 278-323 K temperature range (Figure 31, showing the SGM anomeric region). An increase in temperature resulted in line broadening of all peaks. The expected doublet splitting of H1' is observed for both the free and the bound forms, however, the resonances corresponding to the bound form are noticeably narrower, suggesting a higher degree of rigidity. With increasing temperature all peaks broaden, and the signal ratios remain unchanged. Above 303 K, the doublet splitting of the free form is no longer observable, while for the bound form this broadening occurs above 313 K. More importantly, in this temperature range the resonances of the free- and bound forms of SGM remain separated and still far from coalescence, indicating that the system is still in the slow exchange regime.

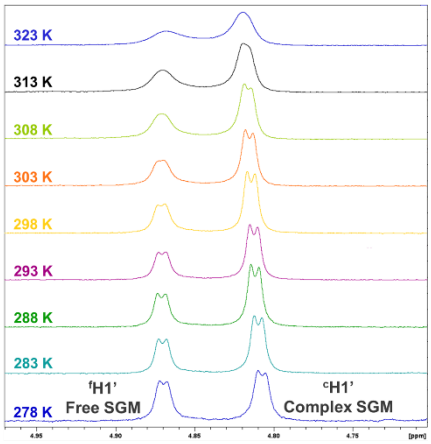

Figure 31. Temperature dependent ^{1}H NMR spectra of SGM:SS 2:1, showing the anomeric region of SGM. (700 MHz, 10% DMSO-d_6 in D_2O, various temperatures) (75).

In the slow exchange regime of the system, EXSY spectroscopy can be employed to calculate pseudo-first order equilibrium constants. Plotting the off- and on-diagonal peak volume integrals for the bound and free forms of SGM protons, the slope of the initial region provides the rate constants k_{fc} and k_{cf} corresponding to the complex formation and dissociation processes, respectively (Figure 32B).

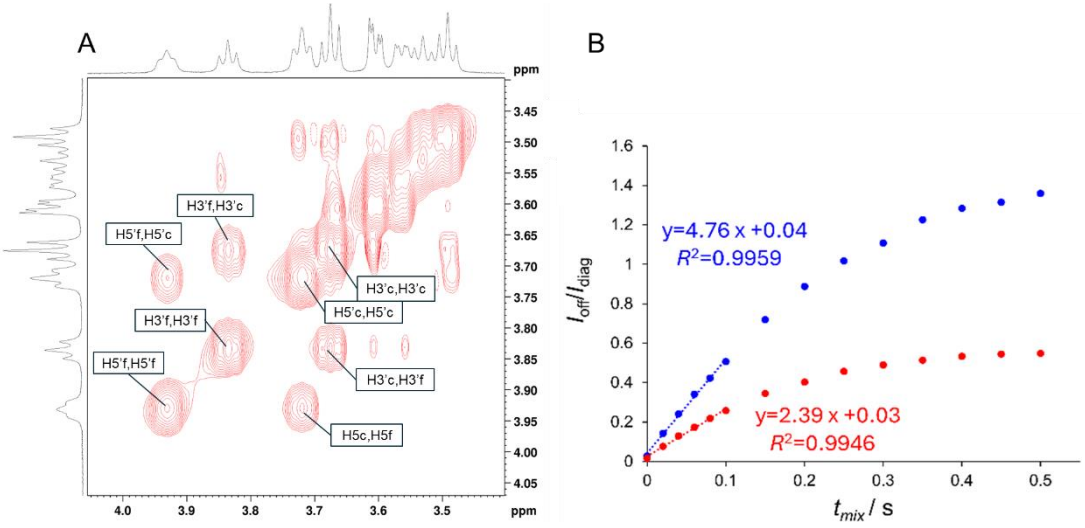

Figure 32. (A) H5' and H3' region of the 2D EXSY spectrum of a sample with SGM:SS 2:1 composition (700 MHz, 298 K, 10% DMSO-d_6 in D_2O) (t_{mix} = 100 ms). (B) Calculation of the k exchange rates from the H3' using the volume integrals extracted from EXSY spectra. Blue points represent the off- and on- diagonal integral ratios for the free H3'; while red points belong to bound H3'. The equation of the linear fit for the initial regime is shown, values of the slope represent the k values (75).

Using Eq. 5, the exchange rate of the equilibrium can be calculated, resulting in k_{ex} = 5.8 s^{-1}.

The temperature dependence of the exchange rate was also tested, in order to determine further thermodynamic parameters. EXSY spectra were acquired at constant 0.1 s mixing time in the temperature range between 278 and 313 K. Calculated values at a given temperature for H3 and H5 environments were in good agreement, therefore, for the Eyring plot representation the average values are used (Figure 33).

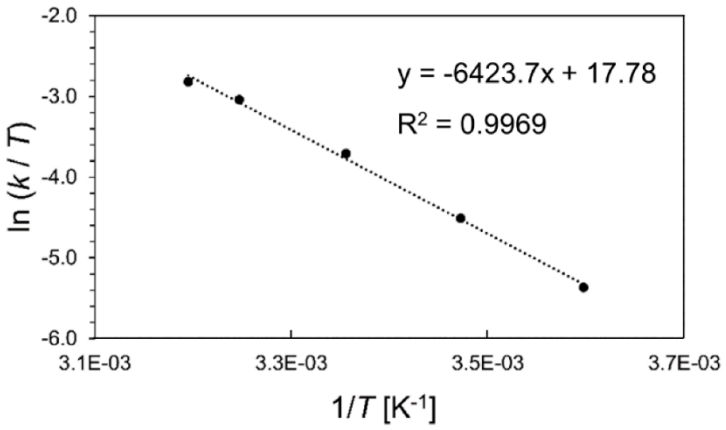

Figure 33. Eyring-plot of the k_{ex} values from the average values of H3' and H5' volume integrals (75).

This linear fitting provided the values of $\Delta H^{\ddagger}$ = 53.2 kJ/mol for the enthalpy of activation and $\Delta S^{\ddagger}$ = -49.7 $JK^{-1}mol^{-1}$ for the entropy of activation, which results in $\Delta G^{\ddagger}$ = 68.0 kJ/mol for the Gibbs energy of activation at 298 K.

4.2.1.5. Effect of glycosylation

To study the effect of glycosylation on the complexation of aminosteroids by SGM, SN and its glycoside ASN were compared. Initially, a complexation study similar to that of described above was carried out for both SN and ASN. To avoid the disrupting effect of DMSO as a co-solvent on the equilibrium, a co-solvent-free approach was used. Initially, SN and ASN were dissolved directly in D_2O and their ^1H NMR spectra were recorded. Equimolar complexes were then prepared by grinding the components together using a mortar and pestle, dissolving in D_2O, and recording the ^1H spectra of the solutions.

Both SN and ASN exhibited limited aqueous solubility on their own but were successfully solubilized by forming equimolar complexes with SGM. The resulting spectra closely resembled those of the SGM/SS complex. In both cases, the bound and free forms of

SGM were detected alongside the signals of the aminosteroid compounds (Figure 34a-b). When excess SGM was added to the samples, the signals of the free SGM emerged, while the signals of the complexes remained unchanged. The observation of a slow exchange regime further indicated the strong nature of the complexes.

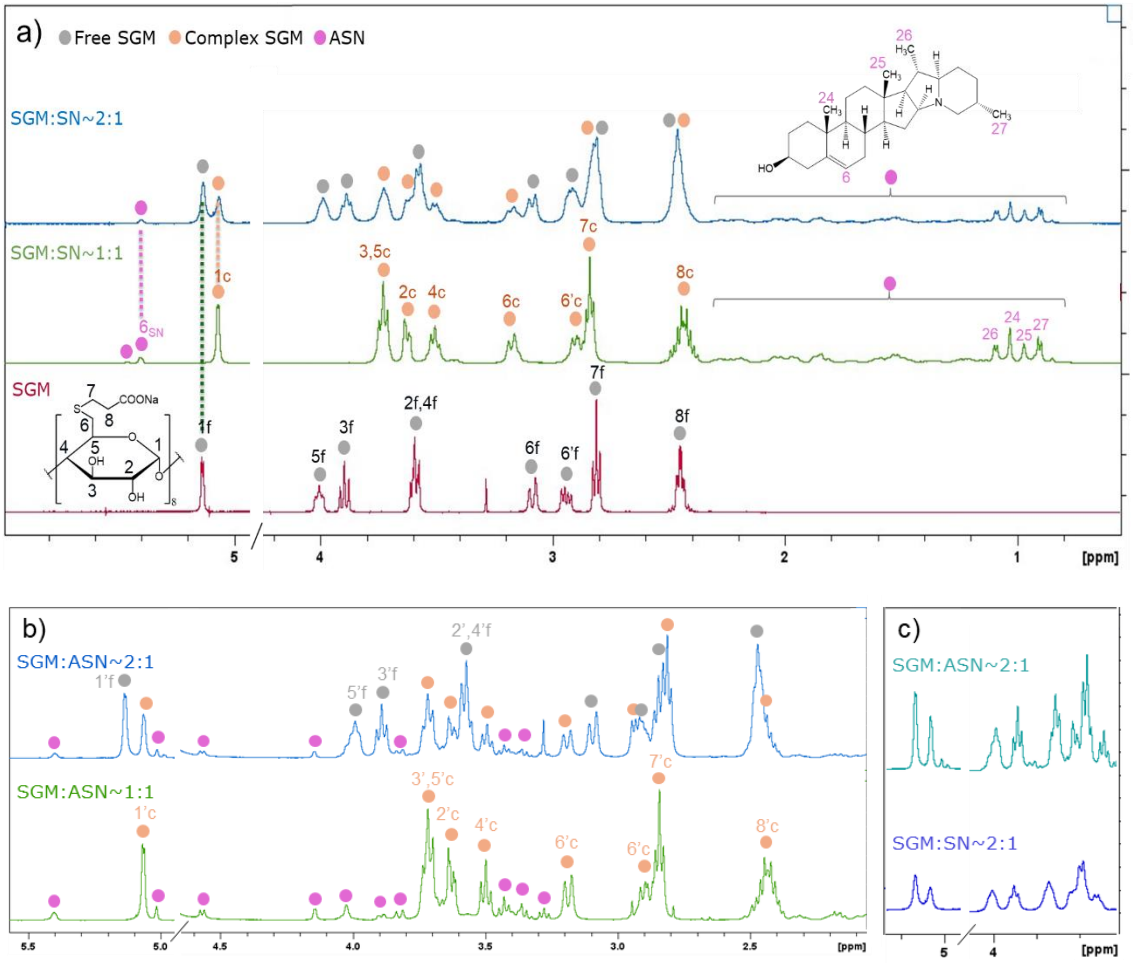

Figure 34. ^{1}H NMR spectra of SGM/SN and SGM/ASN complexes. a) Stacked ^{1}H NMR spectra of SGM alone (red), SGM:SN 1:1 ground mixture (green) and SGM:SN 2:1 mixture (blue) (D_2O, neutral pH, 500 MHz, 298 K, pH ~6.2, pD ~6.6). b) comparison of SGM:ASN 1:1(green) and SGM:ASN 2:1 (blue) systems, and c) comparison of SGM:SN 2:1(blue) and SGM:ASN 2:1 (turquoise) systems (500 MHz, 298 K, D_2O) (91).

A comparison of the ^{1}H NMR spectra of the SGM/SN and SGM/ASN complexes revealed slight differences. When excess SGM was added, signal broadening was observed in the SGM/SN system, whereas no such changes were noted in the SGM/ASN system (Figure 34c). This suggests the presence of a secondary, intermediate-rate process in the SGM/SN system. It is likely that a second SGM molecule binds to SN, similar to the interaction

previously reported between cholesterol and heptakis(2,3,6-tri-*O*-methyl)-β-CD [5]. In contrast, such binding is unlikely to occur between ASN and SGM due to the steric hindrance posed by the attached trisaccharide moiety.

The complex stability was tested by heating the complexes up to 313 K (the limit of the physiological range) and also by dilution up to 2-3-fold. Both complexes remained intact, as no disruption of the equilibrium was detected in any of the cases, proving the high stability of the associations.

The structures of the complexes were explored by 2D ROESY NMR experiments. The orientation of the guests was studied by the inspection of the intermolecular correlations of the well separated H6 and the methyl protons H24, H25, H26 and H27, starting with the spectrally less crowded SN. Correlations with the cavity protons H3' and H5' of SGM confirmed the inclusion of the guest. At the studied pH, H3' and H5' of SGM overlap make it difficult to directly deduce the guest's orientation; however, proximity to H6' and the side-chain protons H7' and H8' can provide insights. Intense cross-peaks were observed between both the cavity protons and H6'a,b and H24 of SN, while the side-chain protons exhibited weaker correlations with the methyl groups H25 and H26. This suggests that SN enters the cavity with the piperidine ring positioned near the primary side and the A and B rings of the steroid deeply embedded in the cavity. Interestingly, weaker correlations were also detected between H6 of SN and both H7' and H8' of SGM, suggesting that an alternative complex with reversed orientation may also form. Additionally, cross-peaks between the guest's H6 and the protons of the CD pointing outward from the cavity (H2' and H4') were identified, indicating the formation of an outer-sphere complex.

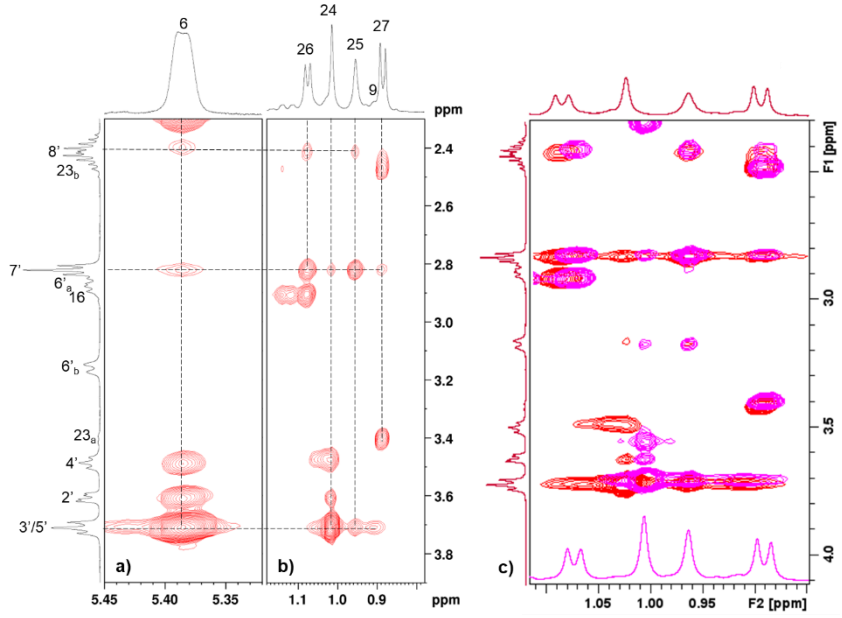

Figure 35. Partial ^{1}H-^{1}H ROESY spectrum of the SGM/SN complex, with magnification of a) the H6 region b) the methyl region of SN c) the methyl region of SN (red) overlapped with the same section of the SGM/ASN spectrum (pink). The non-apostrophized numbers correspond to SN signals, while those apostrophized numbers correspond to SGM protons (91).

The structure elucidation of the SGM/ASN complex was hindered by the numerous signal overlap, as the trisaccharide residue signals appeared in the same spectral region as those of the SGM frequencies. However, the side-by-side comparison of the ROESY spectra of the two complexes revealed an identical cross-peak pattern (Figure 35c), indicating that the guest molecules adopt the same orientation in both complexes.

In contrast to the SGM/SN complex, no proximities were detected between H6 of the steroid core and the sidechain protons H7 and H8 of SGM in the glycoside complex, ruling out the presence of an alternative orientation of ASN.

4.2.1.6. Effect of pH

Both the CD and the alkaloids exhibit pH-dependent charges. SGM is an octavalent acid, with the pK_a values ranging from 3.8 (lowest) through 6.6 (highest) (92), while SN and ASN are tertiary amines with estimated pK_a values exceeding 9. Consequently, at physiological pH (7.4) the amines are positively charged, whereas SGM is present as a heptaanion. As acidity increases, SGM becomes gradually protonated, resulting in a decrease in total charge, while the alkaloids remain monocationic. Conversely, under basic conditions, SN and ASN deprotonate, resulting in the loss of their positive charge.

Consequently, at physiological pH, SGM and the phytotoxins carry opposite charges, leading to the emergence of intermolecular ionic interactions that are believed to stabilize the complexes (7). To assess the significance of these ionic interactions on complex stability, ^{1}H NMR spectra were recorded for both complexes under various pH conditions (Figure 36).

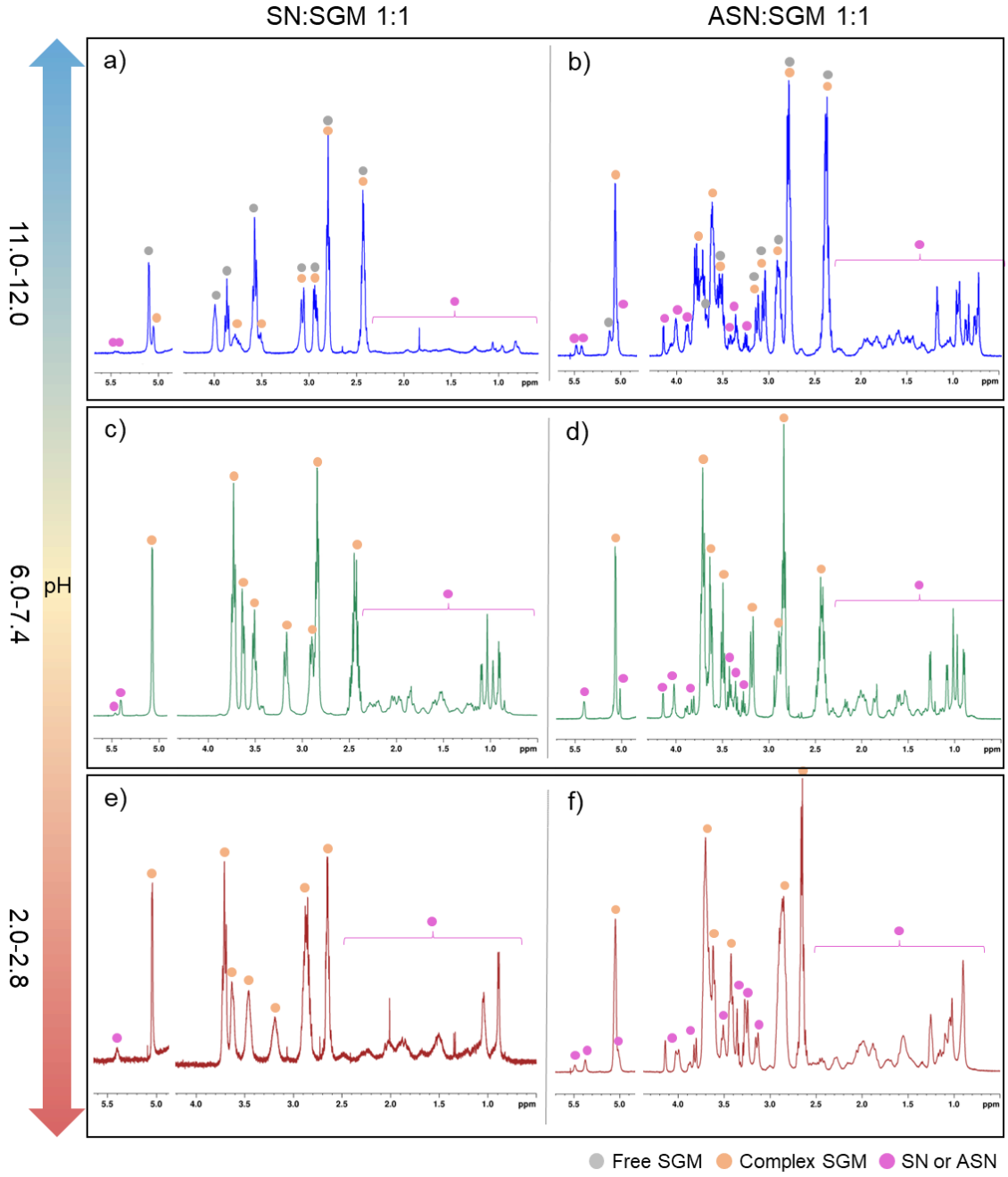

Figure 36. pH-dependent ^{1}H NMR spectra of SGM/SN (a, c, e) and SGM/ASN (b, d, f) complexes (1:1 ratio) (500 MHz, 298 K, D_2O) (91).

4.2.1.6.1. Host-guest interactions under basic conditions

As the pH approaches the pK_a of SN, the tertiary amine begins to lose its positive charge through deprotonation. In the case of the SGM/SN complex, precipitation was observed when the pH reached 9.5 after the addition of base. The ^{1}H NMR spectrum revealed that approximately 70% of the complex dissociated (Figure 36a), as evidenced by the appearance of SGM signals (denoted by orange and grey), which correspond to those previously identified for the free form of SGM. Concurrently, the signal intensities of SN decreased significantly. Further increase in pH (to 11.5 and 13.0), aimed at full deprotonation of SN, did not result in additional dissociation of the complex. The remaining SN in solution exhibited two sets of signals, characterized by the splitting of the well-separated H6 signals and the broadening of the other peaks. These two forms of SN are assumed to represent opposite orientations within the cavity, a conclusion supported by previous findings from the 2D ROESY NMR experiment. Upon re-neutralization of the system, the solid precipitate resolubilized rapidly, and the ^{1}H NMR analysis revealed the immediate reassembly of the complex (Figure 36c).

In contrast, when the solution of the SGM/ASN complex was adjusted to pH 10, no significant decrease in the signal intensities of ASN was observed, and no immediate precipitation occurred. Only a small amount of free SGM was detected in the ^{1}H NMR spectrum (Figure 36b). However, the signals of both ASN and SGM separated into two distinct sets of resonances with similar intensities. (Figure 36b). Analysis of the ROESY spectrum revealed the presence of two distinct types of SGM/ASN complexes within the system (Figure 37).

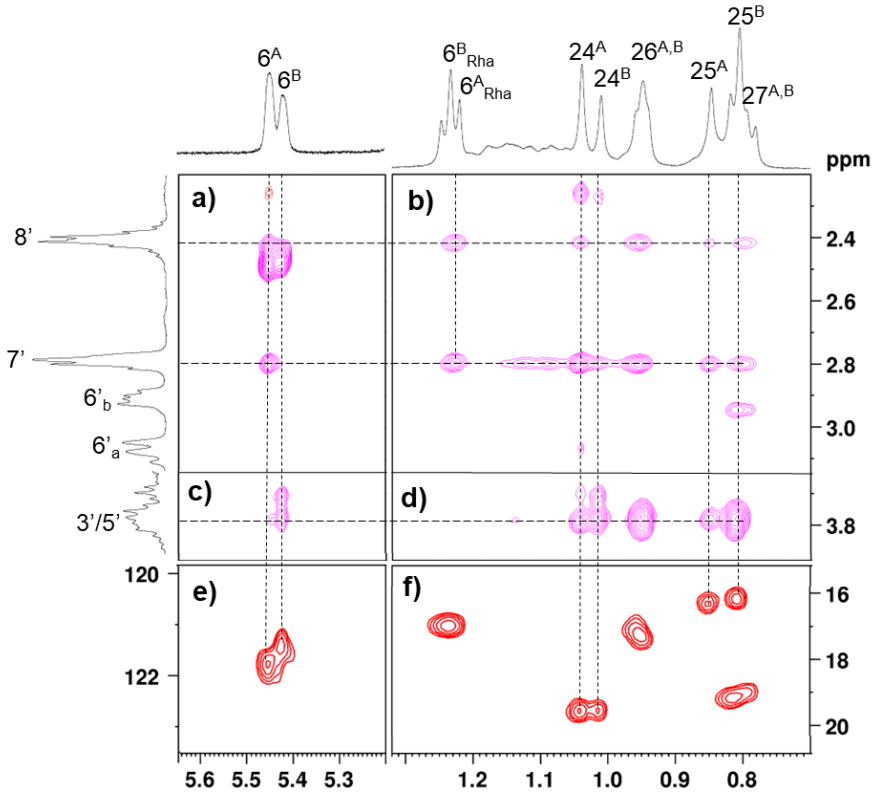

Figure 37. Overlapped 2D spectra of the SGM/ASN complex in basic solution. a-d) Partial ROESY spectra zoomed to the region of the correlations of H6 (a,c) and the methyl groups (b,d) of ASN with the sidechain (a,b) and cavity (c,d) protons of SGM e-f), HSQC spectra zoomed to H6 (e) and methyl (f) signals of ASN (500 MHz, 298 K, D_2O, pH ~10.5). The non-apostrophized numbers indicate SN signals, while those apostrophized correspond to SGM protons (91).

The region corresponding to the duplicated H6 signal of ASN (Figure 37 a, c, e) provides demonstrative evidence for the distinct orientations of the guest in SGM cavitys: While 6A correlates with H7' and H8 of the SGM sidechain, 6B shows clear cross-peaks with the cavity protons but not with the sidechain protons, indicating opposite orientations within the cavity. The same conclusion can be drawn from the methyl region of the spectrum (Figure 37 b, d, f): only one of the doublet methyl signals from the rhamnose unit (6Rha) exhibits clear correlations with the SGM sidechains, suggesting that the trisaccharide faces the primary side of the cone. Conversely, correlations with the cavity protons are absent, as the trisaccharide did not enter the cavity. In a similar manner to H6, one of the pair of H24 singlets correlates with the sidechain protons (H7 and H8) of SGM, while both show intense cross-peaks with the inner protons of the cavity (H3 and H5). However, the overlapping signals of the separated H25 methyls with H27 protons hinder the determination of their orientation based on the detected cross-peaks.

These findings underscore the critical role of ionic interactions between the tertiary amine moiety of the steroid and SGM sidechains to stabilize and to drive the direction of inclusion in the supramolecular complex. Furthermore, they demonstrate that the steroid backbone can also form hydrophobic interactions with the cavity of SGM, albeit with a lower affinity. The additional stabilizing effect of the trisaccharide sidechain of the glycoside is also clearly highlighted.

4.2.1.6.2. Host-guest interactions under acidic conditions

In case of the SGM/SN complex, adjusting the pH to 1.5, resulted in precipitation of the sample and broadening of the signals in the ^{1}H spectrum (Figure 36e). This signal broadening is attributed to the reduced solubility of the complex, which occurs due to the complete protonation of SGM. The assumption that the observed precipitate is indeed the complex is supported by the absence of free SGM signals and the presence of a 1:1 complex, as confirmed by the integration of SN and SGM signals. This suggests that the neutral form of SGM and the cationic form of SN can still form a stable inclusion-type complex. These findings further emphasize the importance of hydrophobic interactions between the steroid backbone of SN and the apolar cavity of SGM in stabilizing the complex, challenging the notion that ionic forces alone maintain the host-guest interaction.

In contrast, no precipitation was observed in the case of SGM/ASN complex at pH 2.0, likely due to the more hydrophilic character of the complex arising from the trisaccharide moiety. Nonetheless, two distinct forms of the complex were identified based on the two separated H6 resonances of ASN and the absence of free SGM signals in the ^{1}H NMR spectrum. Given that different protonation states can be ruled out under these conditions, it can be concluded that two distinct structures of the SGM/ASN complex coexist simultaneously in the system, similarly to those seen in basic environment.

4.2.2. X-ray crystallography study of the SGM/SN complex

The structure at 1.04 Å resolution comprises two crystallographically independent SGM molecules, SGM_a and SGM_b, that form a tail-to-tail dimer centered and parallel to the 4-fold axis of the unit cell, in the cavity of which the SN guest molecule is enclosed (Figure 38). The asymmetric unit contains in fact: one quarter of the host (two glucopyranose moieties of each SGM_a and SGM_b, the full SGM host generated by application of the

four-fold symmetry around the 4-fold axis). Each SGM dimer fully encapsulates one SN guest molecule disordered over four positions, i.e. each SN molecule is found in one only of the four crystallographically equivalent positions of the cavity related by the 4-fold symmetry and has partial occupancy of 0.25, because there is not enough space within the dimer inner space to accommodate even a second guest. However, on average, all possible orientations of SN in the cavity are found in the crystal. In addition, the asymmetric unit comprises 2 sodium cations and 23 water molecules (each with occupancy fixed at 0.25) distributed over 8 and 92 sites, respectively.

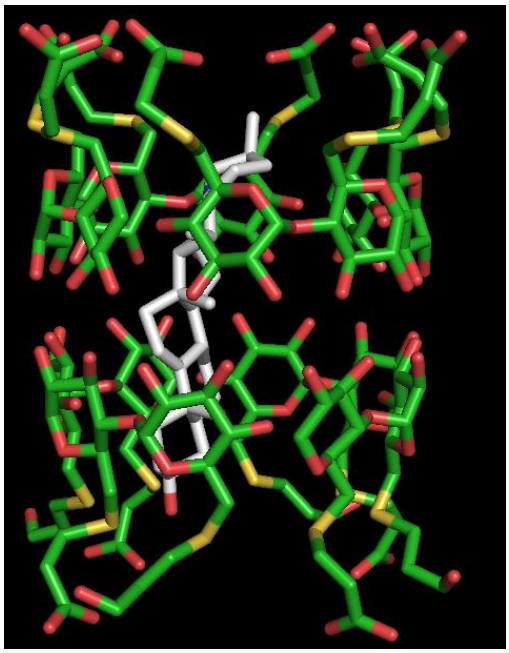

Figure 38. Crystal structure of the SGM/SN complex (solvent molecules are removed for clarity) (created by pymol) (91).

The dimer is stabilized by numerous intermolecular H-bonds between the secondary OH groups of SGM_a and SGM_b. Each O3A of SGM_a H-bonds to O3B and O2B of SGM_b, as was found in other cases of dimeric cyclodextrin-guest complexes (93,94). Intramolecular H-bonds between secondary OH groups of adjacent glucopyranose subunits contribute to the rigidity of each cyclodextrin ring, leading to a rather undistorted geometry. Rings A and B of the SN guest are found inside SGM_b, rings C and D are mostly in the space between the two SN monomers, whereas rings E and F are inside SGM_a. The guest sits parallel to the 4-fold axis of the dimer and somewhat off-center, due to the above-mentioned disorder.

The OH group (ring A) of SN is placed at the SGM_b primary side of the dimer and H-bonds to the nearest sulfur atoms of SGM_b (*O-S* distances of 2.64 Å), this being the closest host-guest interactions in the structure. The primary sides of the hosts along the dimer's channels interact with each other either directly *via* the carboxyl groups of SGM_a and SGM_b or indirectly by a dense network of sodium ions and 12 water molecules located in the interdimer space along the 4-fold axis.

4.2.3. ITC studies

Despite the rather high sensitivity of ITC, SS and SN exhibited insufficient intrinsic solubility for the conventional non-competitive setup, where the solution of the guest is titrated by the sequential addition of the solution of the host. In this arrangement, the free aminosteroids in the cell were either completely consumed by the first 1-2 injections of SGM, inhibiting a proper data fitting, or the generated heat per injection was too small (at the magnitude of the baseline) when the SGM solution was diluted and the injection volume decreased, preventing accurate data collection.

Consequently, distinct approaches were used for the glycoside and the aglycon complexes. While in the first case the solubility was suitable for direct titration both at physiological and acidic pH, the complex stability between SS, SN and SGM was determined by a competitive titration method.

4.2.3.1. Binding stability of the SGM/ASN complex

To explore the effect of pH on the binding affinities between ASN and SGM, the titration was carried out at pH 7.4 as well as at pH 4.0 at 30 °C. In acidic environment, the stability decreased from $K_a = 6.02\times10^6$ M^{-1} to $K_a = 1.61\times10^6$ M^{-1}, indicating the slight influence of the overall charge on the complex stability. While at physiological pH SGM is predominantly octaanionic, at pH of 4.0, it is primarily in a monoanionic form [6]. The complete protonation of SGM was omitted to avoid the precipitation during titration.

The temperature-dependence of the complex stability was also determined at physiological pH (Table 5). By increasing the temperature from 20 to 37 °C, the association constant decreased from 1.2×10^7 M^{-1} to 5.7×10^6 M^{-1}, which shows only minor influence of the temperature on the binding affinity.

Table 5. Complex stabilities of ASN with SGM and γ-CD (GCD) at different temperatures (91).

T / °C	K_a(SGM)/M^{-1}	K_a(GCD)/M^{-1}
20	$1.2\times10^7 \pm 3.9\times10^6$	$2.4\times10^4 \pm 1.0\times10^4$
25	$9.9\times10^6 \pm 2.7\times10^6$	$3.5\times10^4 \pm 8.9\times10^3$
30	$6.0\times10^6 \pm 2.0\times10^5$	$3.6\times10^4 \pm 5.6\times10^3$
37	$5.7\times10^6 \pm 1.5\times10^6$	$2.9\times10^4 \pm 4.5\times10^3$

By examining the temperature dependence of the contribution of ΔH and $-T\Delta S$ by varying temperature (Figure 39A), it is observed that as the temperature increases, electrostatic and Van der Waals interactions become more significant in the complexation process. Additionally, the change in molar heat capacity was calculated, resulting in -911 ± 17 J/mol/K (Figure 39B).

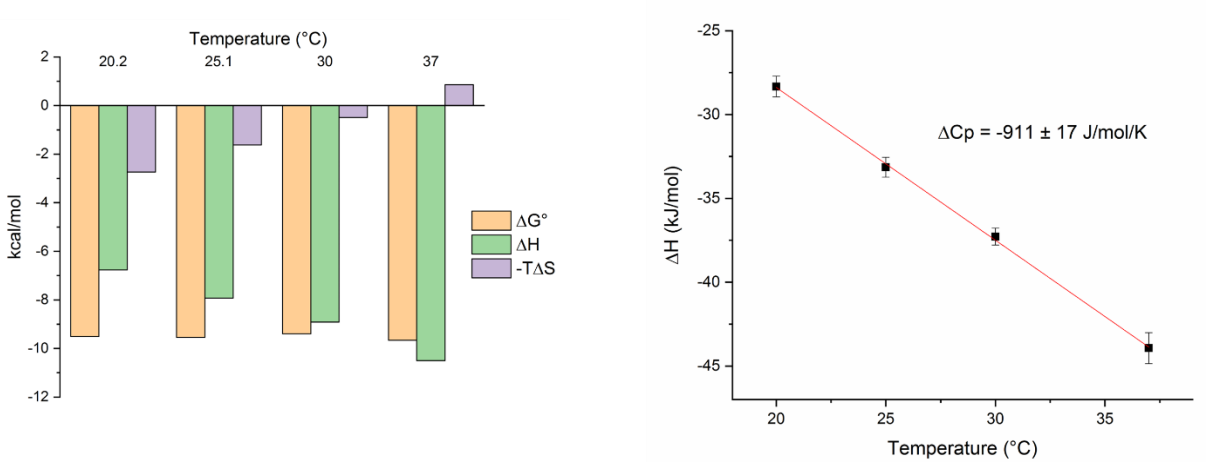

Figure 39. A) Change in the contribution of ΔH and –TΔS by temperature change. By increasing temperature, Van der Waals interactions become decisive in the complexation process. B) Calculation of the molar heat capacity change of ASN-SGM binding (91).

To assess the impact of the thiopropionic acid sidechains of SGM on complex stability, the same series of experiments were carried out with native GCD as well. At each recorded temperature, the ASN/GCD complex stability is 2-3 order of magnitude lower compared to SGM/ASN (Table 5). However, the temperature-dependence of the ASN/GCD complex was found to be lower compared to the SGM/ASN complex, with a calculated change in molar heat capacity of -210± 60 J/mol/K.

4.2.3.2. Binding stability of the SGM/SS and SGM/SN complexes

To determine the complex stability of SGM with the aglycons, a competitive binding approach was employed. Given that the K_a for both SGM/SS and SGM/SN complexes was anticipated to be greater than 10^5 M^{-1}, a competitor host with medium-range binding affinity was needed. If the competitor's binding affinity were too weak, insufficient aminosteroid would be solubilized preventing the achievement of an adequate concentration in the solution. Conversely, if the complexation were too strong (and the affinity difference is insufficiently low), it would be difficult to saturate all guest molecules with the injected SGM. In these regards, GCD was chosen as the competitor host, as its K_a(GCD/aglycon) values were estimated to be in the range of 10^3-10^4 M^{-1}.

To determine the complex stability, the following experimental arrangement was used: SS and SN was (pre)solubilized by the addition of known amount of GCD and titrated by the solution of SGM (with known concentration as well).

However, competitive titration traditionally has the limitation that the parameters of the competing binding process must be determined independently. In our case, neither of the complexes could be measured independently. To address this issue, a new approach was applied to simultaneously determine the binding constants for both the GCD and SGM complexes.

While the concentration of SGM in the syringe was kept constant at 500 μM, several experiments were carried out with varying concentrations of the competing GCD in the range of 0.5–5 mM in the cell. As the concentration of the competitor increased the slope of the thermogram decreased (Figure 40), indicating that more SGM was required to reach saturation.

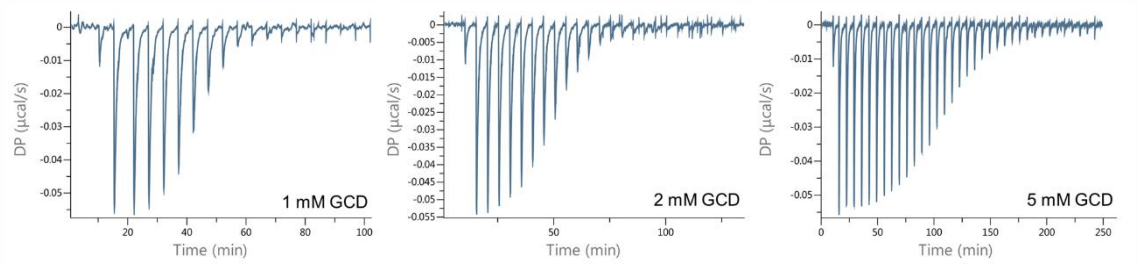

Figure 40. Isothermal calorimetry titration of SS with SGM at 25 °C in the presence of various concentrations of GCD in the reaction cell (75).

The stability constants were calculated based on the reasonable assumption that using the correct binding constant of the weak binder (GCD) in fittings with the competitive model should yield consistent results for the strong binder (SGM) across experiments with varying concentrations of the competitor. Initially, a series of K_d values for GCD/SS in the expected range were set as input parameters in the competitive evaluation model. The corresponding K_d values for SGM/SS were then calculated for all the experiments. The relative standard deviation (SD/mean) for the K_a(SGM/SS) values was plotted against K_a(GCD/SS) (Figure 41). The curve reached a minimum at the best fitting K_d(GCD/SS) value. In this manner, K_d(GCD/SS) has been calculated to be 468 μM at 25°C and 514 μM at 37 °C, equivalent to K_a values of 2.14×10^3 M^{-1} and 1.95×10^3 M^{-1}, respectively, which indeed falls in the preliminary estimated range.

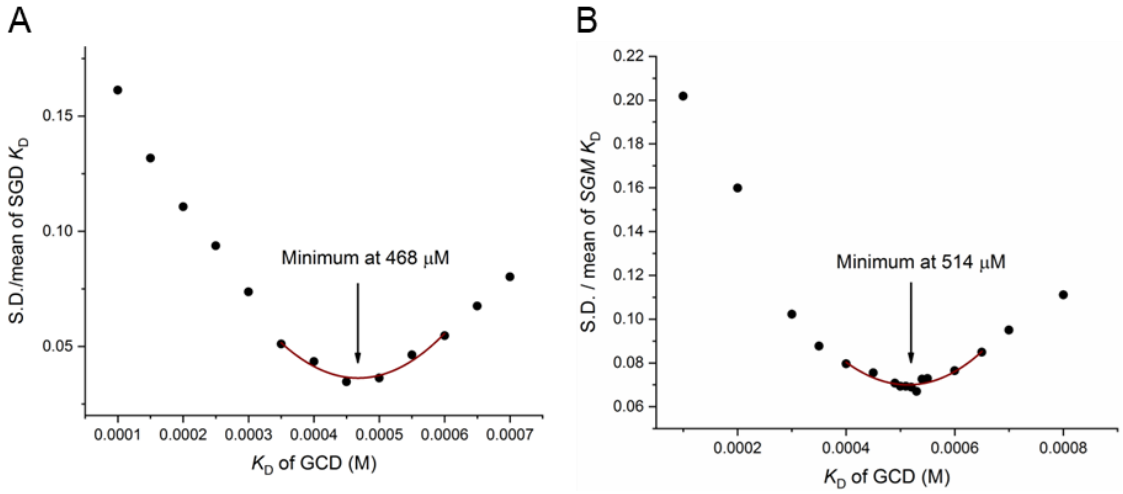

Figure 41. Assessment of the binding constant for the GCD/SS complex (K_d(GCD/SS)) at (A) 25 °C, (B) 37 °C (75).

Using the obtained stability constants as input parameters, the desired association constants of SGM/SS could be derived, resulting in K_d values of 142±5 nM (mean±SD) at 25 °C and 241±17 nM at 37 °C. These translate to K_a values of 7.03×10^6 M^{-1} and 4.17×10^6 M^{-1}, respectively.

The average thermodynamic parameters obtained at both investigated temperatures are listed in Table 6. Similarly to the calculation of K_a(SGM/SS) using the competitive method, deriving the molar enthalpy and entropy change for the SGM/SS complex formation requires the ΔH for the competing GCD/SS complex formation. However, this parameter could not be independently determined. Therefore, based on previous results, a tentative value of ΔH = -4 kcal/mol was used to derive the missing parameters.

While ΔG (and thus the binding affinity) does not change remarkably with varying temperature, the increased influence of electrostatic and van der Waals forces is observed from the decreasing value of the molar enthalpy change, and the increasing entropy contribution at higher temperatures. The average ΔH is calculated to be -9.33 kcal/mol along with an average ΔG of -9.34 kcal/mol at 25 °C for the SGM/SS binding process.

To demonstrate experimentally, and to highlight the specificity of SGM in the formed inclusion complexes, the binding affinity of sulfobuthylether-γ-CD (SB-GCD), a randomly substituted anionic CD derivative towards SS was tested. First, SB-GCD was titrated into an SS solution stabilized by 1 mM GCD, but no clear binding was observed, likely due to similar binding enthalpies or weak SB-GCD affinity. Next, SS was presolubilized with SB-GCD, and titrated with SGM, producing an exothermic response. The calculated K_d values for SB-GCD/SS were 96 μM at 25 °C and 103 μM at 37 °C. These values were about 3 orders of magnitude weaker than those for the SGM/SS complex (Table 6.), reinforcing that the unique structure of SGM is crucial to achieve the high specificity for the SS aminosteroid.

Table 6. Binding parameters of SGM, GCD, and SB-GCD for SS derived from ITC competitive titration (75).

	ΔH (kcal/mol)[a]	ΔG (kcal/mol)[b]	$T\Delta S$ (kcal/mol)[b]	K_a(GCD) (M^{-1})	K_a(SB-GCD) (M^{-1})	K_a(SGM) (M^{-1})
25 °C	-9.33±0.67	-9.34	-0.01	2.14×10^3	1.04×10^3	$7.03\times10^6\pm2.3\times10^5$
37 °C	-10.56±0.59	-9.39	1.19	1.95×10^3	9.71×10^3	$4.17\times10^6\pm2.8\times10^5$

[a]Mean ± SD values for ΔH of SGM-SS binding. We have to note that a -4 kcal/mol value for ΔH of GCD-SS binding was fixed upon calculations.

[b]ΔG and $T\Delta S$ for SGM-SS binding.

The binding affinity of the SGM/SN complex was determined using a similar approach. GCD was added at concentrations of 1 mM or 5mM concentrations for competitive titration. However, unlike the SGM/SS binding, an additional process that influenced the binding isotherm was observed in the final phase of the titration, after the SN was transferred from the GCD into SGM cavity. The phenomenon was more pronounced at higher concentration of GCD. Based on the previous results, the binding of a second CD is assumed. We hypothesize that a competing process between GCD and SGM occurs to accommodate the position of the second host. This additional process influences the apparent binding constant, consequently no proper value for K_a(GCD) could be calculated. Hence, based on the values obtained for the SGM/SS complex (Figure 41), K_d(GCD/SN) = 500 μM was assumed to calculate K_d(SGM/SN). The obtained stability constant at 25°C was K_d(SGM/SN) = 4.5×10^{-7} M, which equals to a K_a(SGM/SN) of 2.22×10^{6} M^{-1}.

4.2.4. Reversal of the toxicity of natural aminosteroids by SGM

To test the hypothesis that the high affinity of SGM for the aminosteroid toxins allows its potential use as an antidote, its protective effect was investigated in the mHippoE-14 mouse hippocampal embryonic cell line.

Two sets of experiments were conducted. First, to determine whether the protective effect is specific to SGM, the antidotal effects of GCD and SB-GCD were also tested against SS. Second, to compare the effect of glycosylation on cell survival and the reversal of toxicity, a viability assay was performed with SN and ASN, as well as their mixtures with SGM.

4.2.4.1. Protective effect of various CDs against the toxicity of SS

SS was proved to be highly toxic to cells at both applied concentrations (Figure 42). Interestingly, SS at 10 μM appeared slightly more toxic than at 20 μM, although the difference was not statistically significant. This could be due to the poor aqueous solubility of SS which was dissolved in DMSO before being added to the cells. Without CDs, SS formed visible precipitates especially at 20 μM. We hypothesize that at 20 μM larger SS particles were formed with a reduced surface area, lowering their effective impact on cells. In the presence of CDs, CD/SS complexes were formed, preventing the precipitation of SS. CDs alone exhibited slight toxicity, however their presence reduced

SS toxicity in most cases (Figure 42). Importantly, SGM showed the strongest protective effect resulting in a marked increase in cell survival (Figure 42C). GCD showed a dual behavior: at 10 µM SS, 0.5 mM GCD increased cell survival, whereas at 20 µM SS, it enhanced cytotoxicity (Figure 42A). This could be attributed to the moderate stability of the GCD/SS complex, where GCD acts as a drug carrier facilitating the delivery of the poorly soluble toxin to the cells at higher SS concentrations.

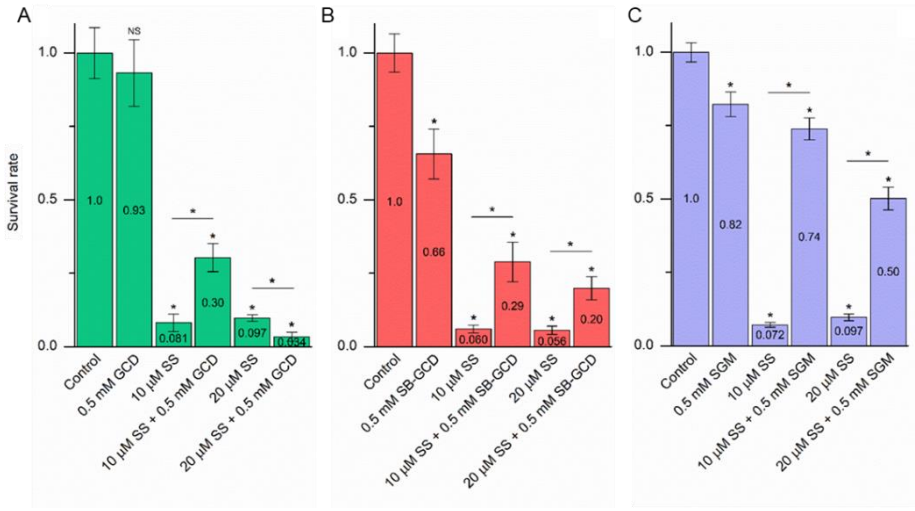

Figure 42. Toxicity of SS on mHippoE-14 cells by MTT assay. Cell survival after 3 days incubation was tested for 10 and 20 µM SS in the absence or presence of 0.5 mM A) GCD B) SB-GCD or C) SGM. Measured absorbances were corrected with the cell-free references and normalized with the 1 % DMSO/buffer control samples to get survival rate. Significance was tested by Mann – Whitney U test, n = 12, *: $p \leq 0.05$ (75).

4.2.4.2. Effect of glycosylation on the protective effect of SGM

Similarly to SS, both SN and ASN were highly toxic, with toxicity increasing at higher concentration. At elevated concentrations, the glycoside showed stronger toxic effect compared to the aglycon, likely due to its higher solubility under physiological conditions (Figure 43). The protective effect of SGM was sufficient at lower concentrations to prevent cell death. However, at higher concentrations, the protective effect of SGM was slightly weaker in most cases, which aligns with the observation that increased SGM concentrations have a modest toxic effect.

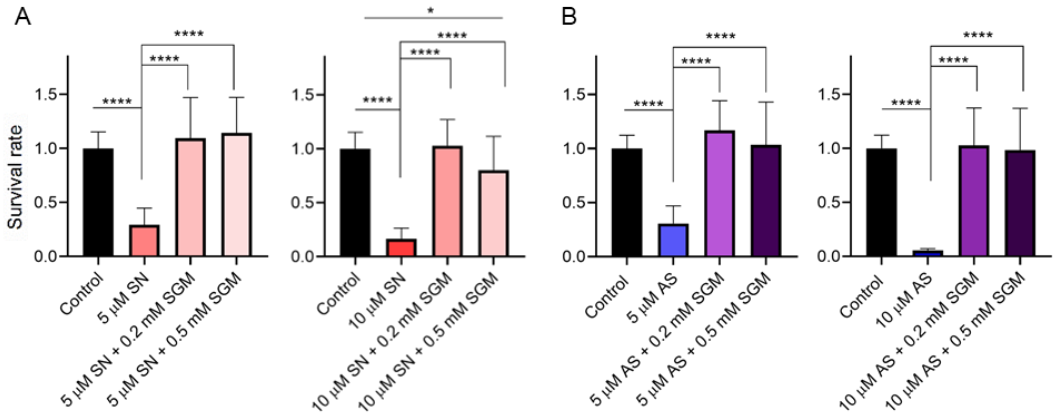

Figure 43. Relative metabolic activity/relative viability of mHippoE-14 cells exposed to various concentrations of SN (A), and ASN (B) and their mixtures with SGM for 72 h, normalized to 1 % DMSO-treated control cells as measured by the MTT. Data are shown as mean and SD. (n = 11-29 per condition, unpaired two-tailed Student's t-test or Mann – Whitney U test depending on normality, asterisks represent statistical significance: * $p \leq 0.05$, ** $p \leq 0.01$, *** $p \leq 0.001$, **** $p \leq 0.0001$) (91).

5. DISCUSSION

5.1. NMR-based determination of the substituent distribution of HPBCD

The presented detailed assignment of the ^{1}H and ^{13}C NMR signals of HPBCD enabled accurate determination of the substituent distribution. It provides a simple and accurate tool to enhance our capability for a more thorough structural characterization of this pharmaceutically important CD. Most of the spectra were recorded on a 400 MHz instrument equipped with probe head operating at room temperature showing that such characterization only requires easily accessible instrumentation. Even though registering ^{13}C spectrum using inverse-gated decoupling requires longer experiment time than the conventional one, HPBCD is easily accessible and generally synthetized over a gram-scale, allowing the preparation of an NMR sample of high concentration. From one NMR sample, the complete characterization of the given batch is feasible through one set of measurements. Recording the ^{1}H NMR spectrum takes only several minutes, and the DS can be directly calculated. Regarding the PS, ^{1}H NMR provides information about the extent of substitution on the OH-2 position, providing a rapid method for comparison of various batches. However, the quantification through ^{1}H NMR is not feasible due to severe signal overlap, impurities can be identified from this simple experiment. In contrary, based on the provided assignment, recording quantitative ^{13}C spectrum of HPBCD allows a more extensive characterization, including DS and PS determination, quantification of impurities (such as propylene glycol, the byproduct of hydroxypropylation), and identification and quantification of sidechain polymerization.

However, it is crucial to acknowledge the limitations of the proposed method. The model presented does not account for GP units with multiple substituents. Accurate assignment and quantification of such units require more advanced instrumentation than what is commonly available. As a result, this method provides only a simplified view of the PS. Nevertheless, for low DS values ($DS \leq 7$) -common in most commercially available HPBCD products- the model delivers a reliable approximation of the PS. This underscores the method's practical utility for rapid and effective structural analysis under typical conditions.

Such comprehensive structural information obtained in a fast, non-destructive and robust way has the potential to serve as an efficient tool for regulatory purposes in controlling the uniformity and the quality of this up-and-coming CD and promising API. By

correlating the DS and PS, it becomes possible to assign an average structure (or several representative structures) that characterize the mixture of HPBCD. This facilitates the development of more realistic models for computational studies, enabling better predictions of interactions with small molecules. Currently, computational studies of RS cyclodextrins often rely solely on experimental DS values, attaching the corresponding number of substituents to a single site of modification (53,95), or a series of hypothetical models are generated by varying the sidechain arrangements(51,96). Incorporating experimentally determined PS can significantly improve the accuracy of these models. Furthermore, understanding PS can enhance structure-activity relationship studies and can help to optimize synthetic conditions for specific applications. This method could be used to select the most suitable PS for a particular use, improving the performance of HPBCD in its intended role.

5.2. Potential of sugammadex to treat aminosteroid intoxication

The investigated aminosteroids predominantly form equimolar, highly stable complexes with SGM exhibiting slow exchange dynamics based on NMR, crystallographic and ITC data. Interestingly, SN seems to form ternary complex by binding to a second SGM molecule. However, this binding occurs to a much lesser extent and with lower stability, as indicated by a faster exchange process in NMR. The physiological relevance of this ternary complex formation remains unclear and warrants further investigation. The highly stable complexes remain intact even by dilution or increased temperatures within the physiologically relevant range, ensuring their robustness under biological conditions. By comparing the pH-dependent spectra of the SGM/SN and SGM/ASN complexes, it can be concluded that hydrophobic interactions between the cavity and the steroid backbone are sufficient to prevent complete dissociation of the complexes, even in the absence of intermolecular ionic interactions between the host and guest. Notably, the glycoside exhibits significantly greater stability with SGM both in acidic and basic environments. This additional stabilization is likely due to hydrogen bonding interactions between the hydroxyl groups of the trisaccharide chain of the glycoside and those of the cyclodextrin. The higher binding affinity was also confirmed by ITC. The complex stability of SGM/SN and of SGM/ASN resulted in K_a(SGM/SN) = 2.22×10^6 M^{-1} and K_a(SGM/ASN) = 9.90×10^6 M^{-1} at 25 °C. Comparing the affinity of the aglycons with SGM, reveals that SS forms a more stable complex with the association constant of K_a(SGM/SS) = 7.03×10^6

M^{-1} at 25 °C. This suggests a tighter fit into the cavity, which may explain why SS is less likely to form a 1:2 complex with SGM in contrast to SN. The high stability of the complexes at elevated temperatures (up to 40 °C) indicates that the physiological temperature does not lead to dissociation of the assemblies.

Additionally, the binding constants obtained by ITC are among the highest ever reported values for CD host-guest complexes, reaching the order of magnitude of SGM/vecuronium and SGM/pancuronium complexes (40). This highlights the exceptional affinity of SGM for aminosteroids. Cell survival studies confirmed SGM's ability to reverse the toxic effect of all the studied aminosteroids.

Quantitative results demonstrated that SGM provides superior protective effects compared to GCD and SB-GCD. These findings underscore the importance of SGM's extended cavity and unique structural features, which enable strong and selective binding to this family of molecules. The combination of high affinity and complex stability positions SGM as a potent agent for treating aminosteroid intoxication.

Finally, the specificity and stability of SGM-aminosteroid complexes, even under challenging conditions, lay a solid foundation for further clinical development and optimization of aminosteroid detoxification protocols.

6. CONCLUSIONS

This thesis provides significant advancements in the structural and functional characterization of CD derivatives, specifically HPBCD and SGM.

Herein we established an efficient NMR-based methodology for the structural characterization of HPBCD. Using widely available instrumentation, we achieved precise differentiation of ^{13}C NMR signals corresponding to hydroxypropyl sidechains attached to different modification sites of glucopyranose units. This approach enables the simultaneous determination of both the DS and the pattern of the substitution from a single set of experiments. Its speed, non-destructive nature, and reliable performance make it as a valuable tool for regulatory purposes, ensuring batch-to-batch consistency and quality control for this industrially and pharmaceutically important CD. Furthermore, it provides essential structural insights that can support future studies on structure-activity relationships and computational modeling

In addition, we demonstrated the potential of SGM to neutralize plant-derived aminosteroid toxins, including SS, SN, and ASN. SGM forms highly stable complexes with these toxins, exhibiting binding constants comparable to those for its primary target, rocuronium. Importantly, cell viability assays confirmed that SGM effectively reverses the cytotoxic effects of these toxins, underscoring its potential for for use as a phytotoxin antidote beyond its current clinical use. These findings highlight the versatility of SGM and suggest its potential for treating intoxication cases involving specific natural toxins.

These findings highlight the great potential to extend the applications of the selected CD as APIs. The developed methodologies not only deepen our understanding of their structural and functional properties but also pave the way for novel therapeutic applications.

7. SUMMARY

During my PhD our aim was to expand the possibility of utilization of two pharmaceutically important CDs, HPBCD and sugammadex as APIs by developing new NMR-based methods for the comprehensive structural characterization of the complex mixture of the RS derivative and exploring new indications to use SGM in antidote-like applications.

As HPBCD is a promising API currently owning orphan drug status, its RS nature hinders its proper structural determination, burdening its acceptance as API. We have developed a fast, reliable and robust method using NMR spectroscopy, that allows to establish an average structure by determining the distribution of the HP substituents over the three possible sites of modification of the GP unit. It was achieved by comprehensive signal identification of the separated frequencies of substituents attached to different positions. This complete signal differentiation was described for the first time. The adequate signal dispersion provides a method for quantitative determination of the extent of substitution on the various positions using the inverse-gated decoupled ^{13}C NMR experiment. It can serve as a simple tool for regulatory purposes in controlling the uniformity and the quality of HPBCD.

The ability of SGM was tested to capture naturally occurring aminosteroid-type phytotoxins. Three model compounds, SS, containing secondary amino head group, SN with tertiary amino group and its glycoside ASN were chosen. The formation of exceptionally stable equimolar complexes was revealed using NMR spectroscopy and ITC. The complexes were found to be stable under the physiological temperature range. The type of the amino head group on the steroid core had no remarkable effect on the complex stability, however SS, containing secondary amino group seems to form a tighter, more stable complex with SGM. In contrary SN is likely to form ternary complex as well by the association with two SGM molecules. The binding of the second CD was found to be a less favorable process. Comparing the aglycon SN and its glycoside ASN, the additional stabilizing effect of the saccharide chain was revealed, as the SGM/ASN complex was found stable in a wide pH range, while the SGM/SN partially dissociated under basic conditions. Cell viability assays revealed the protective effect of SGM against the toxicity of all three investigated aminosteroids. The low protecting effect of GCD and SB-GCD underlined the specificity of SGM towards the studied aminosteroids.

8. REFERENCES

1. Szejtli J. Introduction and General Overview of Cyclodextrin Chemistry. Chem Rev. 1998;(98):1743–1753.

2. Loftsson T, Brewster ME. Cyclodextrins as Functional Excipients: Methods to Enhance Complexation Efficiency. J Pharm Sci. 2012 Sep;101(9):3019–3032.

3. Liu L, Guo QX. The driving forces in the inclusion complexation of cyclodextrins. J Incl Phenom Macrocycl Chem. 2002;42(1–2):1–14.

4. Santos EH, Kamimura JA, Hill LE, Gomes CL. Characterization of carvacrol beta-cyclodextrin inclusion complexes as delivery systems for antibacterial and antioxidant applications. Food Science and Technology. 2015 Jan;60(1):583–592.

5. Wang JW, Yu KX, Ji XY, Bai H, Zhang WH, Hu X, Tang G. Structural insights into the host–guest complexation between β-cyclodextrin and bio-conjugatable adamantane derivatives. Molecules. 2021;26(9):1–13.

6. Li H, Zhang G, Wang W, Chen C, Jiao L, Wu W. Preparation, Characterization, and Bioavailability of Host-Guest Inclusion Complex of Ginsenoside Re with Gamma-Cyclodextrin. Molecules. 2021 Nov 29;26(23):7227.

7. Welliver M, McDonough J, Kalynych N, Redfern R. Discovery, development, and clinical application of sugammadex sodium, a selective relaxant binding agent. Drug Des Devel Ther. 2008;(2):49–59.

8. Rawat S, Jain SK. Solubility enhancement of celecoxib using β-cyclodextrin inclusion complexes. Eur J Pharm Biopharm. 2004;57(2):263–267.

9. Popielec A, Loftsson T. Effects of cyclodextrins on the chemical stability of drugs. Int J Pharm. 2017;531(2):532–542.

10. Fernández-Rosas J, Pessêgo M, Cepeda-Plaza M, Basilio N, Parajó M, Rodríguez-Dafonte P, García-Río L. γ-Cyclodextrin modulates the chemical

reactivity by multiple complexation. Org Biomol Chem. 2015;13(4):1213–1224.

11. Loftsson T, Brewster ME, Másson M. Role of Cyclodextrins in Improving Oral Drug Delivery. Am J Drug Deliv. 2004;2(4):261–275.

12. Cyclodextrin Market Size - By Type (Alpha, Beta, Gamma), By Application (Pharmaceutical, Food and Beverage, Chemicals, Cosmetics and Personal Care) & Forecast, 2024-2032 [Internet]. [cited 2024 Nov 1]. Available from: https://www.gminsights.com/industry-analysis/global-cyclodextrin-market

13. Szejtli J, Szente L. Elimination of bitter, disgusting tastes of drugs and foods by cyclodextrins. Eur J Pharm Biopharm. 2005 Oct;61(3):115–125.

14. Matencio A, Navarro-Orcajada S, García-Carmona F, López-Nicolás JM. Applications of cyclodextrins in food science. A review. Trends Food Sci Technol. 2020;104(July):132–143.

15. Ferreira L, Mascarenhas-Melo F, Rabaça S, Mathur A, Sharma A, Giram PS, Pawar KD, Rahdar A, Raza F, Veiga F, Mazzola PG, Paiva-Santos AC. Cyclodextrin-based dermatological formulations: Dermopharmaceutical and cosmetic applications. Colloids Surf B Biointerfaces. 2023;221(August 2022).

16. Velázquez-Contreras F, Zamora-Ledezma C, López-González I, Meseguer-Olmo L, Núñez-Delicado E, Gabaldón JA. Cyclodextrins in Polymer-Based Active Food Packaging: A Fresh Look at Nontoxic, Biodegradable, and Sustainable Technology Trends. Polymers (Basel). 2021 Dec 28;14(1):104.

17. Liu Z, Xu W, Kovaleva EG, Cheng J, Li H. Recent progress in encapsulation and controlled release of pesticides based on cyclodextrin derivative carriers. Advanced Agrochem. 2022 Dec;1(2):89–99.

18. Rizzi V, Gubitosa J, Signorile R, Fini P, Cecone C, Matencio A, Trotta F, Cosma P. Cyclodextrin nanosponges as adsorbent material to remove hazardous pollutants from water: The case of ciprofloxacin. Chemical Engineering Journal. 2021 May;411(November 2020):128514.

19. Zhu B, Shao R, Li N, Min C, Liu S, Xu Z, Qian X, Wang L. Progress of cyclodextrin based-membranes in water treatment: special 3D bowl-like structure to achieve excellent separation. Chemical Engineering Journal. 2022 Dec;449(April):137013.

20. Teixeira J, Tiritan ME, Pinto MMM, Fernandes C. Chiral stationary phases for liquid chromatography: Recent developments. Molecules. 2019;24(5).

21. Fejős I, Kalydi E, Malanga M, Benkovics G, Béni S. Single isomer cyclodextrins as chiral selectors in capillary electrophoresis. J Chromatogr A. 2020 Sep 13;1627:461375.

22. Schneiderman E, Stalcup AM. Cyclodextrins: a versatile tool in separation science. J Chromatogr B Biomed Sci Appl. 2000 Aug 4;745(1):83–102.

23. Popr M, Hybelbauerová S, Jindřich J. A complete series of 6-deoxy-monosubstituted tetraalkylammonium derivatives of α-, β-, and γ-cyclodextrin with 1, 2, and 3 permanent positive charges. Beilstein J Org Chem. 2014;10:1390–1396.

24. Novokshonov V V., Hoi NC, Shaglaeva NS. Selective monoallylation of β-cyclodextrin. Russ J Gen Chem. 2017 Jun 2;87(6):1172–1174.

25. García-López JJ, Hernández-Mateo F, Isac-García J, Kim JM, Roy R, Santoyo-González F, Vargas-Berenguel A. Synthesis of per-glycosylated β-cyclodextrins having enhanced lectin binding affinity. J Org Chem. 1999 Jan 1;64(2):522–531.

26. Cravotto G, Martina K, Caporaso M, Heropoulos G, Jicsinszky L. Highly efficient Synthesis of per -substituted amino-cyclodextrins under Microwave Irradiation in a closed Cavity. MRS Proceedings. 2013 Feb 18;1492:177–182.

27. Ortega-Caballero F, Giménez-Martínez JJ, Vargas-Berenguel A. Diverse Motifs of Mannoside Clustering on a β-Cyclodextrin Core. Org Lett. 2003 Jul 1;5(14):2389–2392.

28. Benkovics G, Bálint M, Fenyvesi É, Varga E, Béni S, Yannakopoulou K, Malanga M. Homo- and hetero-difunctionalized β-cyclodextrins: Short direct synthesis in gram scale and analysis of regiochemistry. Beilstein J Org Chem. 2019 Mar 18;15:710–720.

29. Liu J, Wang B, Przybylski C, Bistri-Aslanoff O, Ménand M, Zhang Y, Sollogoub M. Programmed Synthesis of Hepta-Differentiated β-Cyclodextrin: 1 out of 117655 Arrangements. Angew Chem Int Ed. 2021 May 17;60(21):12090–12096.

30. Malanga M, Fejős I, Varga E, Benkovics G, Darcsi A, Szemán J, Béni S. Synthesis, analytical characterization and capillary electrophoretic use of the single-isomer heptakis-(6-O-sulfobutyl)-beta-cyclodextrin. J Chromatogr A. 2017;1514:127–133.

31. Benkovics G, Fejős I, Darcsi A, Varga E, Malanga M, Fenyvesi É, Sohajda T, Szente L, Béni S, Szemán J. Single-isomer carboxymethyl-γ-cyclodextrin as chiral resolving agent for capillary electrophoresis. J Chromatogr A. 2016;1467:445–453.

32. Pitha J, Milecki J, Fales H, Pannell L, Uekama K. Hydroxypropyl-β-cyclodextrin: preparation and characterization; effects on solubility of drugs. Int J Pharm. 1986;29(1):73–82.

33. Jindrich J, Pitha J, Lindberg B, Seffers P, Harata K. Regioselectivity of alkylation of cyclomaltoheptaose (β-cyclodextrin) and synthesis of its mono-2-O-methyl, -ethyl, -allyl, and -propyl derivatives. Carbohydr Res. 1995 Jan 3;266(1):75–80.

34. Pitha J, Trinadha Rao C, Lindberg B, Seffers P. Distribution of substituents in 2-hydroxypropyl ethers of cyclomaltoheptaose. Carbohydr Res. 1990;200(C):429–435.

35. Fenyvesi É, Szemán J, Csabai K, Malanga M, Szente L. Methyl-beta-cyclodextrins: The role of number and types of substituents in solubilizing power. J Pharm Sci. 2014;103(5):1443–1452.

36. Loftsson T, Brewster ME. Pharmaceutical applications of cyclodextrins: basic science and product development. J Pharm Pharmacol. 2010 Nov 1;62(11):1607–1621.

37. European Medicines Agency. Background review for cyclodextrins used as excipients In the context of the revision of the guideline on “Excipients in the label” [Internet]. 2014 [cited 2024 Mar 19]. Available from: https://www.ema.europa.eu/en/documents/report/background-review-cyclodextrins-used-excipients-context-revision-guideline-excipients-label-and-package-leaflet-medicinal-products-human-use-draft-report_en.pdf

38. Jansook P, Ogawa N, Loftsson T. Cyclodextrins: structure, physicochemical properties and pharmaceutical applications. Int J Pharm. 2018 Jan 15;535(1–2):272–284.

39. Nag K, Singh D, Shetti A, Kumar H, Sivashanmugam T, Parthasarathy S. Sugammadex: A revolutionary drug in neuromuscular pharmacology. Anesth Essays Res. 2013;7(3):302.

40. Zwiers A, Van Den Heuvel M, Smeets J, Rutherford S. Assessment of the potential for displacement interactions with sugammadex: A pharmacokinetic-pharmacodynamic modelling approach. Clin Drug Investig. 2011;31(2):101–111.

41. Stair C, Fernandez-Bustamante A. Sugammadex, the first selective relaxant binding agent for neuromuscular block reversal. Drugs of Today. 2012;48(6):405.

42. Gijsenbergh F, Ramael S, Houwing N, Van Iersel T. First human exposure of Org 25969, a novel agent to reverse the action of rocuronium bromide. Anesthesiology. 2005;103(4):695–703.

43. Bom A, Bradley M, Cameron K, Clark JK, van Egmond J, Feilden H, MacLean EJ, Muir AW, Palin R, Rees DC, Zhang MQ. A Novel Concept of Reversing Neuromuscular Block: Chemical Encapsulation of Rocuronium Bromide by a Cyclodextrin-Based Synthetic Host. Angew Chem Int Ed. 2002 Jan 18;41(2):265.

44. Adam JM, Bennett DJ, Bom A, Clark JK, Feilden H, Hutchinson EJ, Palin R, Prosser A, Rees DC, Rosair GM, Stevenson D, Tarver GJ, Zhang MQ. Cyclodextrin-derived host molecules as reversal agents for the neuromuscular blocker rocuronium bromide: Synthesis and structure-activity relationships. J Med Chem. 2002;45(9):1806–1816.

45. Calias P. 2-Hydroxypropyl-β-cyclodextrins and the Blood-Brain Barrier: Considerations for Niemann-Pick Disease Type C1. Curr Pharm Des. 2018;23(40):6231–6238.

46. Chang TY, Reid PC, Sugii S, Ohgami N, Cruz JC, Chang CCY. Niemann-Pick Type C Disease and Intracellular Cholesterol Trafficking. J Biol Chem. 2005 Jun;280(22):20917–20920.

47. Kovacs T, Nagy P, Panyi G, Szente L, Varga Z, Zakany F. Cyclodextrins: Only Pharmaceutical Excipients or Full-Fledged Drug Candidates? Pharmaceutics. 2022 Nov 22;14(12):2559.

48. Pitha J, Szabo L, Fales HM. Reaction of cyclodextrins with propylene oxide or with glycidol: Analysis of product distribution. Carbohydr Res. 1987;168(2):191–198.

49. Li Z, Li K, Teng M, Li M, Sui X, Liu B, Tian B, Fu Q. Functionality-related characteristics of hydroxypropyl-β-cyclodextrin for the complexation. J Mol Liq. 2022;365.

50. Buvári-Barcza Á, Barcza L. Influence of the guests, the type and degree of substitution on inclusion complex formation of substituted β-cyclodextrins. Talanta. 1999;49(3):577–585.

51. Kerdpol K, Kicuntod J, Wolschann P, Mori S, Rungnim C, Kunaseth M, Okumura H, Kungwan N, Rungrotmongkol T. Cavity closure of 2-hydroxypropyl-β-cyclodextrin: Replica exchange molecular dynamics simulations. Polymers (Basel). 2019;11(1):1–15.

52. Schönbeck C, Westh P, Madsen JC, Larsen KL, Städe LW, Holm R. Hydroxypropyl-substituted β-cyclodextrins: Influence of degree of

substitution on the thermodynamics of complexation with tauroconjugated and glycoconjugated bile salts. Langmuir. 2010;26(23):17949–17957.

53. Yan X, Wang Y, Meng T, Yan H. Computational Insights Into the Influence of Substitution Groups on the Inclusion Complexation of β-Cyclodextrin. Front Chem. 2021;9(May):1–11.

54. Sohajda T, Béni S, Varga E, Iványi R, Rácz Á, Szente L, Noszál B. Characterization of aspartame-cyclodextrin complexation. J Pharm Biomed Anal. 2009;50(5):737–745.

55. Liu XL, Zhu CF, Liu HC, Zhu JM. Quantitative analysis of degree of substitution/molar substitution of etherified polysaccharide derivatives. Des Monomers Polym. 2022 Dec 31;25(1):75–88.

56. Szente L, Szemán J, Sohajda T. Analytical characterization of cyclodextrins: History, official methods and recommended new techniques. J Pharm Biomed Anal. 2016 Oct;130:347–365.

57. Hakomori S. A Rapid Permethylation Of Glycolipid, And Polysaccharide Catalyzed By Methylsulfinyl Carbanion In Dimethyl Sulfoxide. J Biochem. 1964 Feb;55:205–208.

58. Miro A, Ungaro F, Balzano F, Masi S, Musto P, La Manna P, Uccello-Barretta G, Quaglia F. Triamcinolone solubilization by (2-hydroxypropyl)-β-cyclodextrin: A spectroscopic and computational approach. Carbohydr Polym. 2012 Oct;90(3):1288–1298.

59. Loftsson T, Jarho P, Másson M, Järvinen T. Cyclodextrins in drug delivery [Internet]. Vol. 2, Expert Opinion on Drug Delivery. Taylor & Francis; 2005 [cited 2022 Mar 22]. p. 335–351. Available from: https://www.tandfonline.com/doi/abs/10.1517/17425247.2.1.335

60. Bertaut E, Landy D. Improving ITC studies of cyclodextrin inclusion compounds by global analysis of conventional and non-conventional experiments. Beilstein J Org Chem. 2014;10:2630–2641.

61. Gómez-Biagi RF, Jagt RBC, Nitz M. Remarkably stable inclusion complexes with heptakis-[6-deoxy-6-(2-aminoethylsulfanyl)]-β-cyclodextrin. Org Biomol Chem. 2008;6(24):4622.

62. Mura P. Analytical techniques for characterization of cyclodextrin complexes in the solid state: A review. J Pharm Biomed Anal. 2015 Sep;113:226–238.

63. Dohárszky A, Kalydi E, Völgyi G, Béni S, Fejős I. Cyclodextrin-Enabled Enantioselective Complexation Study of Cathinone Analogs. Molecules. 2024;29(4).

64. Job P. Formation and Stability of Inorganic Complexes in Solution. Ann Chim (Paris). 1928;10(9):113–203.

65. Schneider HJ, Hacket F, Rüdiger V, Ikeda H. NMR studies of cyclodextrins and cyclodextrin complexes. Chem Rev. 1998;98(5):1755–1785.

66. Duus JØ, Gotfredsen CH, Bock K. Carbohydrate Structural Determination by NMR Spectroscopy: Modern Methods and Limitations. Chem Rev. 2000 Dec 1;100(12):4589–4614.

67. Speciale I, Notaro A, Garcia-Vello P, Di Lorenzo F, Armiento S, Molinaro A, Marchetti R, Silipo A, De Castro C. Liquid-state NMR spectroscopy for complex carbohydrate structural analysis: A hitchhiker's guide. Carbohydr Polym. 2022 Feb;277(November 2021):118885.

68. Buda S, Nawój M, Mlynarski J. Recent Advances in NMR Studies of Carbohydrates. Annu Rep NMR Spectrosc. 2016;89:185–223.

69. Chuang WL, Christ MD, Rabenstein DL. Determination of the primary structures of heparin- and heparan sulfate-derived oligosaccharides using band-selective homonuclear-decoupled two-dimensional 1H NMR experiments. Anal Chem. 2001;73(10):2310–2316.

70. Malanga M, Szemán J, Fenyvesi É, Puskás I, Csabai K, Gyémánt G, Fenyvesi F, Szente L. "Back to the Future": A New Look at Hydroxypropyl Beta-Cyclodextrins. J Pharm Sci. 2016 Sep;105(9):2921–2931.

71. Schneider HJ, Hacket F, Rüdiger V, Ikeda H. NMR Studies of Cyclodextrins and Cyclodextrin Complexes. Chem Rev. 1998 Jul 30;98(5):1755–1786.

72. Bryant RG. The NMR time scale. J Chem Educ. 1983;60(11):933–935.

73. Fielding L. Determination of association constants (Ka) from solution NMR data. Tetrahedron. 2000;56(34):6151–6170.

74. Perrin CL, Dwyer TJ. Application of Two-Dimensional NMR to Kinetics of Chemical Exchange. Chem Rev. 1990;90(6):935–967.

75. Kalydi E, Sebák F, Fiser B, Minofar B, Moussong É, Malanga M, Bodor A, Kardos J, Béni S. Exceptional stability of the sugammadex-solasodine complex: Insights from experimental and theoretical studies. Carbohydr Polym. 2025;348(July 2024).

76. Bain AD. Chemical Exchange Effects in NMR. Encyclopedia of Spectroscopy and Spectrometry. 1999;229–237.

77. Ali SM, Muzaffar S. Quantitative ROESY analysis for unravelling structure of glafenine and β-cyclodextrin complex. J Incl Phenom Macrocycl Chem. 2019 Jun 15;94(1–2):95–102.

78. Nishijo J, Moriyama S, Shiota S, Kamigauchi M, Sugiura M. Interaction of Heptakis (2,3,6-Tri-O-methyl)-β-cyclodextrin with Cholesterol in Aqueous Solution. Chem Pharm Bull (Tokyo). 2004;52(12):1405–1410.

79. Ujj D, Kalydi E, Malanga M, Varga E, Sohajda T, Béni S, Benkovics G. Sugammadex analogue cyclodextrins as chiral selectors for enantioseparation of cathinone derivatives by capillary electrophoresis. J Chromatogr A. 2022 Nov;1683:463506.

80. Atri MS, Saboury AA, Ahmad F. Biological Applications of Isothermal Titration Calorimetry. Phys Chem Res. 2015;3(4):319–330.

81. Su H, Xu Y. Application of ITC-Based Characterization of Thermodynamic and Kinetic Association of Ligands With Proteins in Drug Design. Front Pharmacol. 2018 Oct 11;9:1–7.

82. Freire E, Mayorga OL, Straume M. Isothermal Titration Calorimetry. Anal Chem. 1990;62(18):135–159.

83. Isothermal Titration Calorimetry (ITC) [Internet]. [cited 2024 Nov 15]. Available from: https://cmi.hms.harvard.edu/isothermal-titration-calorimetry

84. Crews C. Natural Toxicants: Alkaloids. In: Encyclopedia of Food Safety. Elsevier; 2014. p. 251–260.

85. Pomilio AB, Falzoni EM, Vitale AA. Toxic chemical compounds of the Solanaceae. Nat Prod Commun. 2008;3(4):593–628.

86. Friedman M. Potato Glycoalkaloids and Metabolites: Roles in the Plant and in the Diet. J Agric Food Chem. 2006 Nov 1;54(23):8655–8681.

87. Anwar M, Turner M, Farrell N, Zomlefer WB, McDougal OM, Morgan BW. Hikers poisoned: Veratrum steroidal alkaloid toxicity following ingestion of foraged Veratrum parviflorum. Clin Toxicol. 2018 Sep 2;56(9):841–845.

88. Kumar P, Sharma B, Bakshi N. Biological activity of alkaloids from Solanum dulcamara L. Nat Prod Res. 2009 May 20;23(8):719–723.

89. Sigurskjold BW. Exact analysis of competition ligand binding by displacement isothermal titration calorimetry. Anal Biochem. 2000;277(2):260–266.

90. Kalydi E, Malanga M, Nielsen TT, Wimmer R, Béni S. Solving the puzzle of 2-hydroxypropyl β-cyclodextrin: Detailed assignment of the substituent distribution by NMR spectroscopy. Carbohydr Polym. 2024 Aug;338(February):122167.

91. Kalydi E, Murvai N, Saridakis E, Mavridis IM, Malanga M, Kardos J, Yannakopoulou K, Béni S. Molecular encapsulation of the aminosteroid phytotoxins solanidine and α-solanine by sugammadex: new insights into atomic-level interactions. Carbohydr Polym. 2025 Oct;366(May):123824.

92. Kalydi E, Malanga M, Ujj D, Benkovics G, Szakács Z, Béni S. Fully Symmetric Cyclodextrin Polycarboxylates: How to Determine Reliable Protonation Constants from NMR Titration Data. Int J Mol Sci. 2022;23(22).

93. Saridakis E, Kasimati EM, Yannakopoulou K, Mavridis IM. A guanidino-γ-cyclodextrin superdimer generates a twin receptor for phosphate dimers assembled by anti-electrostatic hydrogen bonds. ChemComm. 2022;58(34):5300–5303.

94. Makedonopoulou S, Mavridis IM. Structure of the inclusion complex of β-cyclodextrin with 1,12-dodecanedioic acid using synchrotron radiation data; a detailed dimeric β-cyclodextrin structure. Acta Crystallogr B. 2000 Apr 1;56(2):322–331.

95. Rodríguez-López MI, Mercader-Ros MT, Lucas-Abellán C, Pellicer JA, Pérez-Garrido A, Pérez-Sánchez H, Yáñez-Gascón MJ, Gabaldón JA, Núñez-Delicado E. Comprehensive Characterization of Linalool-HP-β-Cyclodextrin Inclusion Complexes. Molecules. 2020;25(21).

96. Yong CW, Washington C, Smith W. Structural behaviour of 2-hydroxypropyl-β-cyclodextrin in water: Molecular dynamics simulation studies. Pharm Res. 2008;25(5):1092–1099.

BIBLIOGRAPHY OF THE CANDIDATE'S PUBLICATIONS

List of publications regarding the topic of the thesis

Kalydi, E., Malanga, M., Nielsen, T. T., Wimmer, R., & Béni, S. (2024). Solving the puzzle of 2-hydroxypropyl β-cyclodextrin: Detailed assignment of the substituent distribution by NMR spectroscopy. Carbohydrate Polymers, 338(February), 122167. https://doi.org/10.1016/j.carbpol.2024.122167

Kalydi, E., Sebák, F., Fiser, B., Minofar, B., Moussong, É., Malanga, M., Bodor, A., Kardos, J., & Béni, S. (2025). Exceptional stability of the sugammadex-solasodine complex: Insights from experimental and theoretical studies. Carbohydrate Polymers, 348(July 2024). https://doi.org/10.1016/j.carbpol.2024.122819

Kalydi E, Murvai N, Saridakis E, Mavridis IM, Malanga M, Kardos J, Yannakopoulou K, Béni S. Molecular encapsulation of the aminosteroid phytotoxins solanidine and α-solanine by sugammadex: new insights into atomic-level interactions. Carbohydrate Polymers, 2025 Oct;366(May):123824. https://doi.org/10.1016/j.carbpol.2025.123824

List of publications not related to the topic of the thesis

Fejős, I., Kalydi, E., Malanga, M., Benkovics, G., & Béni, S. (2020). Single isomer cyclodextrins as chiral selectors in capillary electrophoresis. Journal of Chromatography A, 1627, 461375. https://doi.org/10.1016/J.CHROMA.2020.461375

Seggio, M., Payamifar, S., Fraix, A., Kalydi, E., Kasal, P., Catanzano, O., Conte, C., Quaglia, F., & Sortino, S. (2021). Visible light-activatable cyclodextrin-conjugates for the efficient delivery of nitric oxide with fluorescent reporter and their inclusion complexes with betaxolol. New Journal of Chemistry, 45(19), 8449–8455. https://doi.org/10.1039/d1nj00039j

Fejős, I., Kalydi, E., Kukk, E. L., Seggio, M., Malanga, M., & Béni, S. (2021). Single isomer n-heterocyclic cyclodextrin derivatives as chiral selectors in capillary electrophoresis. Molecules, 26(17). https://doi.org/10.3390/molecules26175271

Kalydi, E., Malanga, M., Ujj, D., Benkovics, G., Szakács, Z., & Béni, S. (2022). Fully Symmetric Cyclodextrin Polycarboxylates: How to Determine Reliable Protonation

Constants from NMR Titration Data. International Journal of Molecular Sciences, 23(22). https://doi.org/10.3390/ijms232214448

Ujj, D., Kalydi, E., Malanga, M., Varga, E., Sohajda, T., Béni, S., & Benkovics, G. (2022). Sugammadex analogue cyclodextrins as chiral selectors for enantioseparation of cathinone derivatives by capillary electrophoresis. Journal of Chromatography A, 1683, 463506. https://doi.org/10.1016/j.chroma.2022.463506

Agnes, M., Mazza, A., Kalydi, E., Béni, S., Malanga, M., & Manet, I. (2023). A Cyclodextrin Polymer as Supramolecular Matrix for Scalable Green Photooxygenation of Hydrophobic Substrates in Homogeneous Phase. Chemistry – A European Journal. https://doi.org/10.1002/chem.202300511

Osztie, R., Czeglédi, T., Ross, S., Stipsicz, B., Kalydi, E., Béni, S., Boldizsár, I., Riethmüller, E., Bősze, S. E., & Alberti, Á. (2024). Comprehensive Characterization of Phytochemical Composition, Membrane Permeability, and Antiproliferative Activity of Juglans nigra Polyphenols. International Journal of Molecular Sciences, 25(13), 1–28. https://doi.org/10.3390/ijms25136930

Dunkel, P., Bogdán, D., Deme, R., Zimber, Á., Ballayová, V., Csizmadia, E., Kontra, B., Kalydi, E., Bényei, A., Mátyus, P., & Mucsi, Z. (2024). C(sp3)-H cyclizations of 2-(2-vinyl)phenoxy-tert-anilines. RSC Advances, 14(24), 16784–16800. https://doi.org/10.1039/d3ra08974f

Dohárszky, A., Kalydi, E., Völgyi, G., Béni, S., & Fejős, I. (2024). Cyclodextrin-Enabled Enantioselective Complexation Study of Cathinone Analogs. Molecules, 29(4). https://doi.org/10.3390/molecules29040876

ACKNOWLEDGEMENTS

First and foremost, I would like to express my deepest thanks to my supervisor, Dr. Szabolcs Béni, for his guidance, support and endless patience with me throughout the years. I am grateful to had the opportunity for my professional development through his insights and expertise.

I also owe my thanks for my previous supervisor, Dr. Gábor Benkovics, who made me to start this journey as a PhD student, which brought me more experience as I have ever expected both professionally and personally.

I am endlessly grateful to my mentor, college and friend, Dr. Milo Malanga, who selflessly supported me though all the highs and downs in every aspect of life. Without his constant support, I may not have finished this journey till the end.

I am not less grateful for Mihály Bálint, who also guided me through doubts and difficulties by encouraging me to do what I truly enjoy doing even if it comes with fundamental changes in life.

I am also grateful to Dr. Konstantina Yannakopoulou, my supervisor during my Erasmus internship in Athens, who I was honored to learn from and work together with. I am also thankful for Dr. Irene Mavridis and Dr. Emanuele Saridakis for their help, shared expertise and kindness.

I am truly thankful to Dr. Ilse Manet, Dr. Marco Agnes and Arianna Mazza for the welcoming and supportive environment during my traineeship at ISOF Bologna within the framework of the Young Investigators Training Program 2020, contributing to one of my most influential life experiences.

I deeply appreciate the contribution of our collaborators from Eötvös Loránd University. I deeply appreciate the meticulous and scrupulous work of Dr. József Kardos, sharing us his expertise in the ITC studies, and I am thankful for Dr. Fanni Sebák and Dr. Andrea Bodor for their helpful insights and invested work in the NMR studies of SGM.

Great appreciation goes to all my colleges at the Department of Pharmacognosy at Semmelweis University, sharing a friendly and supporting environment to work in. Special thanks go to Zsófia Garádi and Dr. Bianka Várnai, supporting me in and out of

the NMR lab and creating great memories to remember. I am also very grateful the supporting attitude of Dr. Ida Fejős, helping me to tackle all the difficulties I've met as a PhD student.

Thanks to all my current colleges at the Organic Chemistry Department for the supporting and encouraging environment. Special thanks go to Dr. István Mándity for his open and supportive attitude.

I am endlessly grateful for all my friends inside and outside of the country, for supporting and encouraging me all the way through this journey.

Finally, this dissertation is dedicated to the memory of my mother, whose love, strength, and support have been the foundation of everything I have achieved.